NASA TM X-72

TECHNICAL MEMORANDUM

X - 72

LOW-SPEED STATIC LONGITUDINAL AND LATERAL STABILITY CHARACTERISTICS OF A VARIABLE-INCIDENCE DELTA-WING CANARD MODEL WITH HIGH-LIFT CANARD SURFACES

By Clarence D. Cone, Jr.

Langley Research Center
Langley Field, Va.

Declassified July 11, 1961

NATIONAL AERONAUTICS AND SPACE ADMINISTRATION

WASHINGTON September 1959

copy 1
case 1

NATIONAL AERONAUTICS AND SPACE ADMINISTRATION

TECHNICAL MEMORANDUM X-72

LOW-SPEED STATIC LONGITUDINAL AND LATERAL STABILITY CHARACTERISTICS OF A VARIABLE-INCIDENCE DELTA-WING CANARD MODEL WITH HIGH-LIFT CANARD SURFACES

By Clarence D. Cone, Jr.

SUMMARY

The present investigation was conducted in the Langley full-scale tunnel to determine the low-speed static longitudinal stability and control and lateral stability characteristics of a variable-incidence delta-wing canard model using high-lift devices on a trapezoidal and a delta canard surface.

The results showed that significant gains in both the maximum trim lift coefficient and allowable center-of-gravity travel were provided by the high-lift canard configurations over the basic canard configurations. The flow field from the high-lift canard surface had an appreciable interference effect on the wing which resulted in increasing stability with increasing lift coefficient. Wing incidence was effective in decreasing the model attitude at which the maximum trim lift coefficient was attained. Directional stability was maintained to lift coefficients above the maximum trim lift coefficient with the high-lift delta canard surface.

INTRODUCTION

The possible gains in high-speed performance attainable with canard airplanes over tailless or tail-rearward designs have been well established. A number of canard configurations possessing satisfactory supersonic longitudinal and lateral stability and control characteristics have been investigated (refs. 1 and 2). However, a basic low-speed problem still exists for canard configurations in that stall of the canard surface at moderate angles of attack prevents attainment of desirable high

trim lift coefficients and, in general, severely limits the allowable center-of-gravity travel. In addition, the attitude limitation imposed by practical landing-gear design necessitates the use of wing flaps for attaining the high lift coefficients desirable for take-off and landing. The increment in nose-down pitching moment which accompanies this use of flaps further aggravates the canard trim situation. In attempts to alleviate this low-speed problem, various high lift devices have been investigated (refs. 3 and 4).

In an extension of these studies an investigation has been conducted in the Langley full-scale tunnel of a canard model with a variable-incidence wing and with high-lift devices on the canard surfaces. The two canard-surface plan forms used in the investigation (delta and trapezoidal) were provided with leading- and trailing-edge flaps, with blowing boundary-layer control on the trailing-edge flaps, in an effort to maximize the lifting capabilities of the canard surfaces and thus to increase the maximum trim lift coefficient and allowable center-of-gravity travel for such an airplane configuration. In considering the use of high-lift canard surfaces, it was fully appreciated that the flow field from the highly loaded controls might have a measurable effect on the aerodynamic characteristics of the wing, and an important aspect of the investigation was to determine the general nature and magnitude of this effect.

L 4 6 8

It was further anticipated that use of a variable-incidence wing would yield high lift coefficients at moderate fuselage attitudes with relatively small pitching moments as compared with those produced by flaps, and thus relieve the canard surface of considerable basic trim requirement and reduce the attitude restrictions.

The investigation consisted primarily in obtaining the longitudinal stability and control characteristics and the lateral stability characteristics with both basic and high-lift canard configurations for wing-incidence angles of 0°, 4°, 8°, and 12°. In consideration of possible high-speed directional-stability requirements, limited tests were also made with twin vertical tails and with wing-mounted ventral fins, for comparison with a center vertical-tail installation.

COEFFICIENTS AND SYMBOLS

The positive directions of force and moment coefficients and angular displacements are shown in figure 1. Forces are referred to the stability axes and moments to the body axes.

C_L lift coefficient, $\frac{\text{Lift}}{qS}$

$C_{L,\text{trim}}$ maximum trim lift coefficient

C_D' approximate drag coefficient, $\frac{\text{Approximate drag}}{qS}$ (equivalent to true drag coefficient at $\beta = 0^o$)

C_Y side-force coefficient, $\frac{\text{Side force}}{qS}$

C_m pitching-moment coefficient, $\frac{\text{Pitching moment}}{qS\bar{c}}$

C_n yawing-moment coefficient, $\frac{\text{Yawing moment}}{qSb}$

C_l rolling-moment coefficient, $\frac{\text{Rolling moment}}{qSb}$

$C_{\mu,t}$ canard-surface momentum coefficient, $\frac{wV_j}{gqS_t}$

q free-stream dynamic pressure, lb/sq ft

V free-stream velocity, ft/sec

V_j velocity of blowing jet, ft/sec

S wing area, sq ft

$\bar{c}$ mean aerodynamic chord of wing, ft

b wing span, ft

S_t canard-surface total area, sq ft

$S_{t(exp)}$ exposed area of canard surface, sq ft

$\bar{c}_t$ mean aerodynamic chord of canard surface, ft

b_t span of canard surface, ft

l_t longitudinal distance from balance pitch center to quarter-chord point of $\bar{c}_t$, ft

x longitudinal distance of center of gravity referred to leading edge of $\bar{c}$, positive rearward, ft

α	angle of attack of fuselage center line, deg
β	angle of sideslip, deg
δ_f	deflection angle of wing flaps, deg
$\delta_{f,t}$	deflection angle of canard-surface trailing-edge flaps, deg
$\delta_{n,t}$	deflection angle of canard-surface leading-edge flaps, deg
i_w	wing-incidence angle relative to fuselage reference line, deg
i_t	incidence angle of canard surface relative to fuselage reference line, deg
Δ	denotes an increment
w	weight rate of air flow, lb/sec
g	gravitational constant, 32.2 ft/sec^2

Subscript:

β	denotes partial derivative of a coefficient with respect to angle of sideslip; for example, $C_{n_\beta} = \frac{\partial C_n}{\partial \beta}$, per deg

Definition:

The canard angle of attack is defined as $\alpha + i_t$.

MODEL DESCRIPTION

The general arrangement and principal dimensions of the model are presented in figure 2 and more detailed geometric data on the model components are given in table I. Figure 3 shows the model mounted in the Langley full-scale tunnel.

The wing of the model was a truncated delta plan form of aspect ratio 1.47, with a 60° swept leading edge, and NACA 65A003 airfoil sections parallel to the plane of symmetry. Full-span constant-chord trailing-edge flaps were provided, and for most longitudinal stability tests a full-span leading-edge extension (fig. 5) was installed on the wing. The wing was pivoted about an axis through the 53-percent point

of the mean aerodynamic chord to allow variation of wing incidence relative to the fuselage center line. The portion of the wing rearward of the pivot point was severed free of the fuselage along the wing-fuselage juncture to allow incidence changes. (See fig. 3(b).) The high wing position was chosen primarily to eliminate a rear wing-fuselage gap at incidence. No attempt was made to fair the forward wing-fuselage gap caused by incidence.

The fuselage consisted of two sections joined at the 63-inch station. The forward portion was a development of modified elliptic sections into a circular cross section at the 52-inch station as shown in figure 2. The rear section was a body of revolution with slight modifications to accommodate the wing.

L
4
6
8

Two canard-surface plan forms were investigated: surface A was trapezoidal with 25.6° of leading-edge sweep and surface B was a truncated delta with 55° of leading-edge sweep. Each surface was equipped with full-span leading- and trailing-edge flaps. Canard-surface details and and dimensions are given in figure 4. Each surface had a projected area of 0.15S and the exposed areas were 0.11S and 0.09S for the trapezoidal and the delta surface, respectively.

The trailing-edge flaps of the canard surfaces were provided with boundary-layer control by ejecting high velocity air over the nose of the flap from a full-span slot in the trailing edge of the main surface. The compressed air was supplied to the canard plenum chambers through flexible tubing connected to the canard undersurface.

The leading-edge flaps of the canard surfaces were deflected by inserting a wedge of proper size in the deflection gap. For all tests using the high-lift configuration of canard surface A (trailing-edge flaps deflected and boundary-layer control used), the leading-edge flap was replaced with a full-span slat, since the slat gave slightly higher maximum canard-surface lift coefficients. Details of the flaps, slat, and air system are shown in figure 4.

The effects of single and twin vertical tails and full-chord wing-mounted ventral fins were investigated. Location and dimensions of the vertical tails are given in figure 2 and those of the ventral fins are given in figure 5. The single (center) vertical tail was used in all tests except those to determine the effects of the twin vertical tails.

TESTS

The tests consisted of measurement of the model forces and moments for an angle-of-attack range of -4° to 32° at wing-incidence angles of 0°,

4°, 8°, and 12°. Control-effectiveness data were obtained in most cases for canard-surface incidence angles of 0°, 5°, and 10°, for both the basic (flaps undeflected) and high-lift (flaps deflected and using boundary-layer control) canard-surface configurations.

To establish the optimum high-lift configuration for each of the canard surfaces (A and B), preliminary tests using tufts to permit observation of the surface flow were made with various combinations of leading- and trailing-edge flap deflections and values of momentum coefficient $C_{\mu,t}$. The optimum configurations and the $C_{\mu,t}$ values thus determined were then used for all subsequent tests with the high-lift canard surfaces. The high-lift configuration of canard surface A consisted of the nose slat deflected 40° (fig. 4) and the trailing-edge flap deflected 45° (normal to flap hinge line). That of canard surface B consisted of a 45° deflection of both leading- and trailing-edge flaps. For both canard surfaces, a nominal $C_{\mu,t}$ of 0.033 was used on the trailing-edge flap.

L 4 6 8

For most of the tests to determine the aerodynamic characteristics, the wing was equipped with a leading-edge extension. Early in the program this extension was found beneficial for increasing the range of directional stability and was retained on the wing for the longitudinal tests.

Lateral stability data were obtained for the model equipped with the center vertical tail with basic canard surfaces A and B, and with high-lift canard surface B at sideslip angles of 0° and 5°. The lateral stability investigation also included tests to determine the effects of wing leading-edge extension, wing-mounted ventral fins, and twin vertical tails on the characteristics of the model at wing-incidence angles of 8° and 12°, with high-lift canard surface B. Some data were also obtained at sideslip angles of -5° and -10°.

Force and moment measurements were made with a six-component internal strain-gage balance. All tests were made at a Reynolds number of 2.6×10^6 (based on the mean aerodynamic chord) and a Mach number of 0.10. Since sample calculations showed jet boundary and buoyancy effects to be negligibly small, such corrections were not applied to the data. No correction was made to the drag coefficient to account for taking the boundary-layer-control air on board.

RESULTS

The aerodynamic characteristics of the wing-fuselage combination with wing incidence and without canard surfaces are presented in figures 6 and 7. Longitudinal stability and control characteristics of

the model with basic canard surfaces A and B with wing incidence are given in figures 8 to 11.

The longitudinal control characteristics with the high-lift configurations of canard surfaces A and B are presented in figures 12 and 13, respectively, at wing incidences of 0°, 4°, 8°, and 12°. The moment-producing capability of each high-lift canard surface is shown in figure 14 and the magnitude of the interference effect of the flow field from the high-lift canard surface on the lift and moment contribution of the wing is indicated in figure 15.

L
4
6
8

The variation of maximum trim lift coefficient with center-of-gravity position is presented in figure 16 for the high-lift configurations of canard surfaces A and B. The effects of twin vertical tails on lift and pitching moment are presented in figure 17 for the high-lift configuration of canard surface B.

The lateral stability derivatives for the model with the basic canard surfaces, with high-lift canard surface B, and without canard surfaces are shown in figure 18. Lateral stability characteristics of the various configurations using high-lift canard surface B are presented in figure 19 for $i_w = 0^\circ$, 4°, 8°, and 12° and in figures 20 to 23 for $i_w = 8^\circ$ and 12°. The effects of sideslip angle on the lift and pitching-moment coefficients of the model are shown in figure 24 for $i_w = 8^\circ$ and 12°.

DISCUSSION OF RESULTS

Longitudinal Stability Characteristics

In the following discussion, the pitching- and yawing-moment data are referred to various center-of-gravity (moment-center) locations, depending upon the model configuration. The center-of-gravity position in each case is located on the model center line and is referred to the projection of the leading edge of the wing mean aerodynamic chord on the center line $(i_w = 0^\circ)$, the positive direction being rearward. With this convention, the actual balance center of the model was located at $x = 0.275\bar{c}$. (See fig. 2.)

Aerodynamic characteristics of the wing-fuselage combination with wing incidence and with canard surface off.- As shown in figure 6, wing incidence increased the lift-curve slope by 11 to 14 percent in the lower angle-of-attack range (0° to 12°), but the value of the maximum lift coefficient decreased slightly with increasing incidence. The

reduction in fuselage attitude for a given lift coefficient afforded by the $i_w = 12^\circ$ over the $i_w = 0^\circ$ configuration was approximately a constant 11° throughout the lift range. The basic wing-fuselage combination was stable at all incidences and at the stall for the center-of-gravity (moment-center) position at $0.275\bar{c}$; however, the stability decreased slightly with increasing wing incidence.

As a representative illustration of the moment reduction resulting from wing incidence, a comparison is made of the model using full-span flaps deflected 20° with the model using 12° of wing incidence (fig. 7). This reduction of the pitching-moment coefficient by approximately 0.16 for a given angle of attack illustrates one advantage of using wing incidence in conjunction with canard controls. Although the wing-incidence configuration stalls at a lower lift coefficient than does the configuration with flaps, this angle of stall (20°) is still well above an assumed ground-attitude limitation of 12° to 14°, which is considered a practical limit.

Stability and control characteristics of the model with basic canard surface A.- The stability characteristics of the model with basic canard surface A for $i_w = 0^\circ$, 4°, 8°, and 12° are presented in figure 8. The moment data of this figure are referred to the center-of-gravity position at $0.275\bar{c}$. Addition of the canard surface resulted in a forward shift of the neutral point by approximately $0.26\bar{c}$ as can be seen by comparison with figure 6(a). The control characteristics of the model with basic canard surface A (fig. 9) show a severe limitation imposed on the maximum trim lift coefficient $(C_{L,trim})$ by early canard-surface stall. This is illustrated by the pitching-moment curves for $i_t = 0^\circ$ and 5° with $\delta_{n,t} = 0^\circ$. When these curves are referred to center-of-gravity positions such that neutral or positive stability is obtained throughout the lift range, the $C_{L,trim}$ is limited to approximately 0.4. Deflecting the canard-surface leading-edge flap 30° to delay stall considerably extended the effective lift range of the canard surface and increased $C_{L,trim}$ to 0.6. However, use of the flap caused a displacement of the pitching-moment curve for a given canard-surface incidence by approximately $\Delta C_m = -0.015$. For neutral stability $\left(\frac{dC_m}{dC_L} = 0 \text{ at } C_L = 0\right)$, this displacement cancelled much of the gain in $C_{L,trim}$ that might otherwise have been realized from the extension of the canard-surface lift range.

Stability and control characteristics of the model with basic canard surface B.- Canard surface B was only about 65 percent as destabilizing as canard surface A thereby causing a forward shift in the neutral point of approximately $0.175\bar{c}$ (fig. 10). The smaller exposed (effective) area

and lower lift-curve slope of the delta plan form contribute to this reduced effectiveness. Basic canard surface B at $i_t = 0^\circ$ showed no tendency to stall within the lift range, even without deflection of the leading-edge flap. Although the basic canard surface does stall at the higher canard angles of attack (approximately 25°), it maintains sufficient effectiveness to trim the model to a lift coefficient of 1.0 (fig. 11), with at least neutral stability. However, a forward center-of-gravity shift of only $0.025\bar{c}$ from the neutral position reduces the $C_{L,trim}$ to about 0.7 and illustrates the limitation imposed on center-of-gravity travel by the basic canard surface.

L
4
6
8

Stability and control characteristics of the model with the high-lift configuration of canard surface A.- The stability and control data for the model with the high-lift configuration of canard surface A (fig. 12) have been referred to a center-of-gravity position at $0.05\bar{c}$ which is considered more consistent with probable stability requirements. For this center-of-gravity position the model was generally unstable in the lower lift-coefficient range but became increasingly stable for lift coefficients above 0.6 for $i_w = 0^\circ$ and 4° and above 0.7 for $i_w = 8^\circ$ and 12° for all positive canard-surface incidences. These stability variations appear to be the result of the canard-surface flow-field interference on the magnitude and distribution of wing lift. In order to illustrate the general nature of this effect, the interference-free lift and pitching-moment curves for the configuration with $i_w = 8^\circ$, $i_t = 0^\circ$ are compared with the experimental values for this configuration (fig. 15(a)). The interference-free curves were obtained by adding the separate contributions of the canard surface and the wing-fuselage combination. As shown, the canard-surface interference caused a considerable lift loss on the wing throughout the lift range. The magnitude of the loss increased up to $\alpha = 8^\circ$ and then decreased steadily with increasing angle of attack. This decreased interference is probably due to the relative position of the wing and the trailing vortices of the canard surface, since the canard surface was effective up to $\alpha = 20^\circ$ (fig. 14). The variation in the lift loss with angle of attack results in a decrease in the lift-curve slope in the lower angle-of-attack range (-4° to 8°) and an increase in slope above 8°. The dashed line in figure 15(a) represents the lift-curve slope at $\alpha = 0^\circ$ of the complete configuration (wing-fuselage combination with canard surfaces, center vertical tail, and leading-edge extension). These changes in slope of the lift curve are reflected in the pitching-moment curve as the stability variations.

The pitching-moment curves of figure 15(a) agree closely for angles of attack between 12° and 24° even though interference still causes an appreciable lift loss in this range. This result suggests that the center-of-pressure location on the wing may also vary as the angle of attack varies.

Because of the similarity of the lift and pitching-moment curves for all positive canard-surface- and wing-incidence angles, the same analysis would also apply for these configurations. The interference-caused lift losses and pitching-moment increments for the high-lift configurations of figure 12 for $i_t = 0^\circ$ are shown in figures 15(b) and 15(c). The apparent gain in lift shown for the higher angles of attack (fig. 15(a)) is not actually caused by the interference but results from the leading-edge extension, which was used on the complete configuration but was not on the wing for the wing-fuselage tests.

The further increase in stability in the high-lift-coefficient range (fig. 12) is attributed to canard-surface stall since the data of figure 14 indicate that canard surface A stalls at a canard angle of attack of 21° to 24°, depending on canard-surface incidence. This coincides in general with the sudden increase in stability at high angles of attack.

For the center-of-gravity position at $0.05\bar{c}$, canard surface A was capable of trimming the model to lift coefficients of the order of 1.3 at all wing-incidence angles. For this center-of-gravity position the model was unstable in the lower lift range. However, it is not probable that an aircraft of this type would fly at the velocities corresponding to these low lift coefficients while using high-lift canard surfaces and/or wing incidence. In connection with this instability region, it might be noted that the wing interference caused by the canard is somewhat beneficial in that it allows the attainment of high trim lift coefficients with a more rearward center-of-gravity position than would have been possible without the stability increase.

Stability and control characteristics of the model with the high-lift configuration of canard surface B.- The stability and control data for the model with high-lift canard surface B (fig. 13) have been referred to the center-of-gravity position at $0.09\bar{c}$, which gives stability except for the lower lift-coefficient range for wing incidences of 4°, 8°, and 12°.

The pitching-moment curves for canard surface B are characterized by the same increasing stability as are those of canard surface A, and from the same causes. However, the increase in stability due to canard-surface interference is considerably less with canard surface B (fig. 13) as might be expected in view of its lower lift at a given canard angle of attack. This reduced interference resulted in somewhat more linear pitching-moment curves. With the center-of-gravity position at $0.09\bar{c}$ it was possible to trim to lift coefficients of approximately 1.3 for the lower wing incidences ($i_w = 0^\circ$ and 4°).

Variation of the maximum trim lift coefficient with center-of-gravity position.- In order to summarize the maximum trim capabilities

of the high-lift canard surfaces, the data of figures 12 and 13 have been used to prepare figure 16, which shows the variation of the maximum trim lift coefficient $(C_{L,trim})$ with center-of-gravity position $x/\bar{c}$, with x referenced to the leading edge of the mean aerodynamic chord. The curves of this figure were obtained by replotting the pitching-moment data for a range of center-of-gravity positions and determining the maximum lift coefficient for which the model could be trimmed for each center-of-gravity position. The angle of attack at which $C_{L,trim}$ occurs is shown on the right side of the figure for each wing incidence for the high-lift canard surface. The curves for the basic model (wing-fuselage combination with basic canard surface and center vertical tail) with $i_w = 0^o$ are included for comparison. It should be pointed out that figure 16 is intended only to summarize the maximum canard-surface trim capabilities and for any specific application these curves must be interpreted in terms of the basic data of figures 12 and 13. The trim capabilities of canard surface A are shown in figure 16(a). In using the $C_{L,trim}$ curves of this figure to establish the allowable center-of-gravity travel, it is first necessary to set a rear center-of-gravity limit. Since the aircraft represented by the model must assume the normal flight configuration at relatively low speeds after take-off and will be in the normal flight configuration before beginning the landing transition, this rear limit cannot exceed the neutral point of the normal flight configuration if stability is to be maintained. This neutral point has been marked on figure 16(a) by a circular symbol. This limit also applies to all of the incidence configurations. This rear limit is, in general, compatible with high-speed requirements.

The neutral point of the model with basic canard surface A was located at $0.05\bar{c}$. This neutral-point position limits the $C_{L,trim}$ of the basic model to values below 0.7. The high-lift canard surface produced an increment in $C_{L,trim}$ of about 0.5 throughout the center-of-gravity travel range. Considering the forward center-of-gravity position limited by the $C_{L,trim}$ required, the extension of possible center-of-gravity travel gained with the high-lift canard surface is significant.

The $C_{L,trim}$ attainable for a given center-of-gravity position was essentially independent of wing incidence. The reason for this appears to be the compensating effect of the canard-surface interference, for a given lift coefficient, as wing incidence increases. That is, for a given C_L and i_t, canard-surface lift decreases as i_w increases so that a larger negative moment would be expected as i_w increases. However, the lower canard-surface lift results in less nose-down moment from the wing, so that the resultant moment changes but little with wing incidence, especially in the high-lift region (C_L of 0.6 to 1.2).

The curves of figure 16(a) show the maximum possible trim lift coefficient attainable for the various center-of-gravity locations for each wing-incidence configuration. However, the amount of this lift that can actually be used for take-off and landing will of course be governed by attitude limitations as set by landing-gear design. If, for example, the model with $i_w = 12^\circ$ is assumed to be attitude limited to an angle of attack of 14°, the maximum usable lift coefficient is 1.15 for all center-of-gravity positions rearward of $0.01\bar{c}$, while the $C_{L,trim}$ varies from 1.38 at $0.05\bar{c}$ to 1.15 at $0.01\bar{c}$. For center-of-gravity positions forward of $0.01\bar{c}$ the full $C_{L,trim}$ can be realized since the angle of attack for $C_{L,trim}$ is below 14° for this center-of-gravity range. The value of $C_{L,trim}$, however, decreases as the center of gravity moves forward as is obvious from the figure. It should be noted that these data do not include possible ground effects on both maximum lift and trim.

The trim capabilities of canard surface B are summarized in figure 16(b). In general the increment in $C_{L,trim}$ for a given center-of-gravity position resulting from the high-lift canard surface is less than that obtained with canard surface A, and the increment decreases with increasing wing incidence. The pronounced effect of wing incidence in this case is apparently due to the smaller interference effect produced by canard surface B, which results in a negative displacement of the pitching-moment curves with increasing incidence (fig. 13). Again, if the model is assumed to be attitude limited at $\alpha = 14^\circ$, the full available $C_{L,trim}$ cannot be realized for center-of-gravity positions rearward of the $0.08\bar{4}\bar{c}$ position even for the case of $i_w = 12^\circ$, although this configuration can be trimmed to a C_L of 1.05.

In summary of the trim capabilities of the two canard-surface plan forms, it can be said that canard surface A offers both higher $C_{L,trim}$ values for a given center-of-gravity position and a more extensive range of possible center-of-gravity travel than does canard surface B. The assumed attitude restriction of $\alpha = 14^\circ$, however, limits the maximum usable lift coefficients to approximately 1.15 and 1.04 for canard surfaces A and B, respectively, so that canard surface A offers only a 10-percent advantage as far as maximum usable lift is concerned. Also, the pitching-moment curves of canard surface A are very nonlinear and in some cases the stability at trim may be excessive.

Longitudinal effects of wing leading-edge extension, wing-mounted ventral fins, and twin vertical tails.- The principal effect of the wing leading-edge extension was to increase the maximum lift coefficient that could be attained, especially for $i_w = 12^\circ$; however, no data on the longitudinal effects of the wing leading-edge extension are presented.

Its effect on the pitching moment at a given lift coefficient was negligible. The wing-mounted ventral fins had practically no effect on either lift or pitching moment.

The twin vertical tails, however, caused a loss in lift coefficient of 0.1 or more at the higher angles of attack for $i_w = 12^\circ$ as shown in figure 17. This lift loss was accompanied by a positive increment in pitching moment for $i_w = 12^\circ$ at the higher lift coefficients. This effect is probably the result of vertical tail interference with the wing leading-edge vortex, which caused stall of the outboard wing areas. Location of the twin vertical tails at the wing tips might reduce such an interference effect.

Lateral Stability Characteristics

Stability characteristics with the basic canard surfaces.- Figure 18 shows that addition of the canard surfaces to the basic model increased the magnitude of both C_{n_β} and $-C_{l_\beta}$ at high lift coefficients. Canard-surface plan form appeared to have no significant effect on lateral stability, except that directional instability occurred at lower lift coefficients with canard surface A for $i_w = 0^\circ$ and 4°.

Stability characteristics with high-lift canard surface B.- Comparison of the derivatives for the basic and high-lift configurations of canard surface B (fig. 18) shows that use of high-lift devices on the canard surface increased the positive effective dihedral at $i_w = 4^\circ$, 8°, and 12°, decreased the directional stability, and reduced the lift coefficient at which directional instability occurred at $i_w = 8^\circ$ and 12°. For more forward center-of-gravity locations, the magnitude of C_{n_β} would be increased due to the increased vertical-tail moment arm.

As previously stated, the lateral stability tests with high-lift canard surfaces were limited to canard surface B, and in most cases to wing incidences of 8° and 12°, since these wing incidences were deemed the more important from take-off and landing considerations.

The effects of wing incidence on the stability derivatives with canard surface B are shown in figure 19. The lift range for which the model is directionally stable increases to a maximum at $i_w = 4^\circ$. Above $i_w = 4^\circ$ the range decreases rapidly to a C_L of 1.0 at $i_w = 12^\circ$. A decrease in effective dihedral also occurs at the two higher wing incidences for the higher lift coefficients.

In an attempt to extend the directional stability range for the higher incidences the wing was fitted with a leading-edge extension. The effects of this extension on the lateral derivatives are shown in figure 20. The lift range for which the model was directionally stable was considerably increased by the extension so that the model was stable up to a lift coefficient of 1.27 at $i_w = 12^\circ$ for the center-of-gravity position at $0.275\bar{c}$. However, the severe increases in positive effective dihedral which occur in the C_L range of 0.5 to 1.0 with the extension may be of some concern since large rolling moments may be produced. Further study of various means of alleviating this excessive effective dihedral while maintaining the directional advantages of the extension is needed.

The stability derivatives of the model with the leading-edge extension and center vertical tail for $i_w = 8^\circ$ and 12° are presented in figure 21. The directional data are referred to the center-of-gravity position at $0.09\bar{c}$ so that they may be compared directly with the basic longitudinal data of figures 13(c) and 13(d). Comparison of these figures shows that directional stability was maintained to a lift coefficient well above that of $C_{L,trim}$ so that maximum trimmed lift is not limited by directional instability. Forward movement of the center of gravity would tend to increase the range between $C_{L,trim}$ and the C_L at which directional instability occurs. The undesirable increases in effective dihedral caused by the leading-edge extension have already been noted.

Since ventral fins have been beneficial in improving high-speed directional stability (ref. 1), limited lateral tests were made with a wing-mounted ventral-fin configuration. The stability characteristics of this configuration are presented in figure 22. The ventral fins were equally as effective as the leading-edge extension in extending the range of directional stability for $i_w = 8^\circ$ and 12° and in reducing the positive dihedral effect, and in this respect are to be preferred to the use of the leading-edge extension. However, the very large gradients in C_{l_β} which occur at $C_L = 0.67$ for $i_w = 8^\circ$ and $i_t = 10^\circ$ and at $C_L = 0.8$ for $i_w = 12^\circ$ and $i_t = 0^\circ$, 10° might be objectionable. Also, at $i_w = 12^\circ$, increasing canard incidence had a sizeable effect in decreasing the lift range for which the model was directionally stable.

Tests were also made with a twin-vertical-tail configuration (wing leading-edge extension off). The twin tails gave directional stability up to maximum lift (fig. 23), but the same excessive values of effective dihedral as caused by the leading-edge extension occurred and were even more pronounced. This effect, combined with the decrease in lift caused by these tails (fig. 17) does not make the twin-tail configuration as

investigated attractive from low-speed considerations. As mentioned previously, however, a more suitable location of the tails might be expected to alleviate such adverse characteristics.

Effect of sideslip on longitudinal characteristics.- In view of the rather pronounced effects of the high-lift canard-surface flow field on the wing pitching moment, it is of interest to examine the magnitude of the changes in longitudinal characteristics which accompany sideslip. The effects of -5° and -10° sideslip for $i_w = 8^\circ$ and 12° for a canard-surface incidence angle of 10° are presented in figure 24 for the model with high-lift canard surface B with center vertical tail and wing leading-edge extension. The effects with $i_w = 8^\circ$ (fig. 24(a)) are small for angles of attack below 14°, even for $\beta = -10^\circ$. For $i_w = 12^\circ$ (fig. 24(b)) the effects are similar, and for angles of attack below 14° they are negligible. Thus no serious changes in longitudinal characteristics appear to accompany sideslip angles up to 10° with high-lift canard surface B in the take-off and landing attitude range.

L
4
6
8

CONCLUSIONS

An investigation to determine the low-speed static longitudinal and lateral stability characteristics of a variable-incidence delta-wing canard model with high-lift devices on the canard surfaces has yielded the following conclusions:

1. The use of high-lift devices and boundary-layer control on the canard surfaces resulted in significant increases in both the maximum trim lift coefficient and allowable center-of-gravity travel, compared to the basic canard configurations.

2. The high-lift configuration of the trapezoidal canard surface gave higher trim lift coefficients for a given center-of-gravity position and offered a larger travel range for the center of gravity than did that of the delta canard surface. Assumed attitude limitations of 14°, however, reduced the maximum usable trim lift coefficient to approximately 1.1 for both configurations at a wing incidence of 12°.

3. The flow field from the high-lift trapezoidal canard surface had a pronounced effect on the wing lift and pitching moment which resulted in increasing stability with positive canard-surface incidence at all wing incidences. Interference effects from the delta canard surface were less severe.

4. Directional stability was maintained to lift coefficients above the maximum trim lift coefficient with the high-lift delta canard surface using the center vertical tail and leading-edge extension for wing incidences of 8° and 12°. However, very large values of positive effective dihedral were caused by the extension.

Langley Research Center,
National Aeronautics and Space Administration,
Langley Field, Va., June 16, 1959.

REFERENCES

1. Spearman, M. Leroy, and Driver, Cornelius: Some Factors Affecting the Stability and Performance Characteristics of Canard Aircraft Configurations. NACA RM L58D16, 1958.

2. Hall, Charles F., and Boyd, John W.: Effects of Canards on Airplane Performance and Stability. NACA RM A58D24, 1958.

3. Johnson, Joseph L., Jr.: A Study of the Use of Various High-Lift Devices on the Horizontal Tail of a Canard Airplane Model as a Means of Increasing the Allowable Center-of-Gravity Travel. NACA RM L52K18a, 1953.

4. Sleeman, William C., Jr.: Investigation at High Subsonic Speeds of the Static Longitudinal and Lateral Stability Characteristics of Two Canard Airplane Configurations. NACA RM L57J08, 1957.

TABLE I

GEOMETRIC DATA ON MODEL COMPONENTS

L
4
6
8

Wing:		
Area, total, sq in.		2135.6
Area, movable, sq in.		1895.6
Span, in.		56
Mean aerodynamic chord, in.		43
Aspect ratio		1.47
Taper ratio		0.223
Airfoil section		NACA 65A003
Fuselage:		
Length, in.		130.0
Maximum diameter, in.		12.0
Fineness ratio		10.82
Horizontal tails:	Canard A	Canard B
S_t/S	0.150	0.150
$S_{t(exp)}/S$	0.110	0.091
b_t/b	0.554	0.409
$l_t/\bar{c}$	1.45	1.50
Aspect ratio	3.0	1.66
Taper ratio	0.407	0.219
Vertical tails:	Single	Twin (each)
Area, total, sq in.	455	242
Span, in.	21	18
Aspect ratio	0.968	1.340
Ventral fins (each):		
Length, in.		26
Maximum width, in.		5
Area, sq in.		109

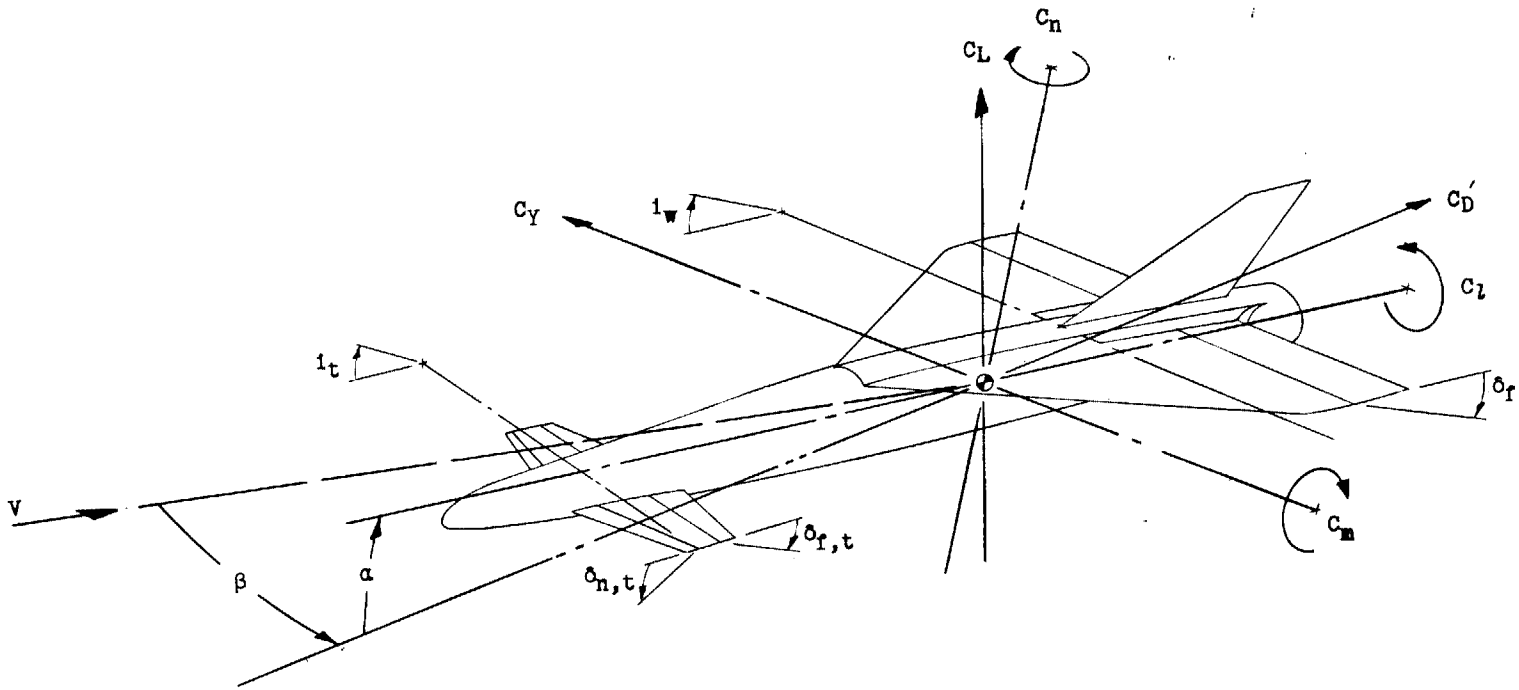

Figure 1.- System of axes used. Arrows indicate positive directions of force and moment coefficients and angular displacements.

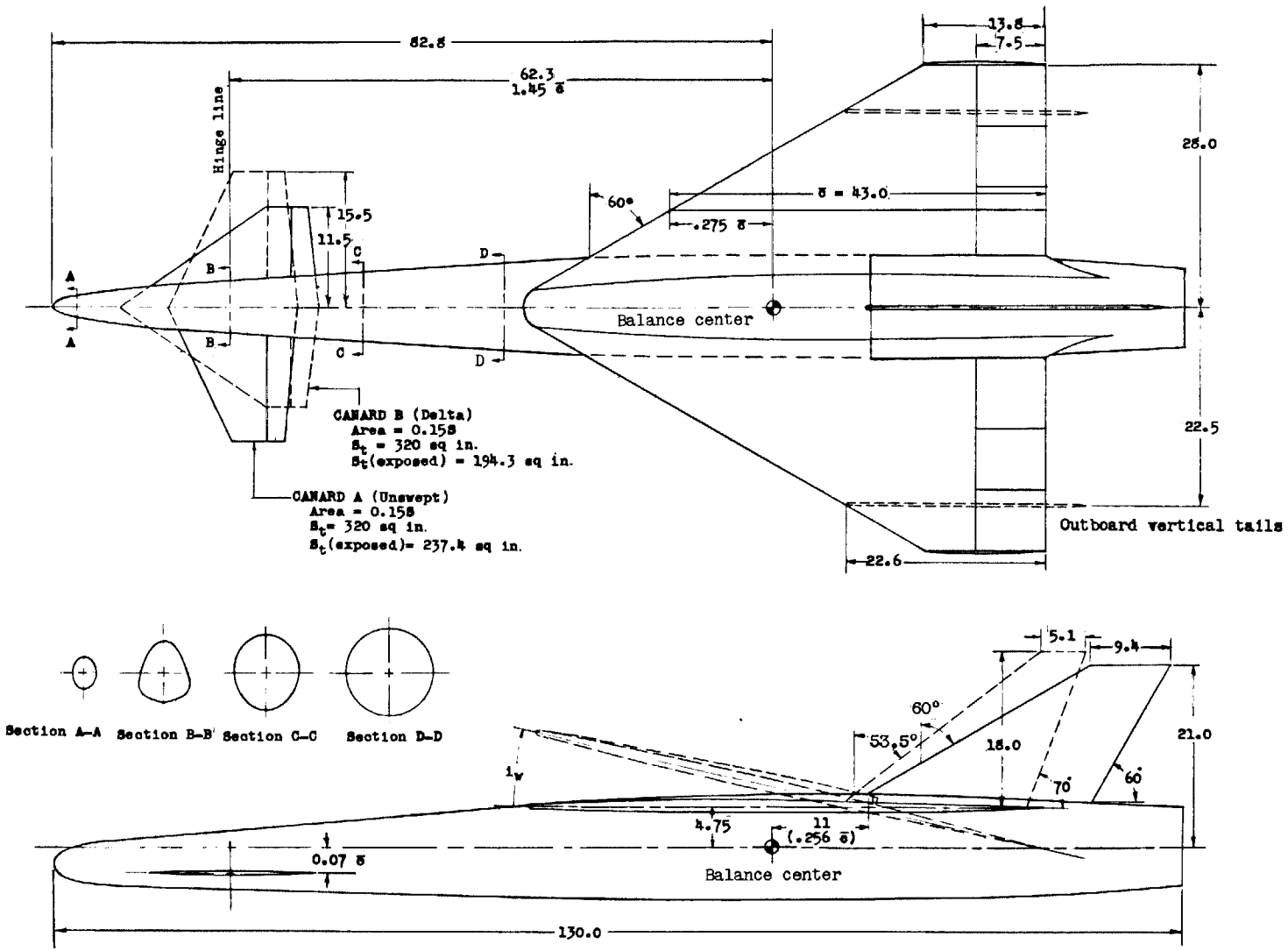

Figure 2.- General arrangement and principal dimensions of model. All dimensions are in inches.

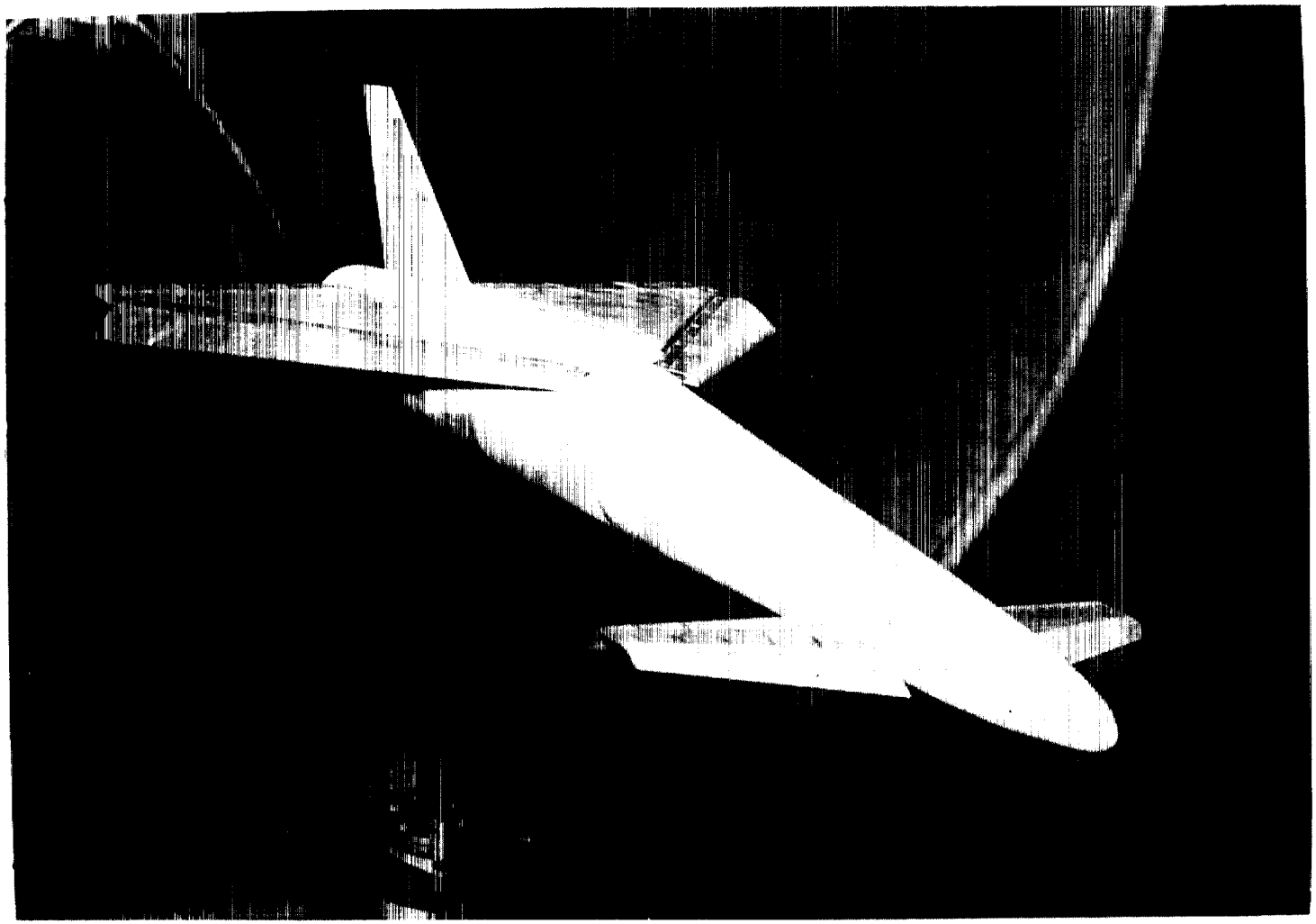

(a) $i_w = 0^\circ$.

L-58-1118

Figure 3.- Photograph of model with high-lift canard surface A, wing leading-edge extension and center vertical tail.

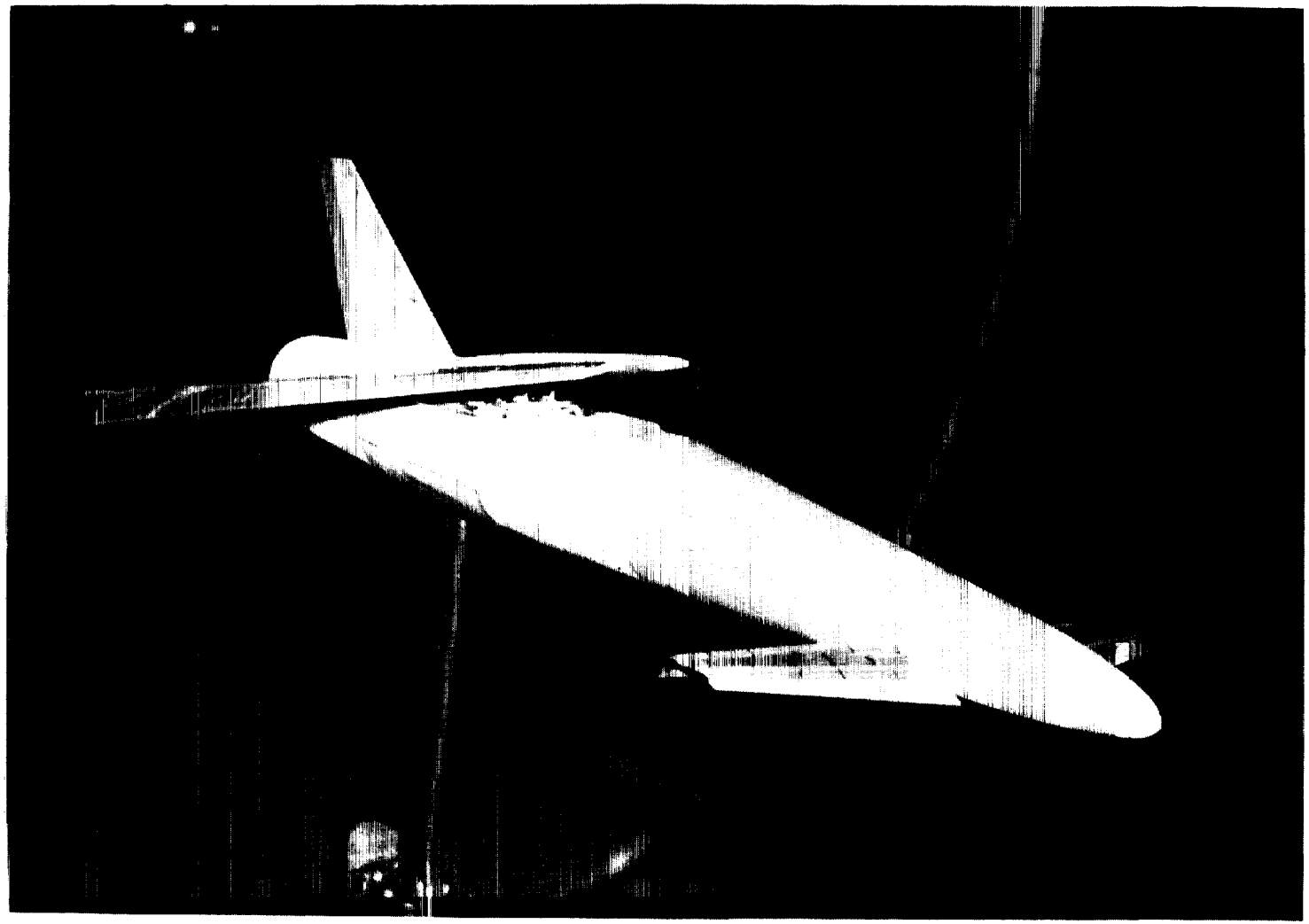

(b) $i_w = 12^\circ$. L-58-1119

Figure 3.- Concluded.

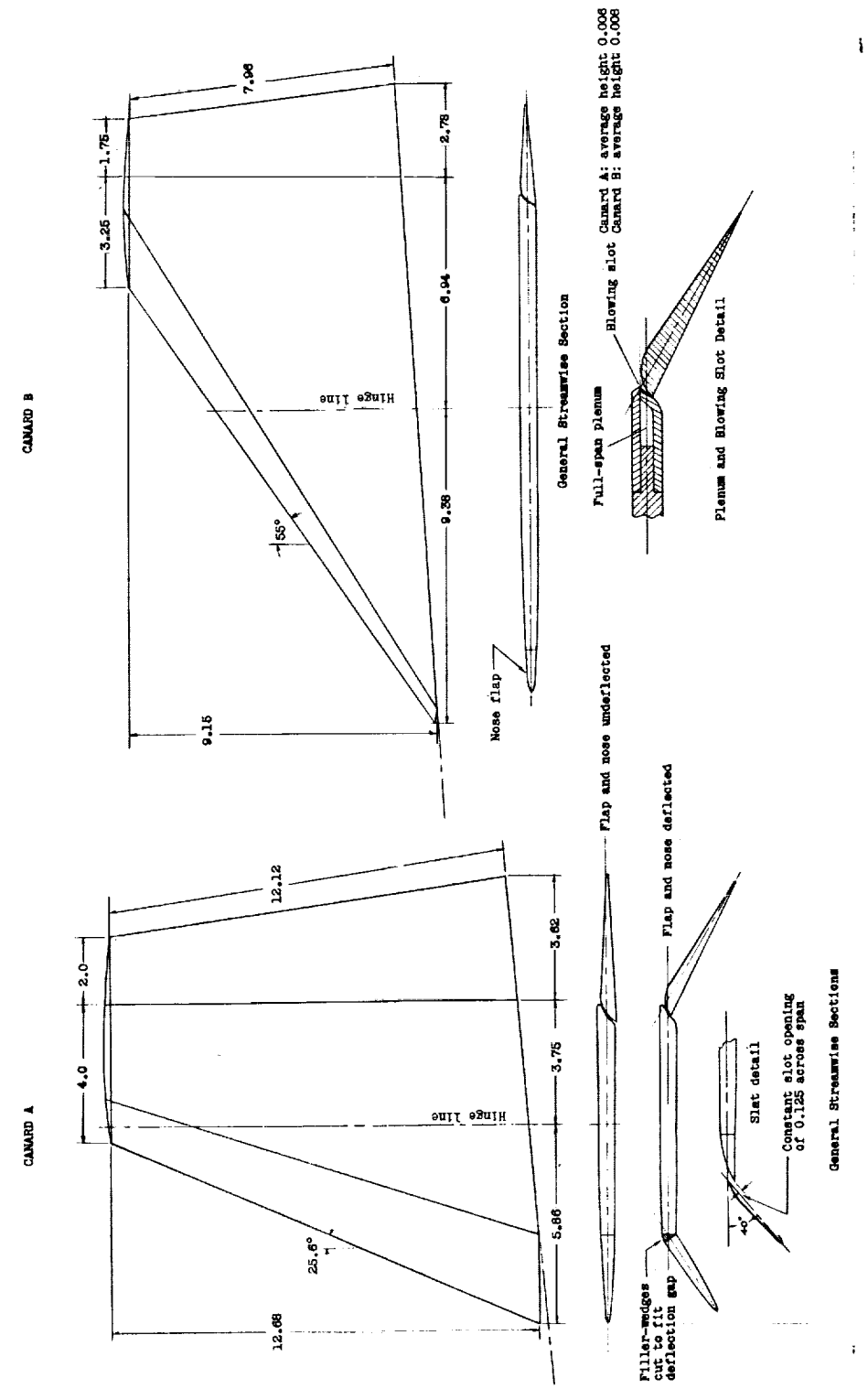

Figure 4.- Dimensions and sections of canard tail surfaces. All dimensions are in inches.

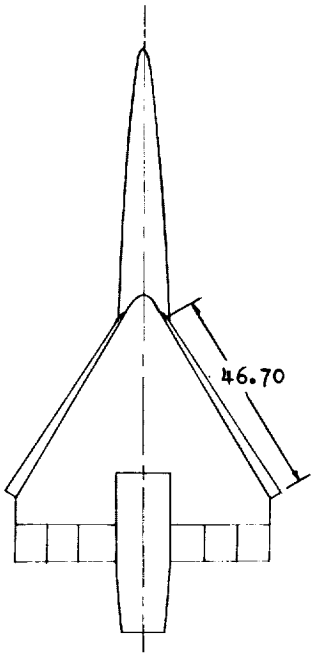

Model with leading-edge extensions

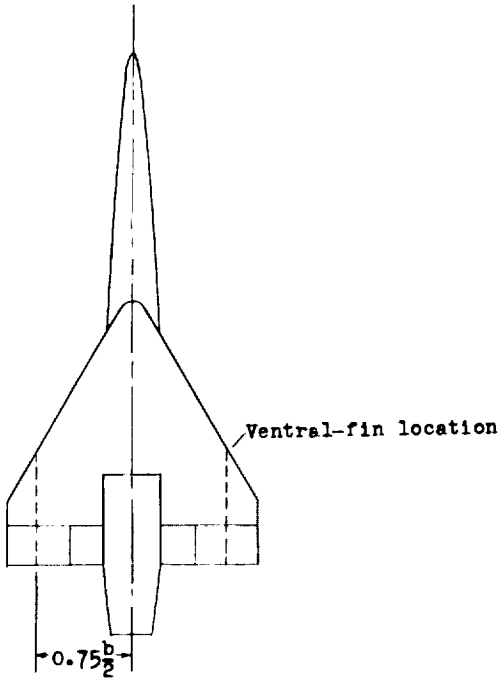

Model with ventral fins

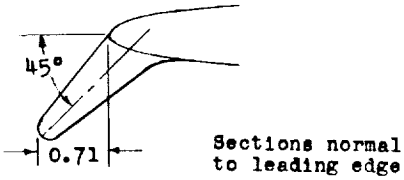

Inboard end

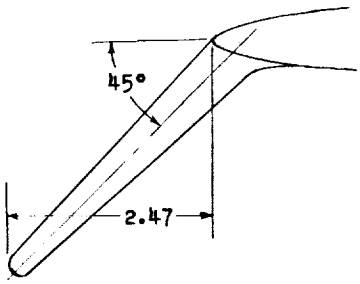

Outboard end

Leading-edge Extension

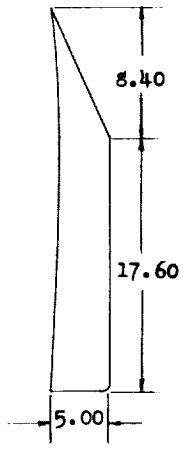

Side view

Ventral Fins

Figure 5.- Details of leading-edge extensions and ventral fins. All dimensions are in inches.

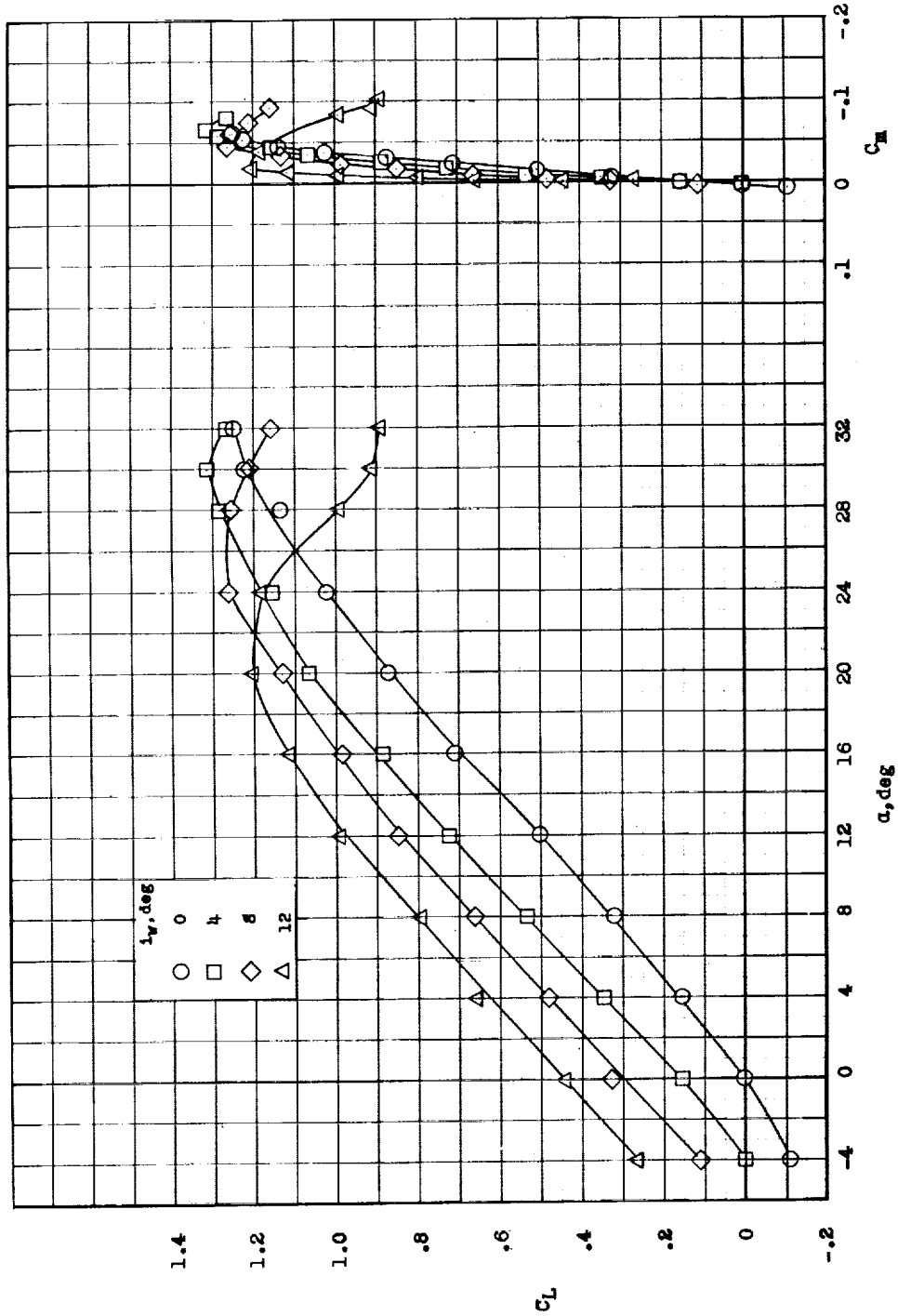

(a) Lift and pitching-moment coefficients.

Figure 6.- Aerodynamic characteristics of wing-fuselage combination with center vertical tail. Canard surface off; center of gravity at 0.275$\bar{c}$.

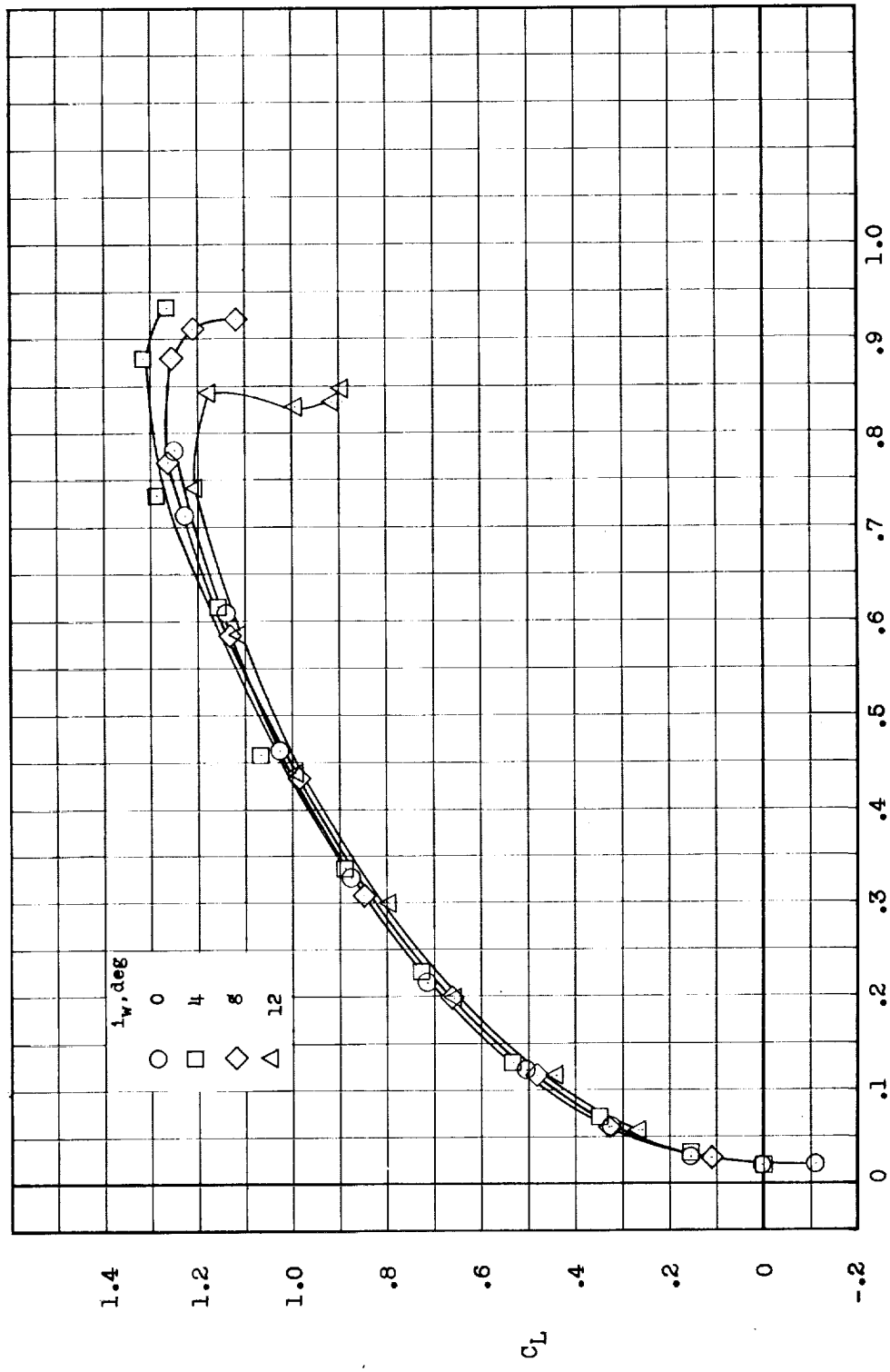

(b) Drag coefficient.

Figure 6.- Concluded.

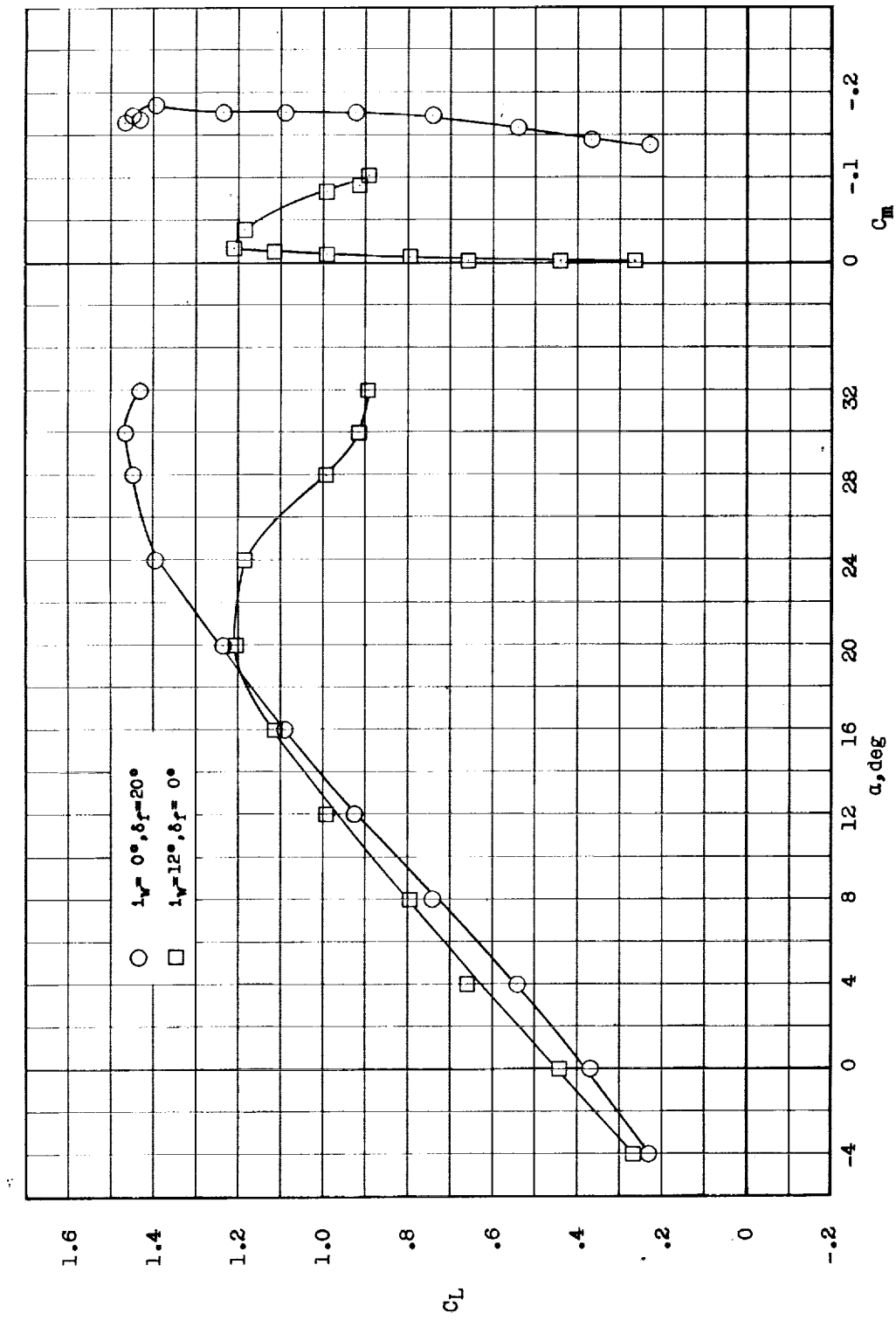

Figure 7.- Comparison of aerodynamic characteristics of wing-fuselage combination with full-span flaps deflected and with wing incidence. Center vertical tail on; canard surface off; center of gravity at 0.275$\bar{c}$.

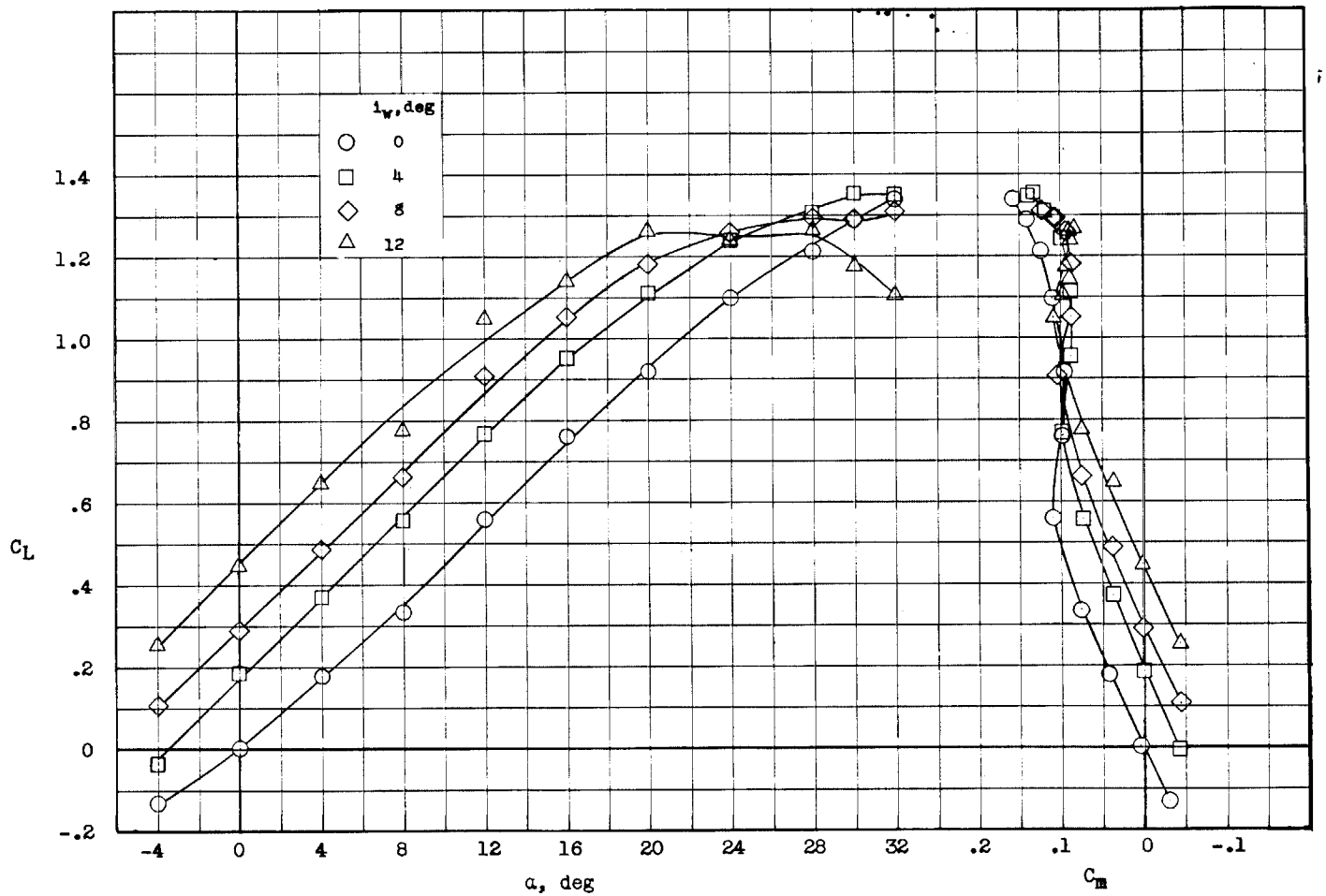

(a) Lift and pitching-moment coefficients.

Figure 8.- Longitudinal characteristics of model with center vertical tail and basic canard surface A. $i_t = 0^\circ$; $\delta_{f,t} = 0^\circ$; center of gravity at $0.275\bar{c}$.

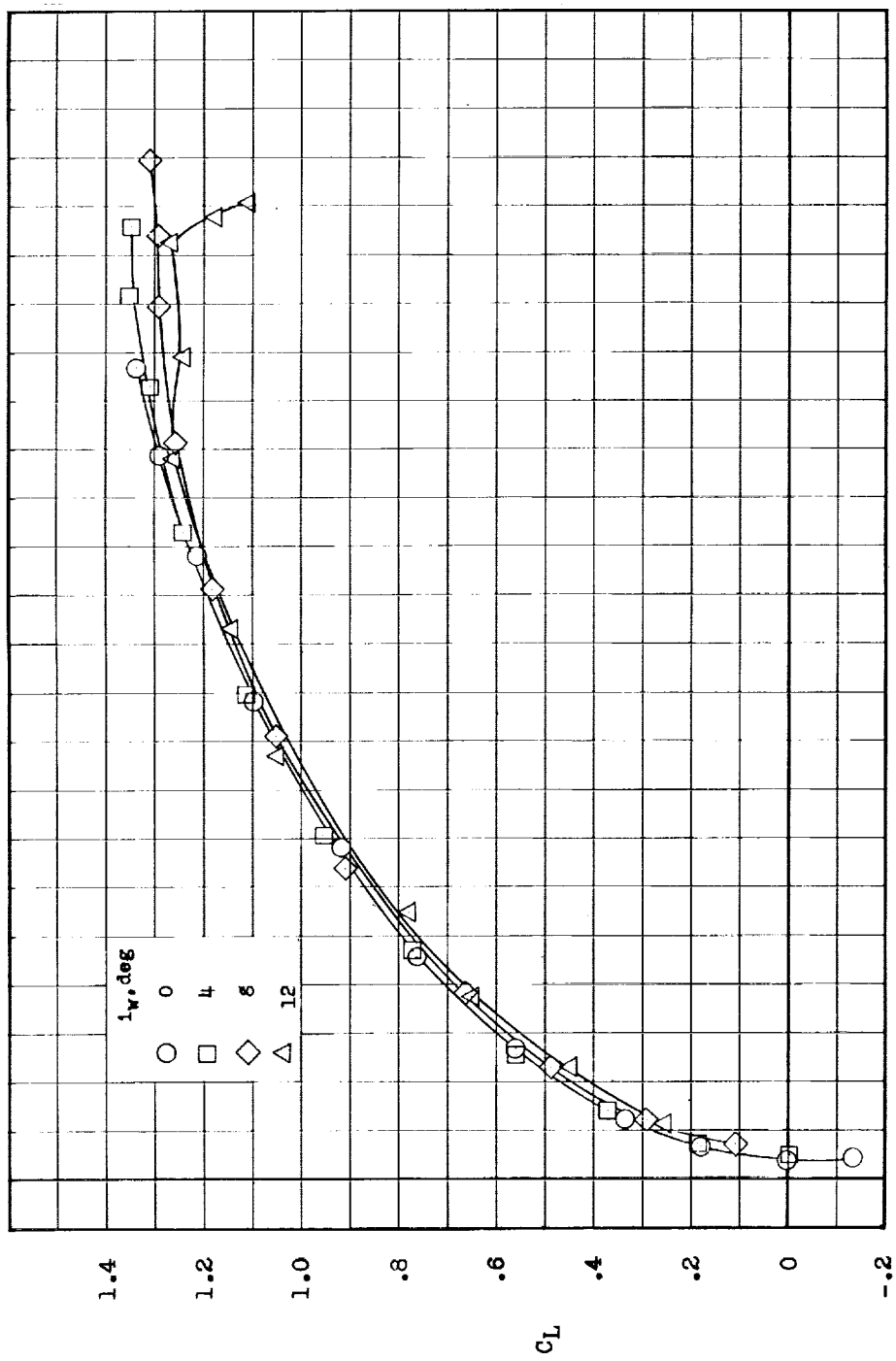

(b) Drag coefficient.

Figure 8.- Concluded.

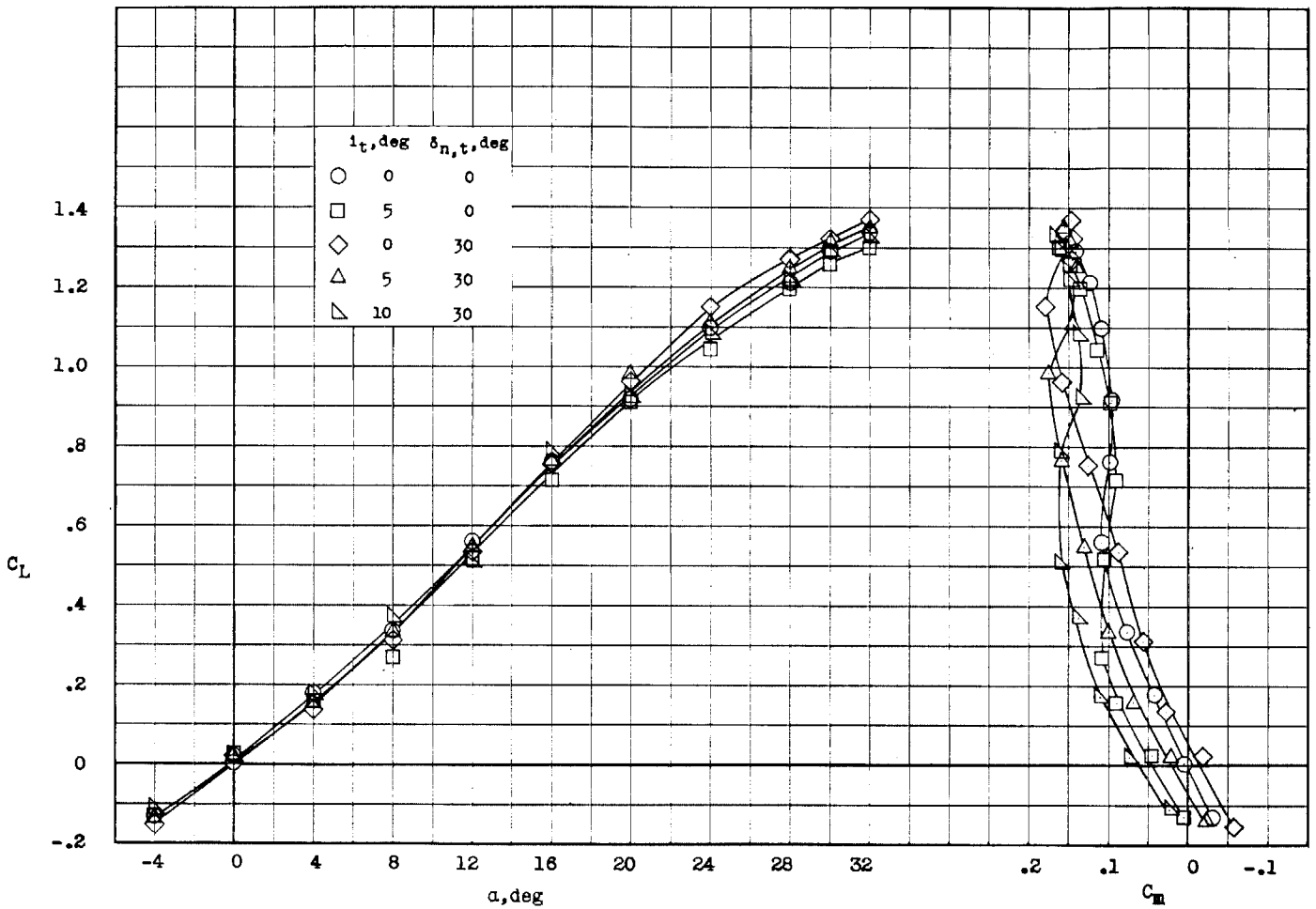

(a) Lift and pitching-moment coefficients.

Figure 9.- Longitudinal control characteristics of model with basic canard surface A. $i_w = 0^\circ$; $\delta_{f,t} = 0^\circ$; center of gravity at $0.275\bar{c}$.

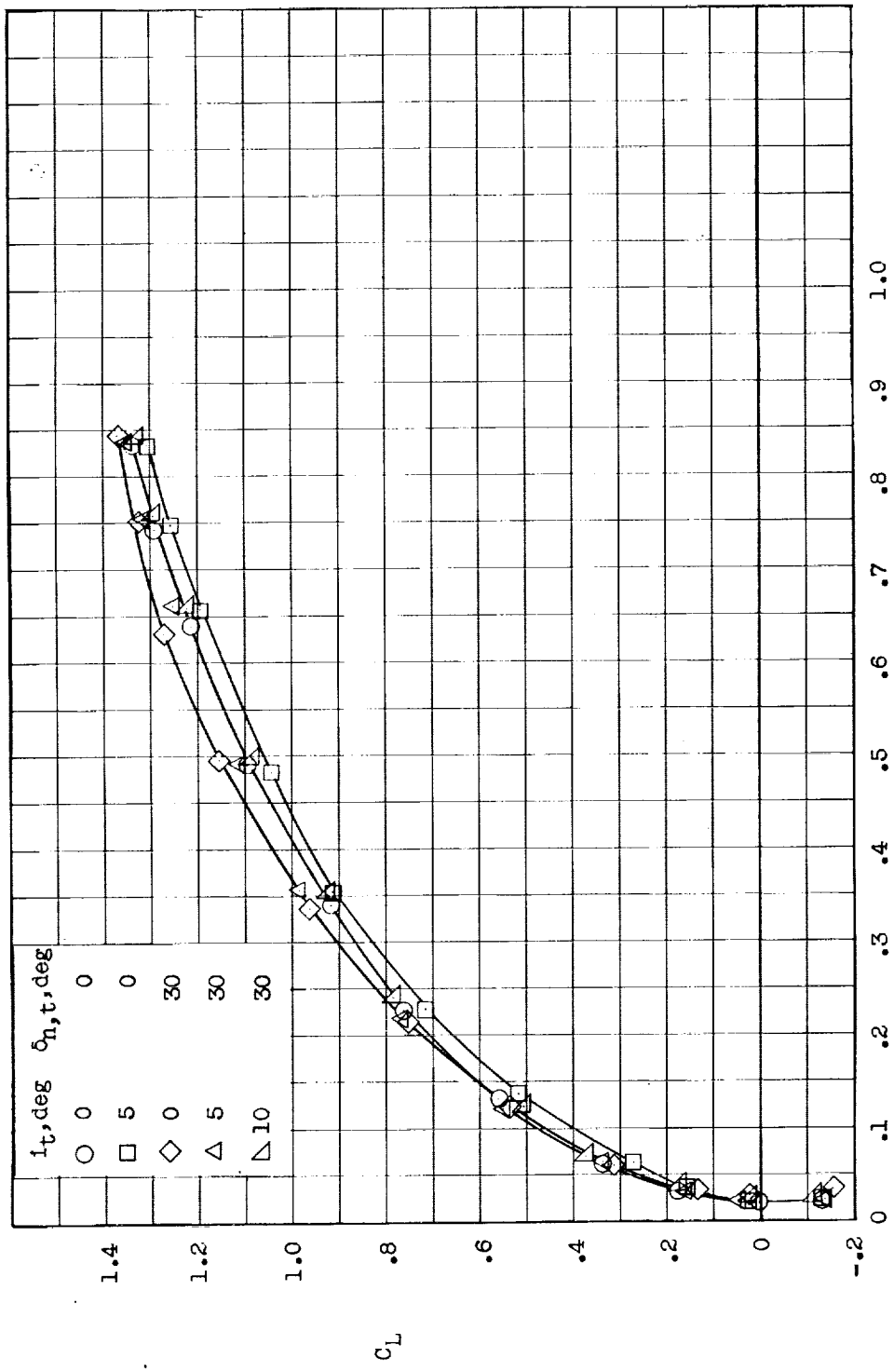

(b) Drag coefficient.

Figure 9.- Concluded.

L-468

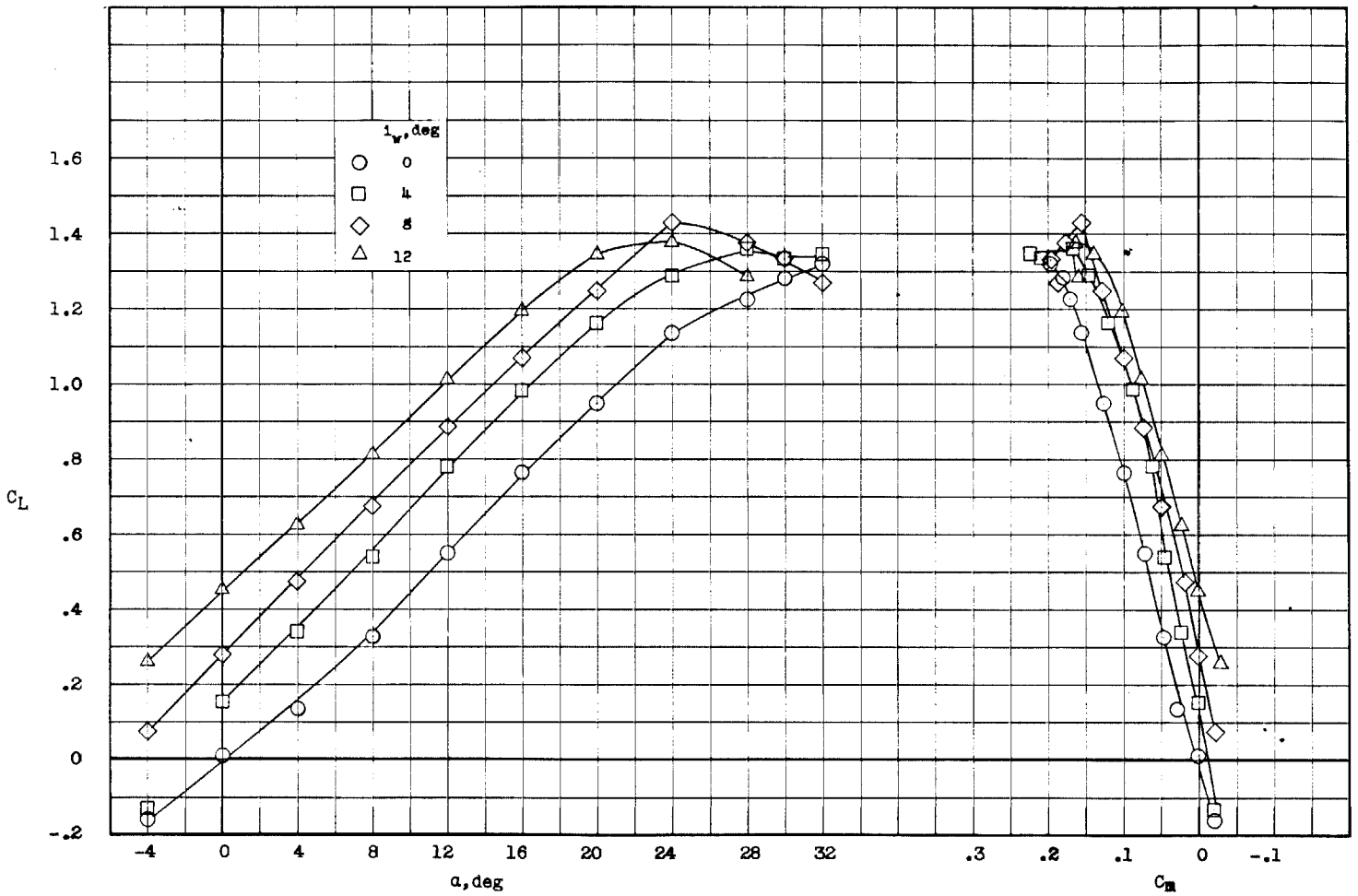

(a) Lift and pitching-moment coefficients.

Figure 10.- Longitudinal characteristics of model with center vertical tail and basic canard surface B. $i_t = 0^\circ$; $\delta_{f,t} = 0^\circ$; center of gravity at $0.275\bar{c}$.

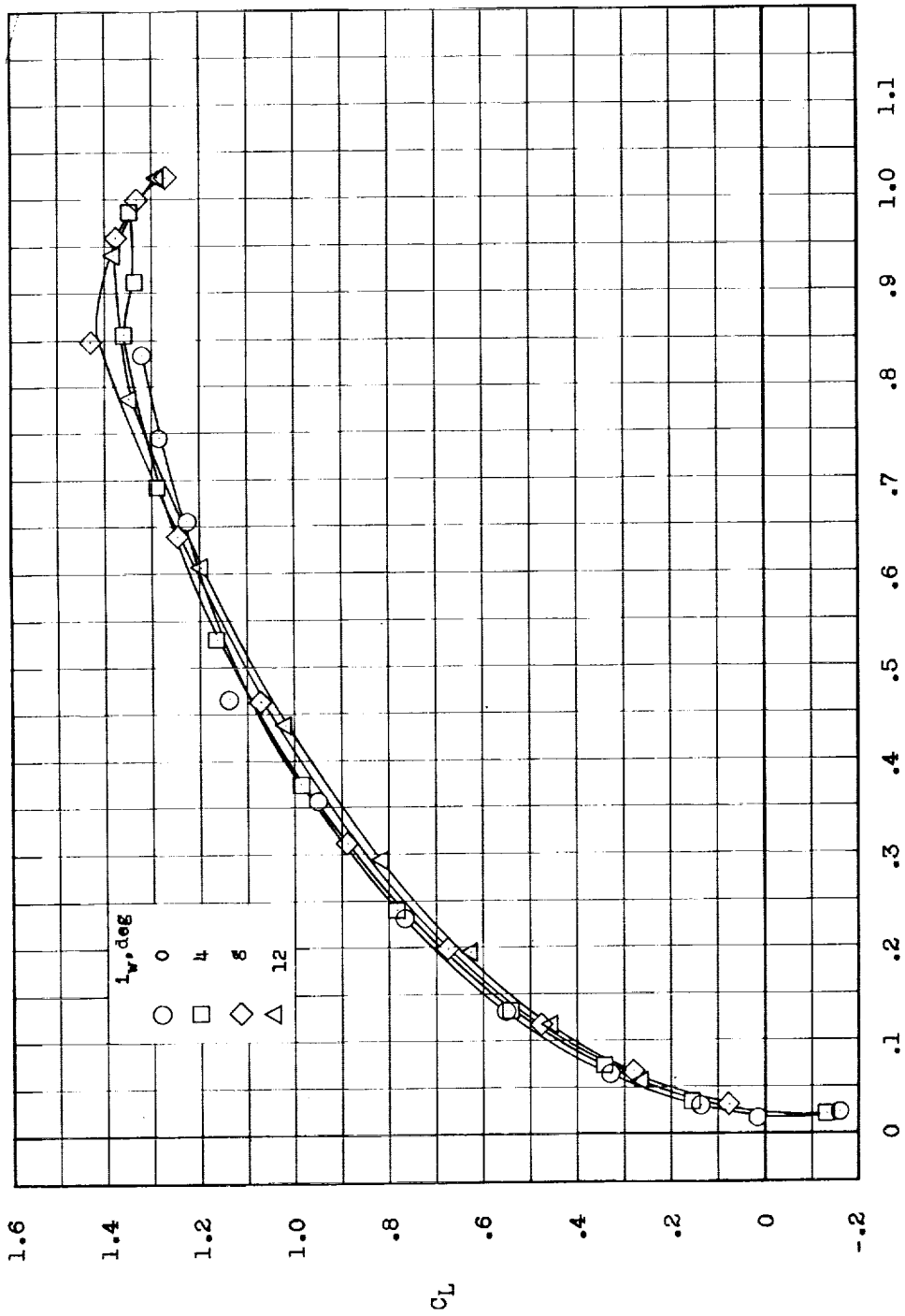

(b) Drag coefficient.

Figure 10.- Concluded.

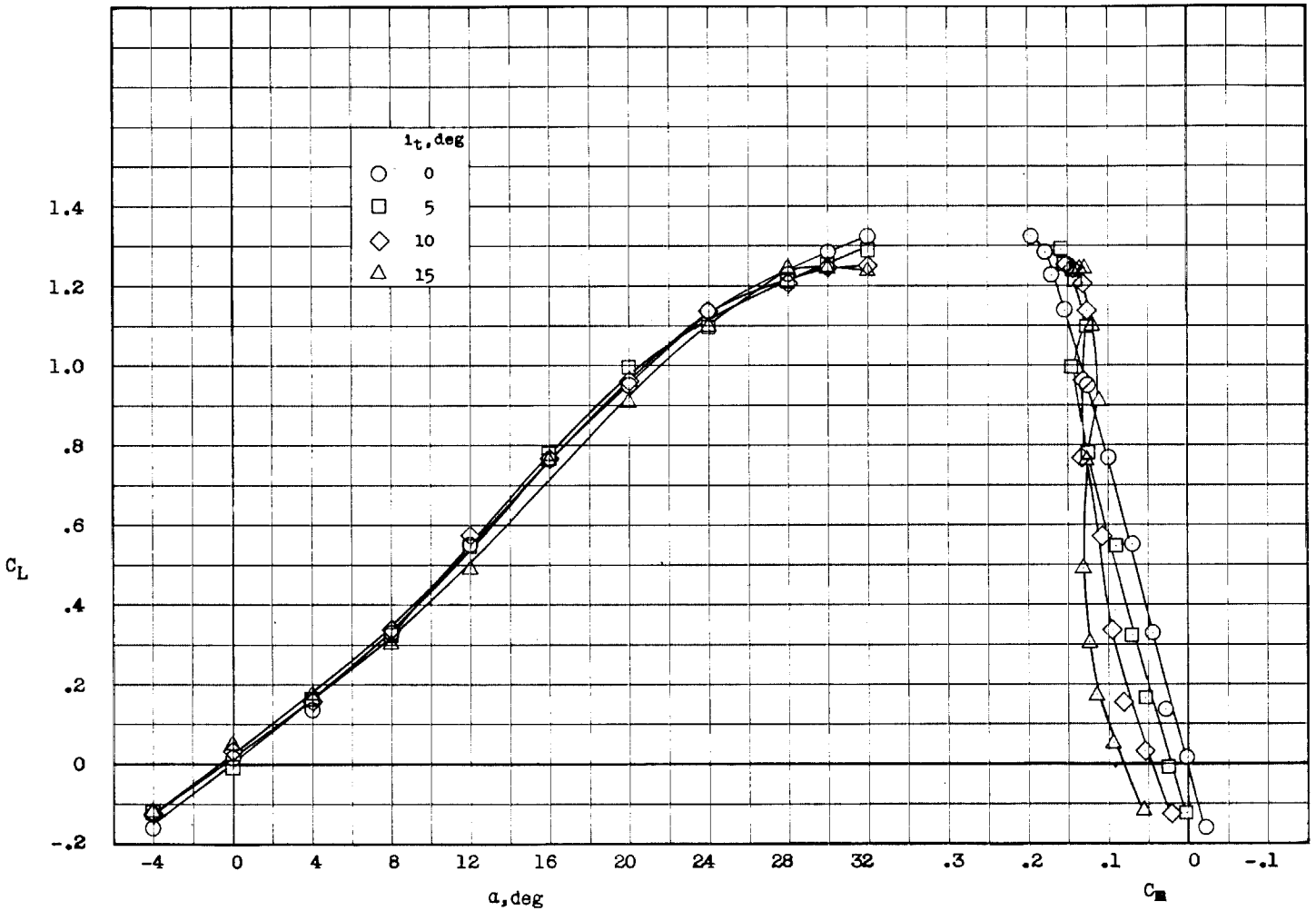

(a) Lift and pitching-moment coefficients.

Figure 11.- Longitudinal control characteristics of model with basic canard surface B. $i_w = 0^\circ$; $\delta_{f,t} = 0^\circ$; center of gravity at $0.275\bar{c}$.

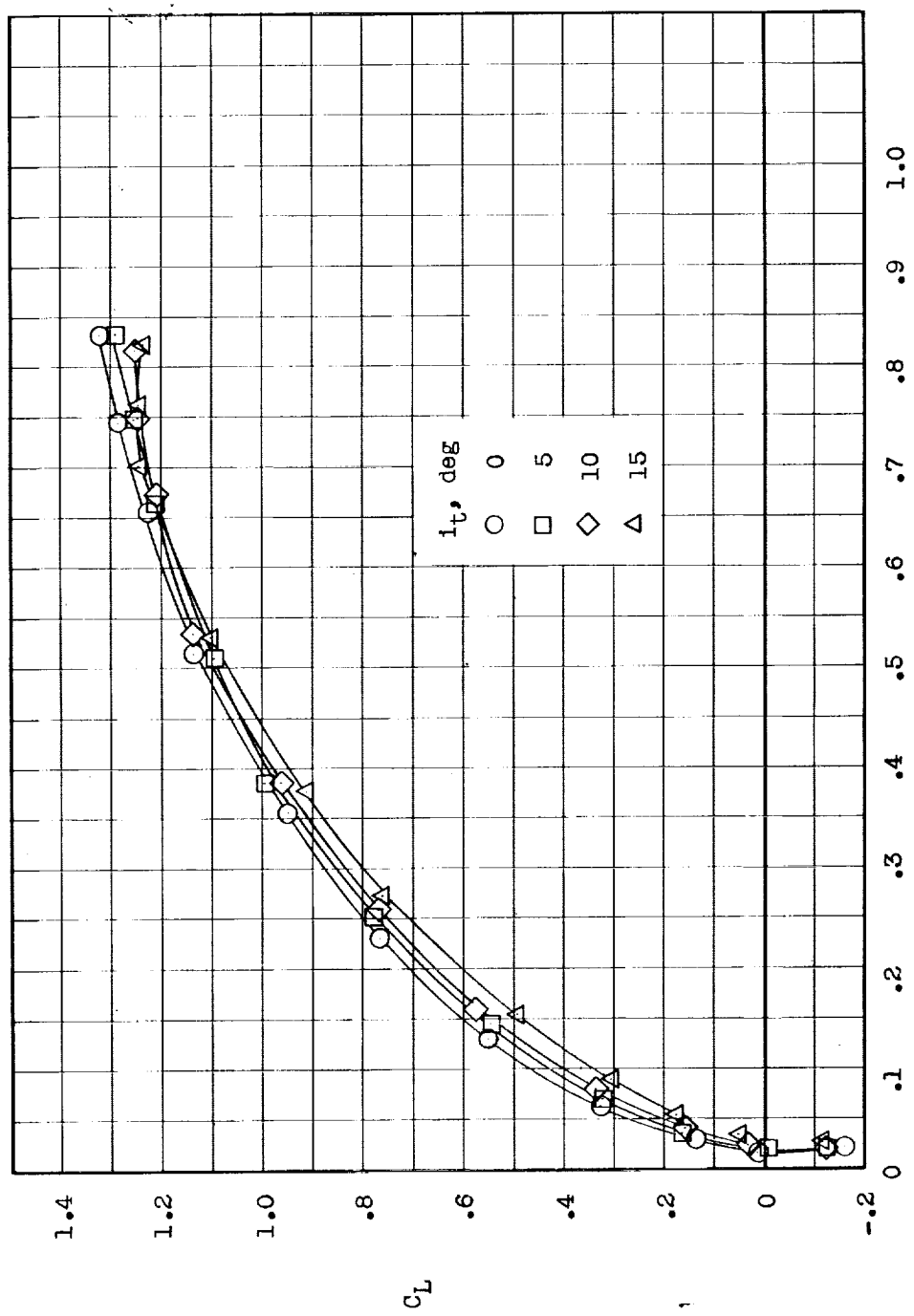

(b) Drag coefficient.

Figure 11.- Concluded.

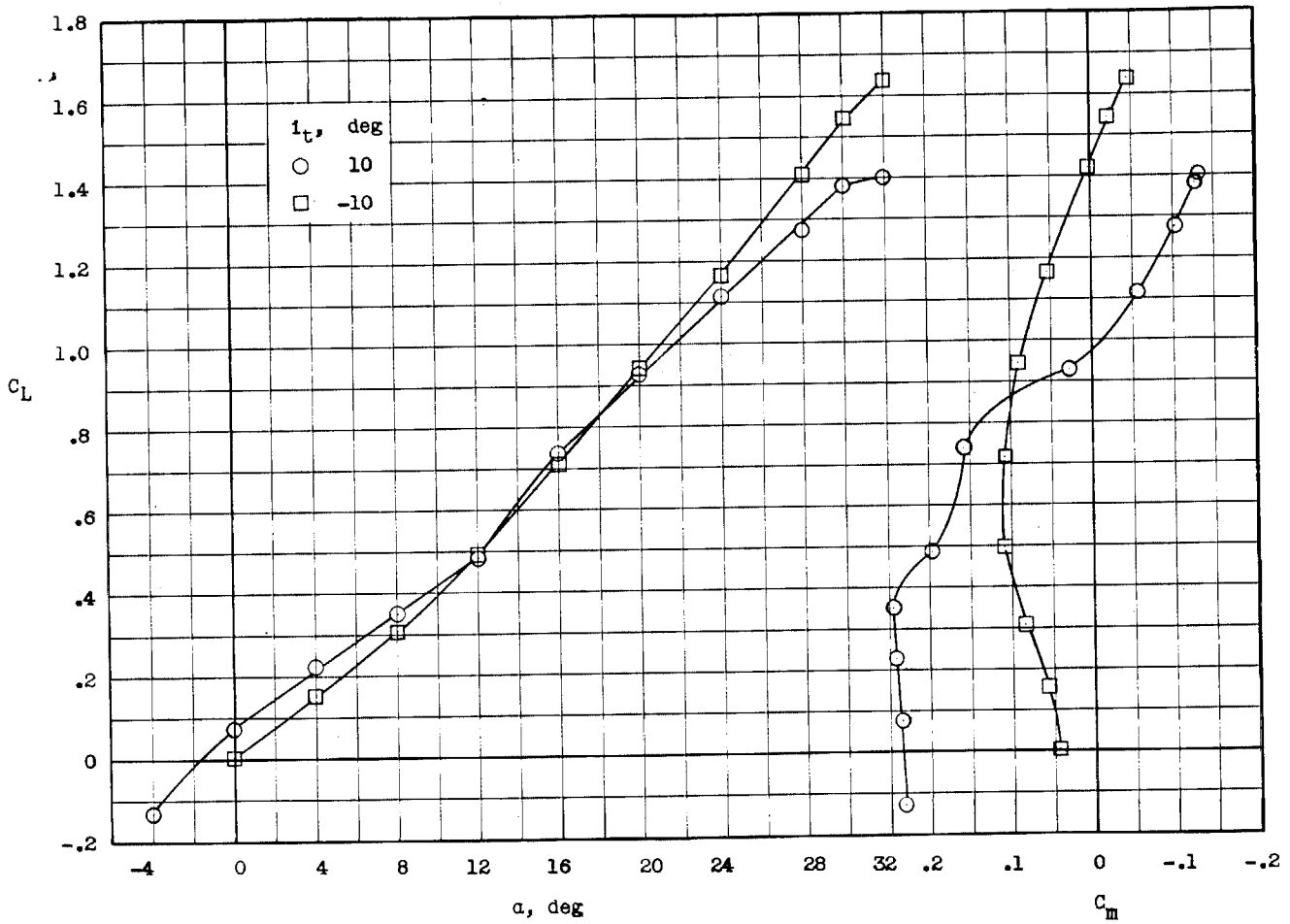

(a) $i_w = 0^\circ$.

Figure 12.- Longitudinal control characteristics of high-lift configuration of canard surface A. Leading-edge extension on; center of gravity at $0.05\bar{c}$.

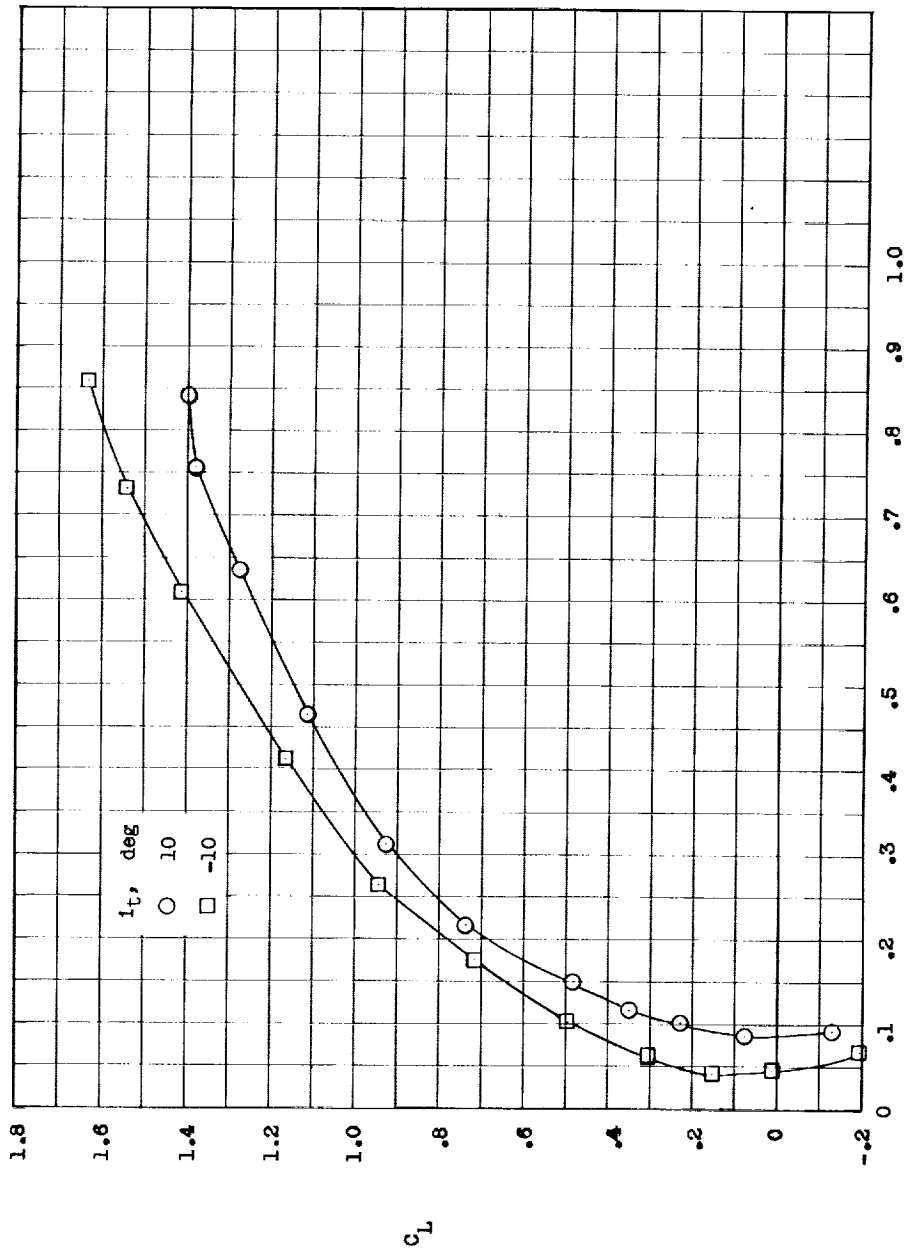

(a) $i_w = 0^o$. Concluded.

Figure 12.- Continued.

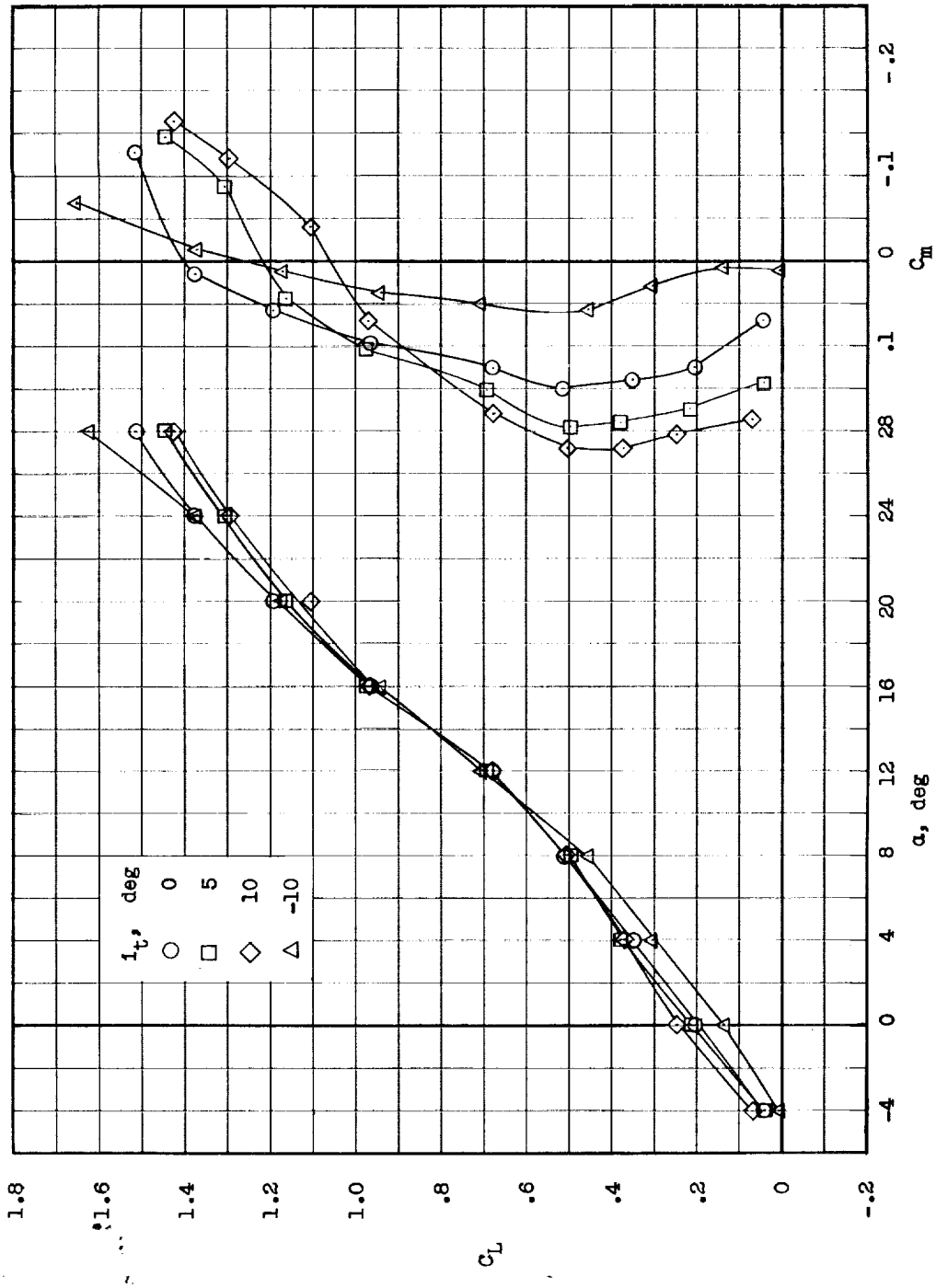

(b) $i_w = 4^\circ$.

Figure 12.- Continued.

L-400

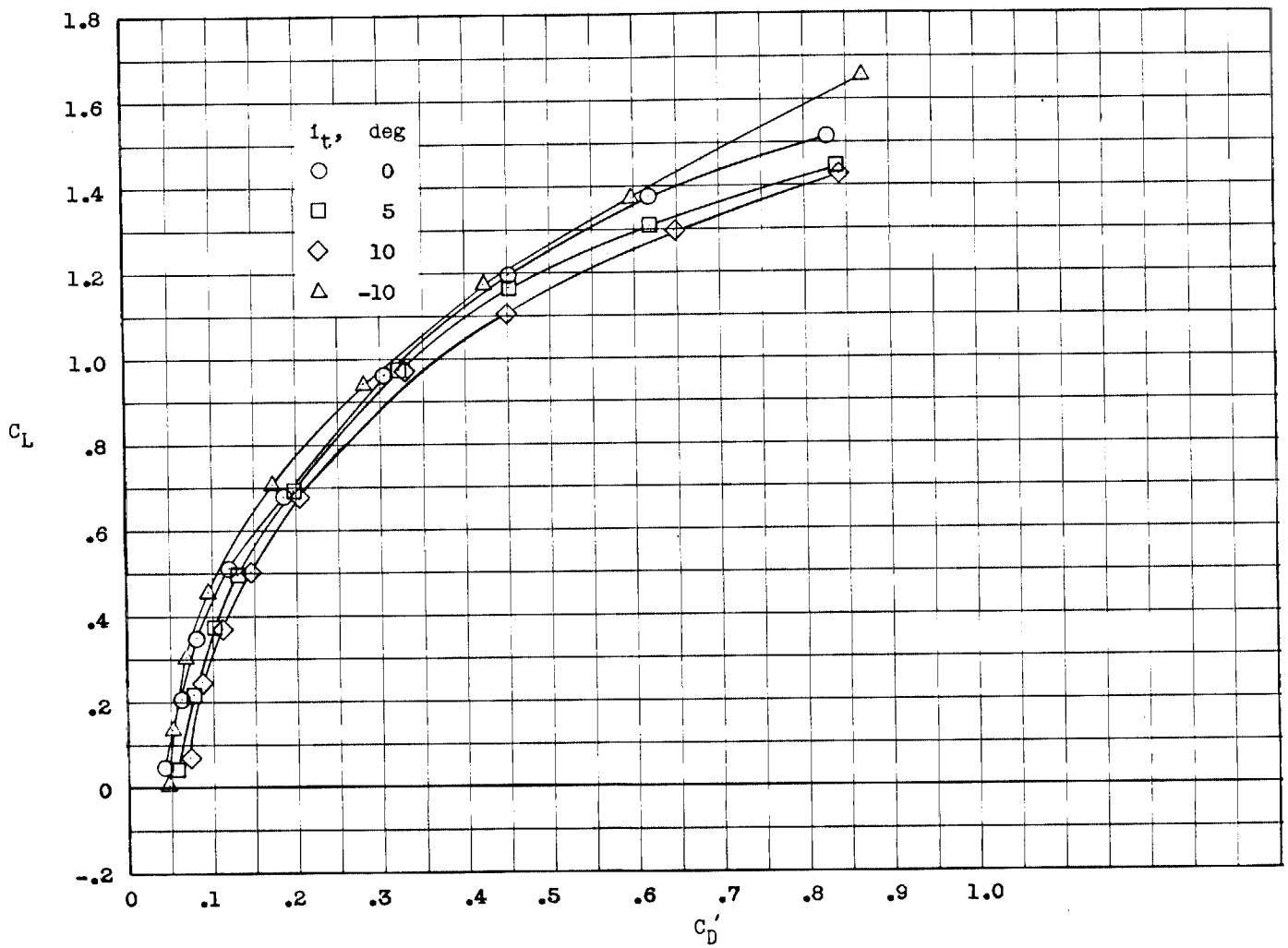

(b) $i_w = 4^\circ$. Concluded.

Figure 12.- Continued.

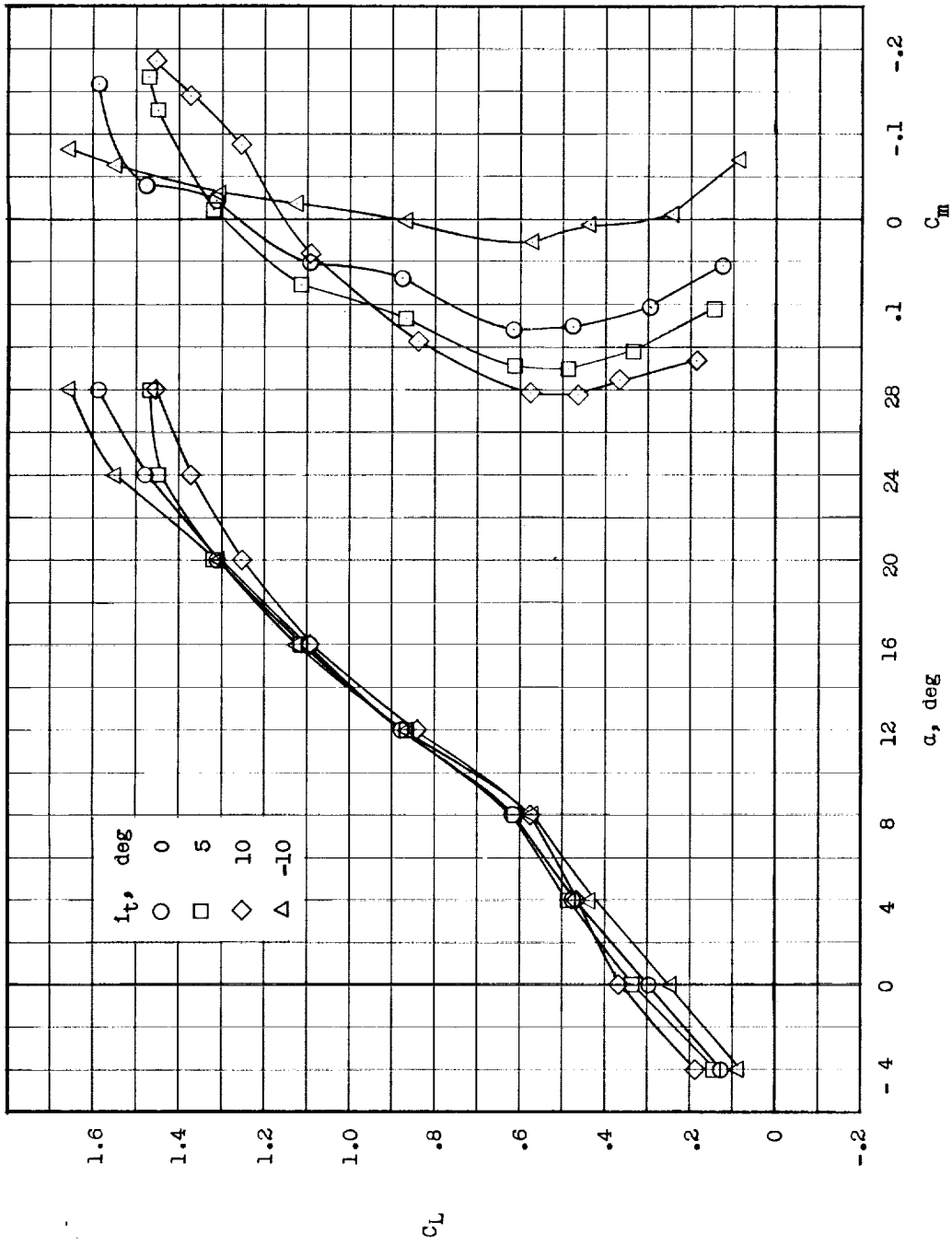

(c) $i_w = 8^o$.

Figure 12.- Continued.

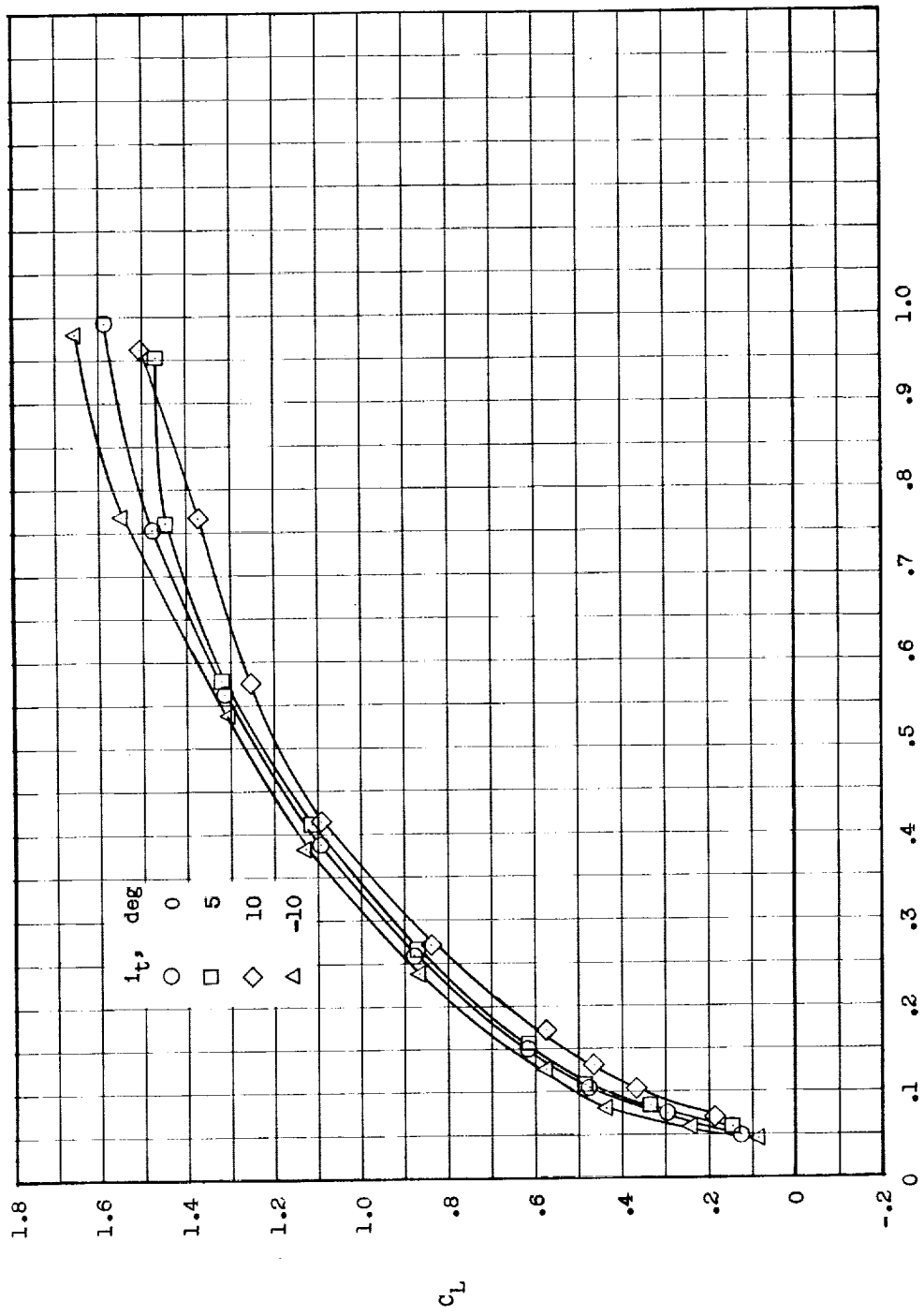

(c) $i_w = 8^o$. Concluded.

Figure 12.- Continued.

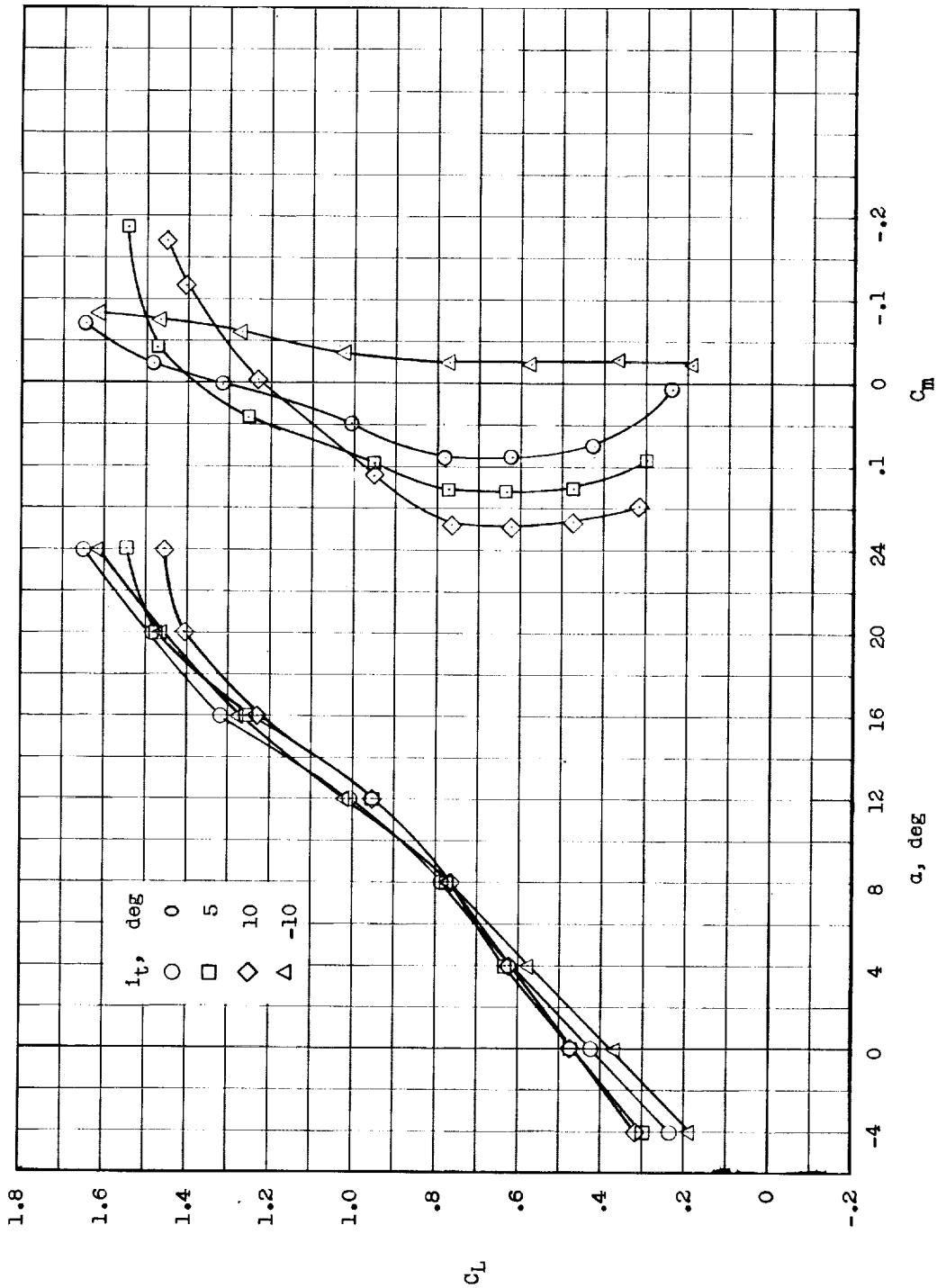

(d) $i_w = 12^\circ$.

Figure 12.- Continued.

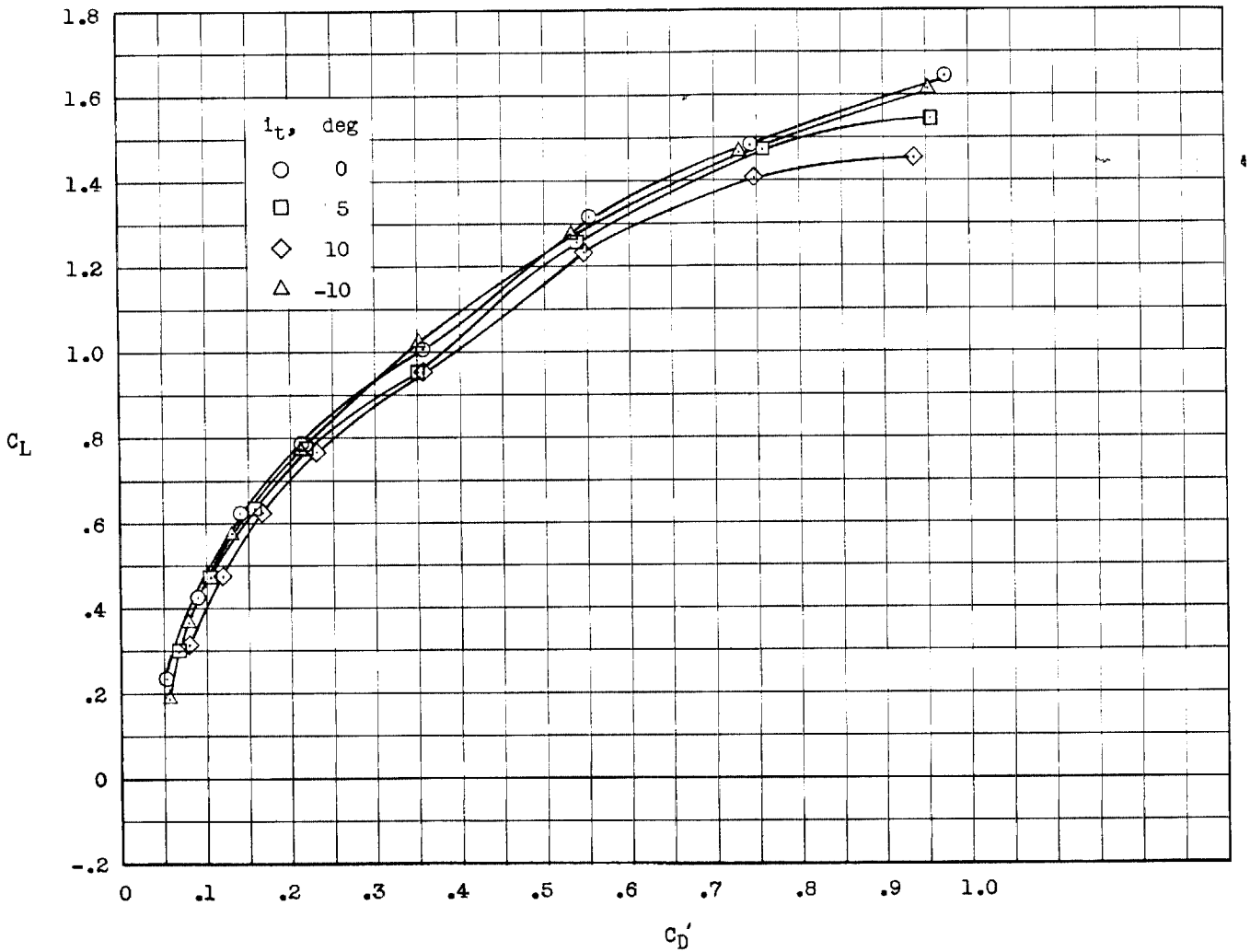

(d) $i_w = 12^o$. Concluded.

Figure 12.- Concluded.

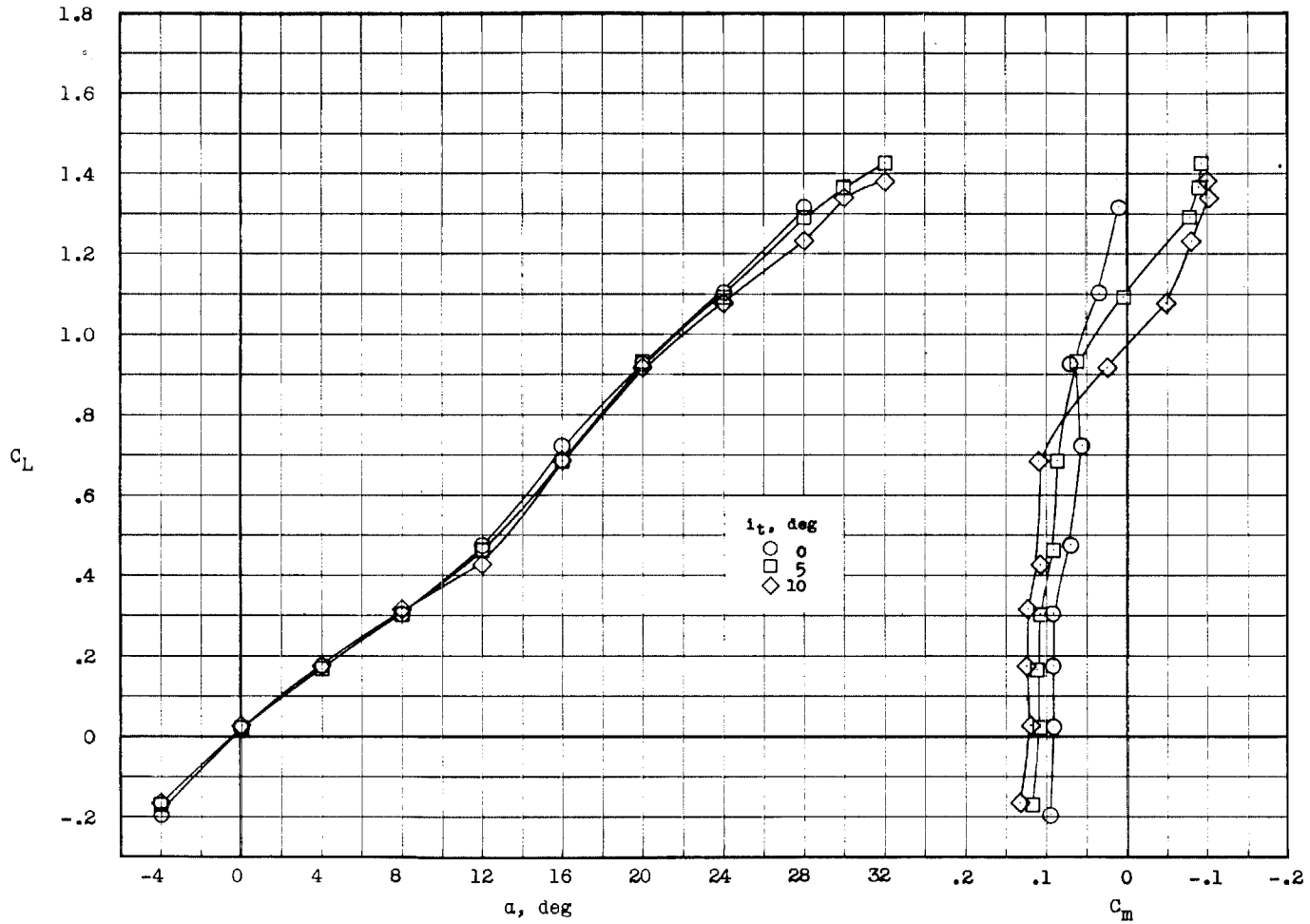

(a) $i_w = 0^\circ$.

Figure 13.- Longitudinal control characteristics of high-lift configuration of canard surface B. Leading-edge extension on; center of gravity at 0.09$\bar{c}$.

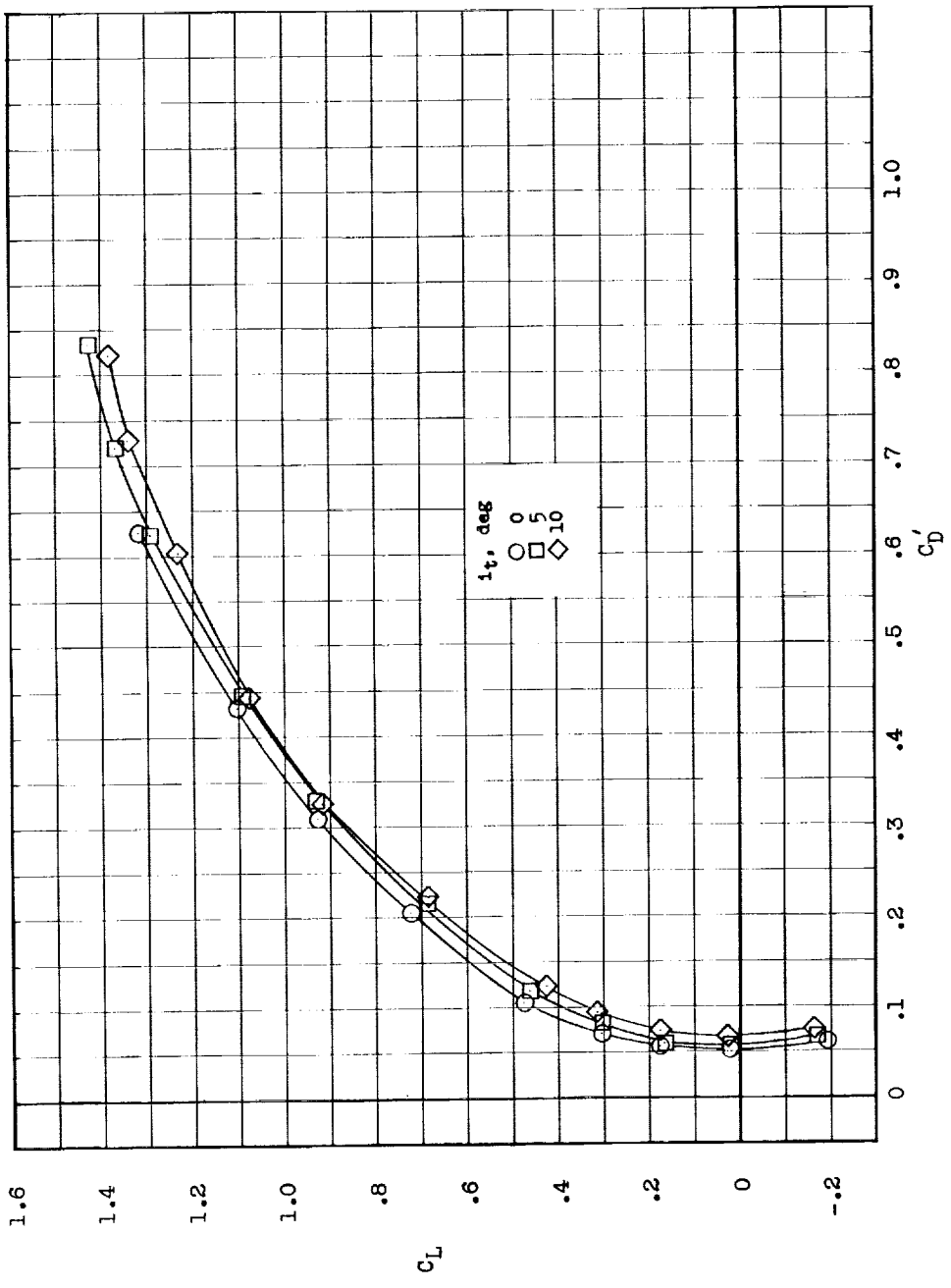

(a) $i_w = 0^o$. Concluded.

Figure 13.- Continued.

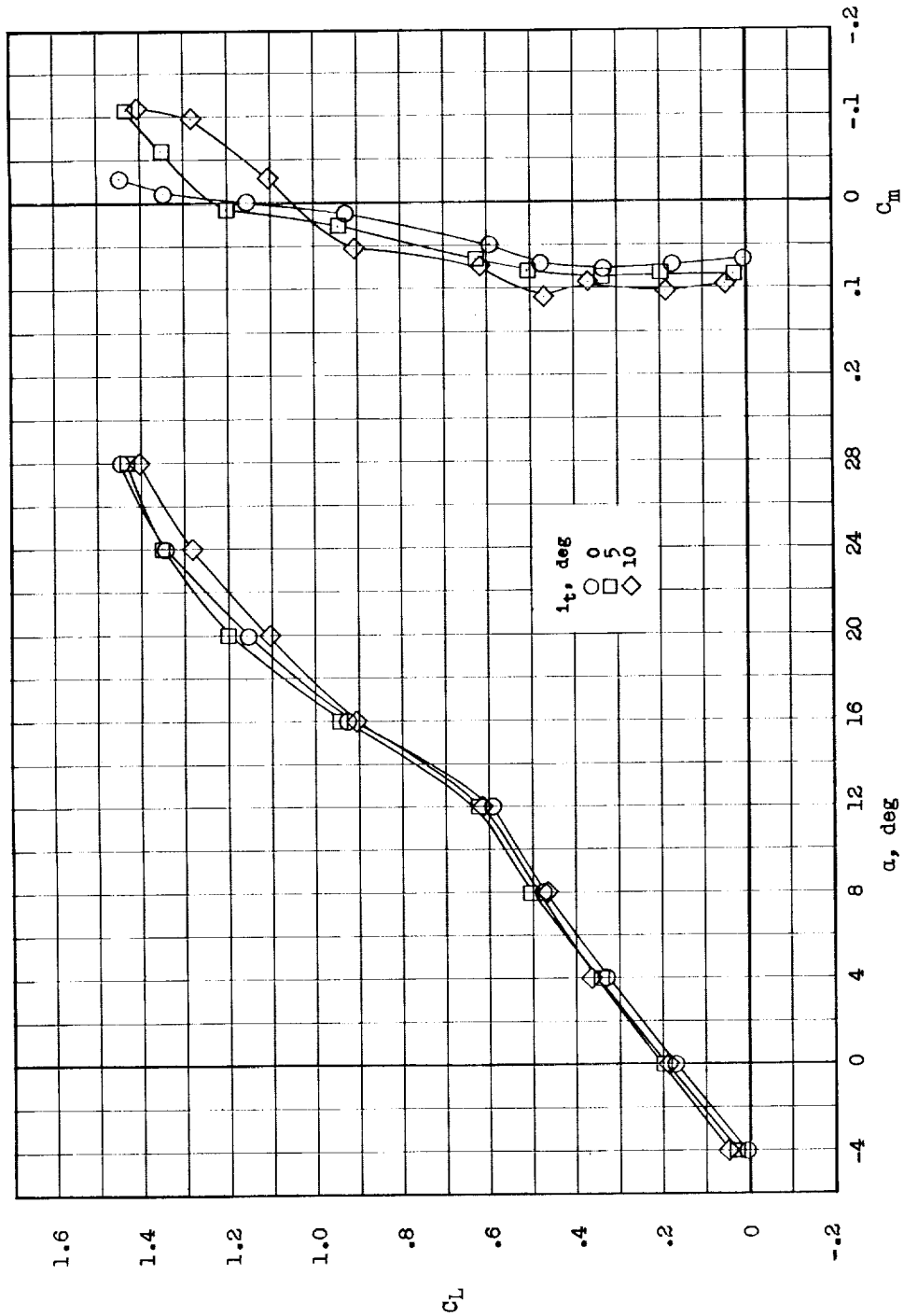

(b) $i_w = 4^\circ$.

Figure 13.- Continued.

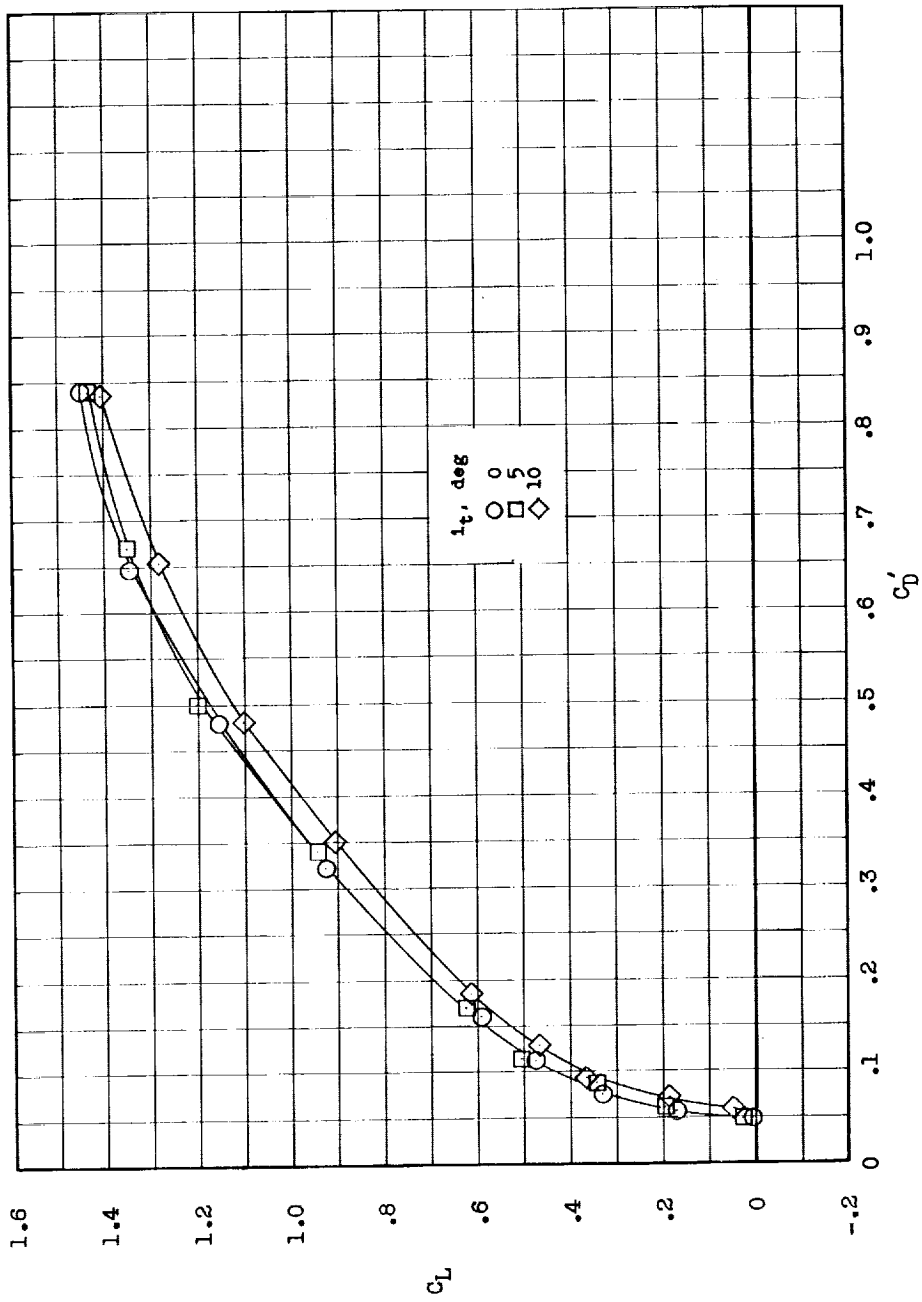

(b) $i_w = 4^o$. Concluded.

Figure 13.- Continued.

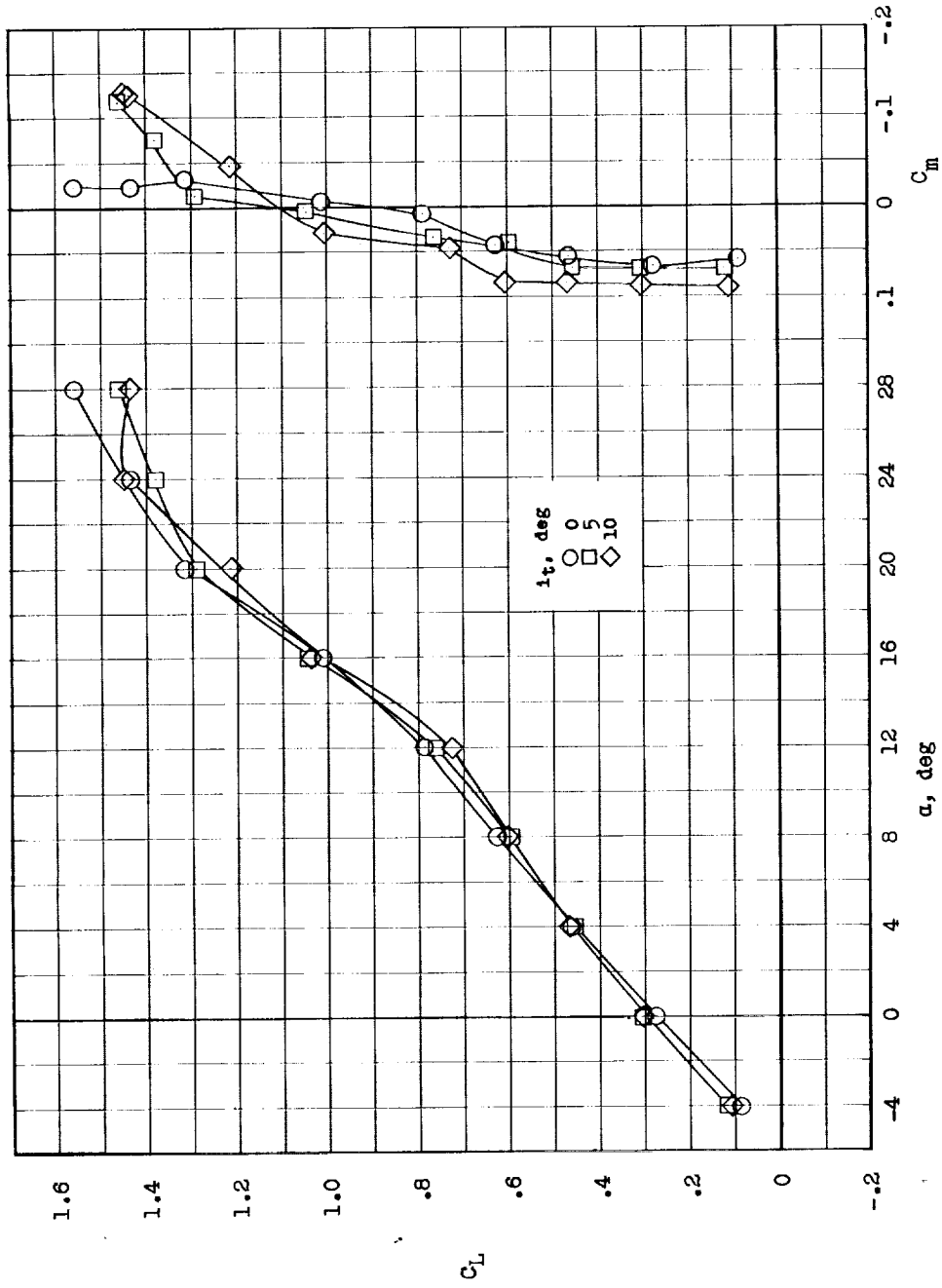

(c) $i_w = 8^o$.

Figure 13.- Continued.

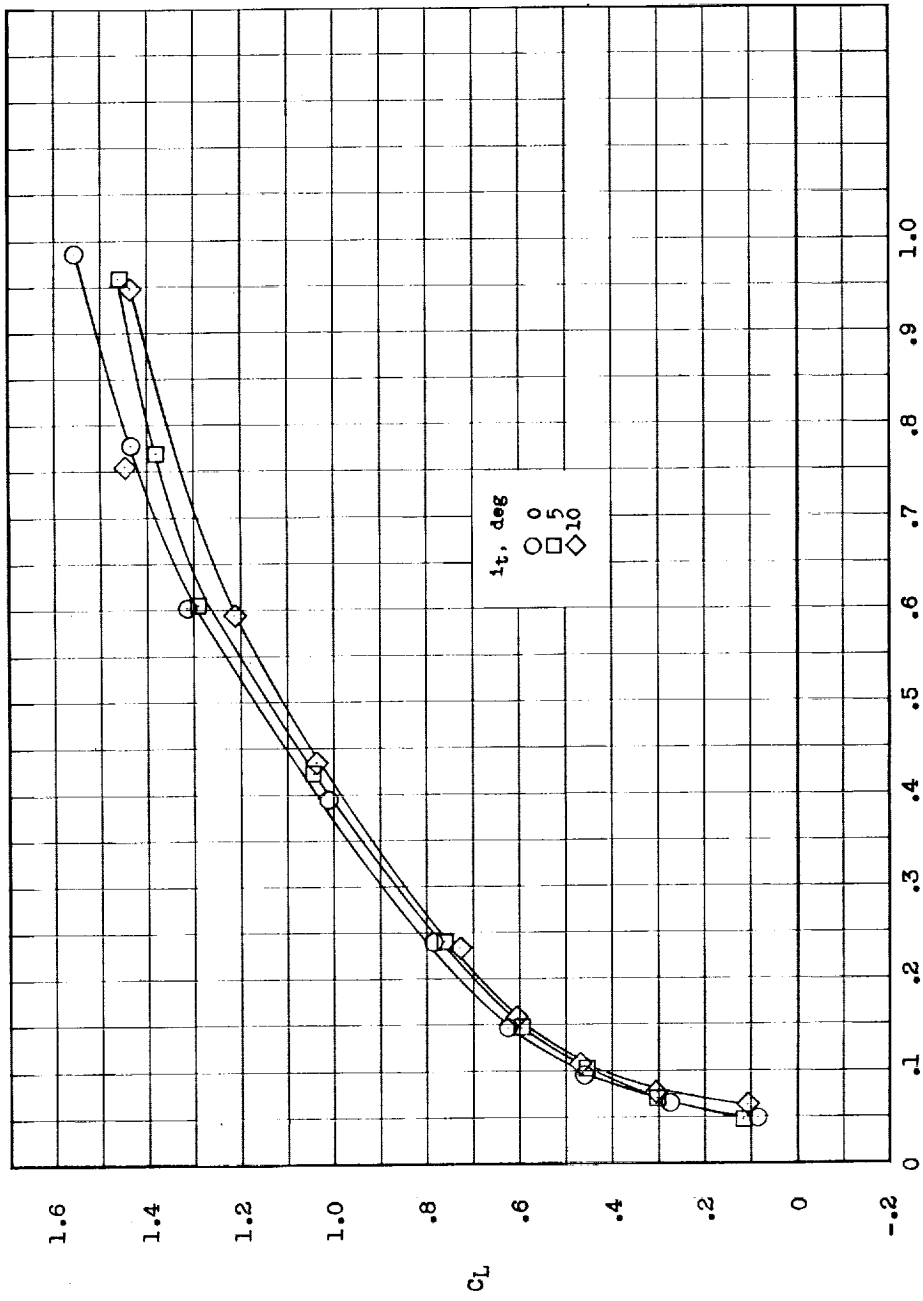

(c) $i_w = 8^\circ$. Concluded.

Figure 13.- Continued.

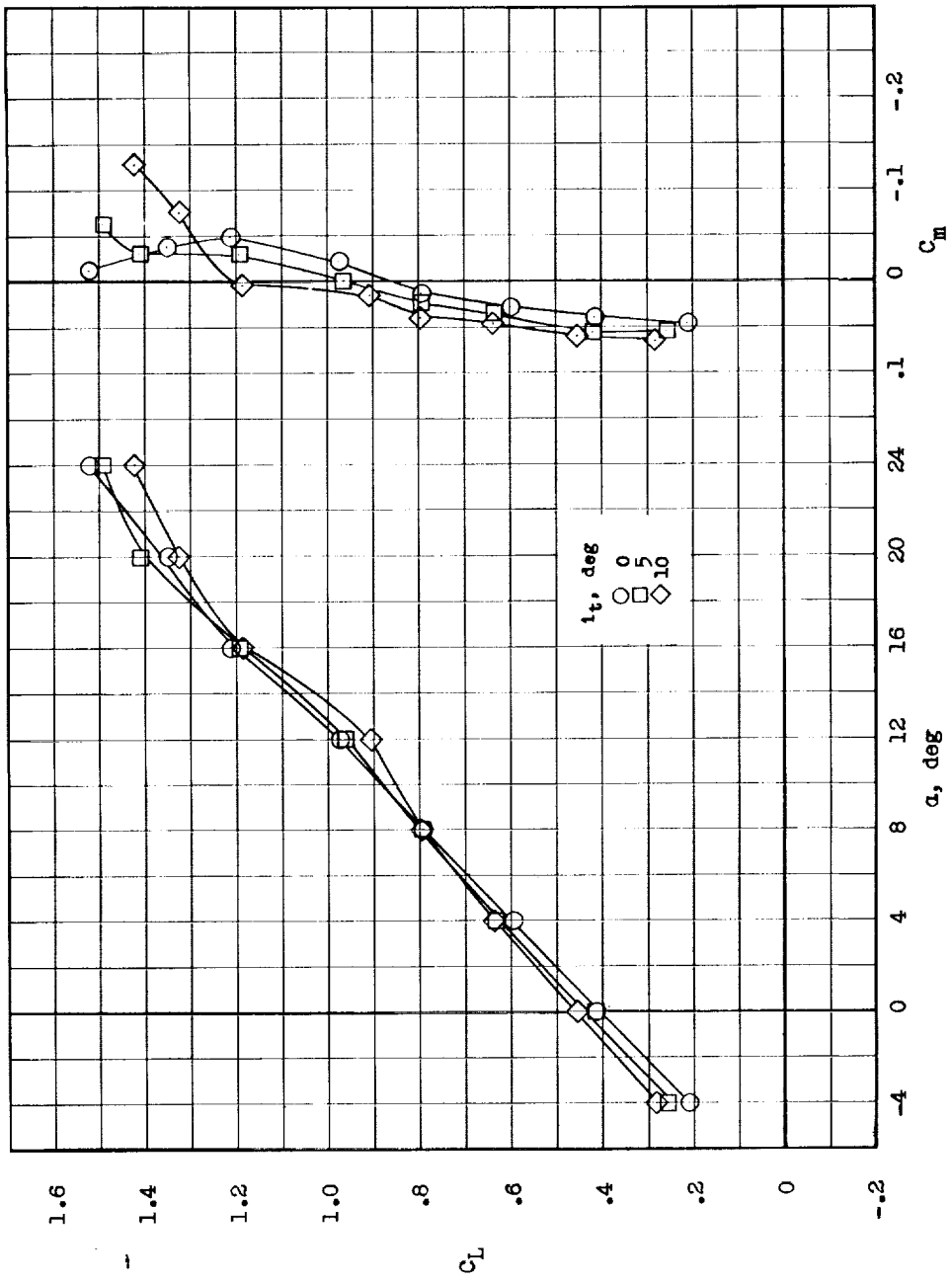

L-468

(d) $i_w = 12^o$.

Figure 13.- Continued.

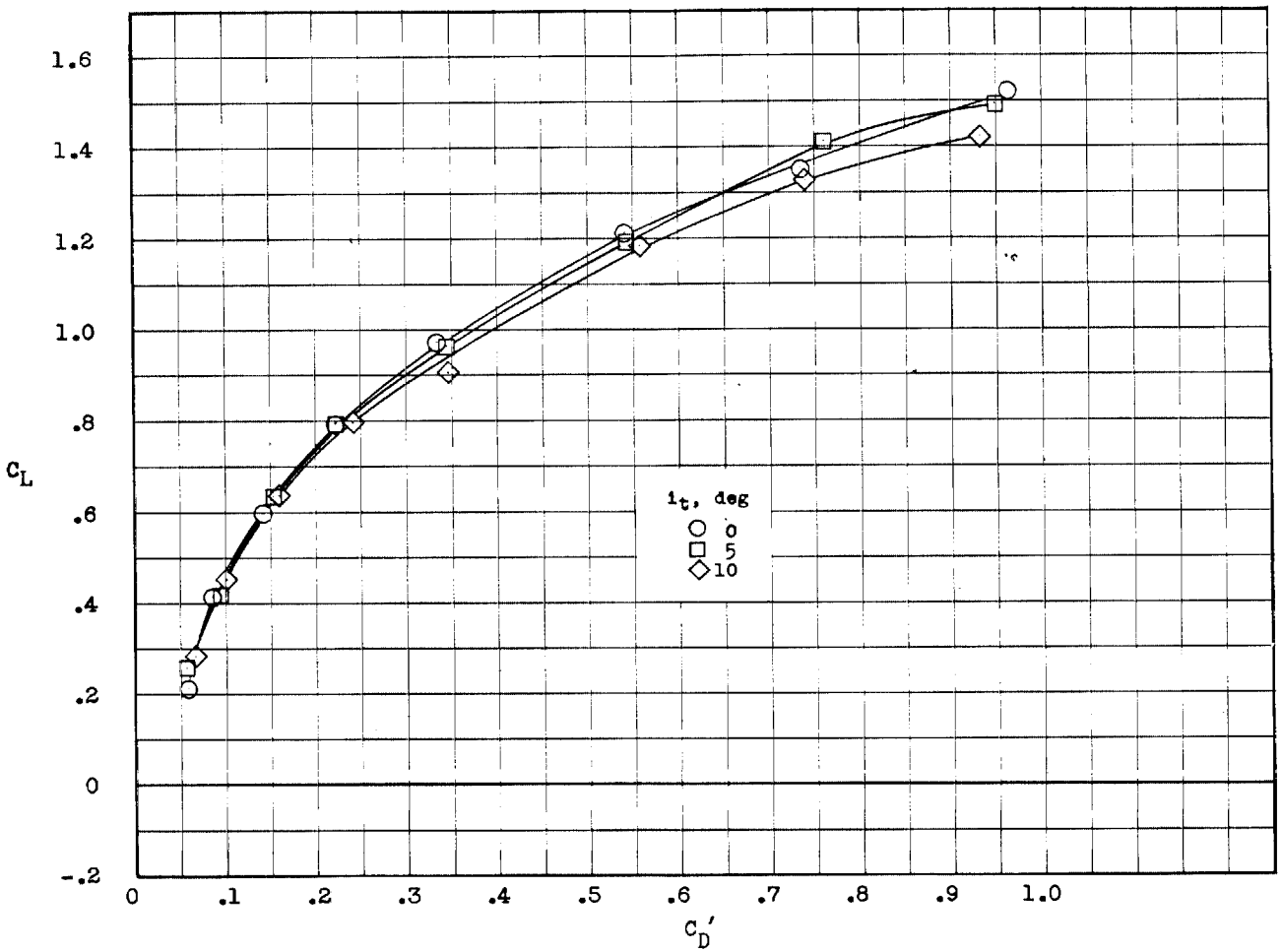

(d) $i_w = 12^\circ$. Concluded.

Figure 13.- Concluded.

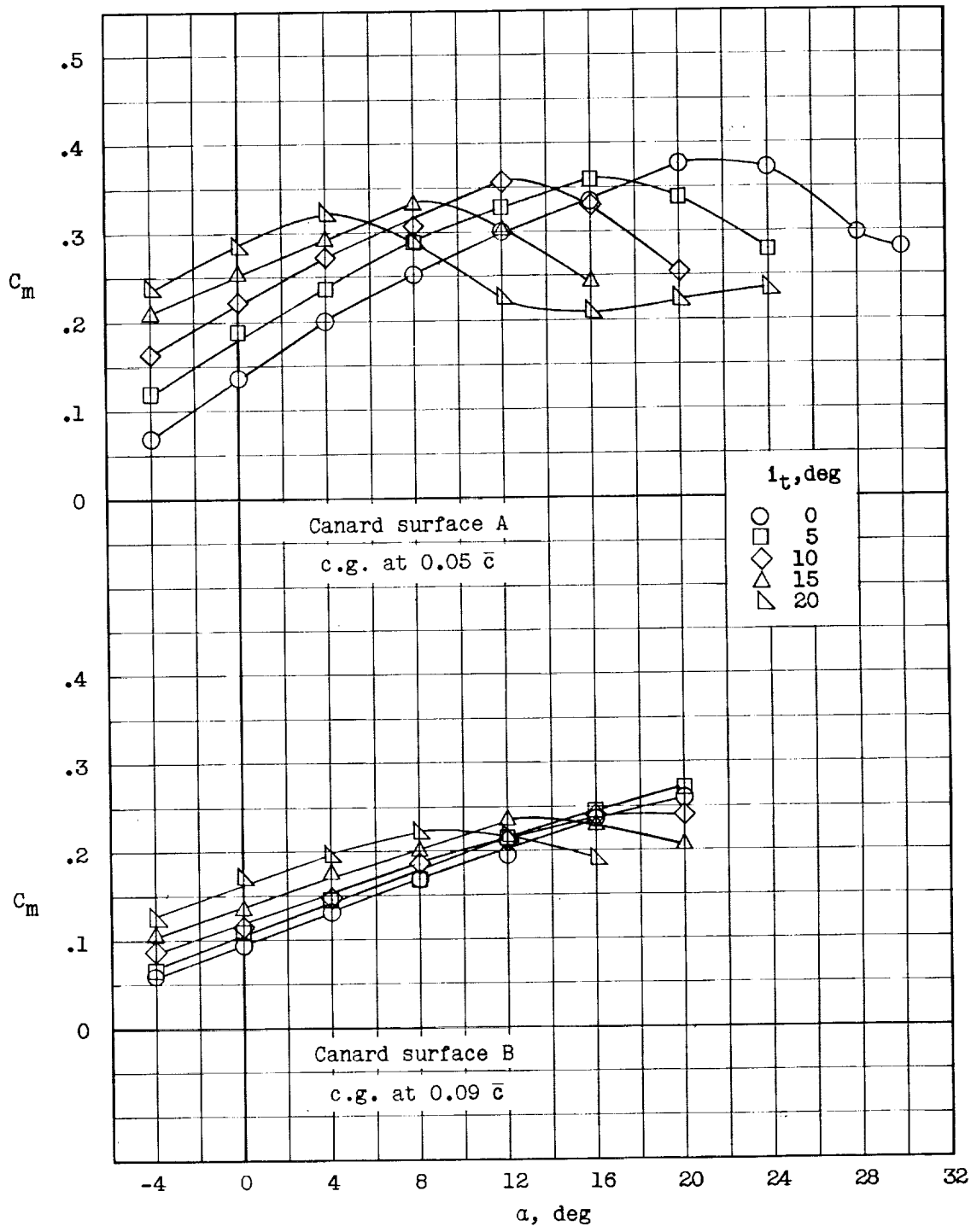

Figure 14.- Moment-producing capability of high-lift canard-surface fuselage combination, wing removed.

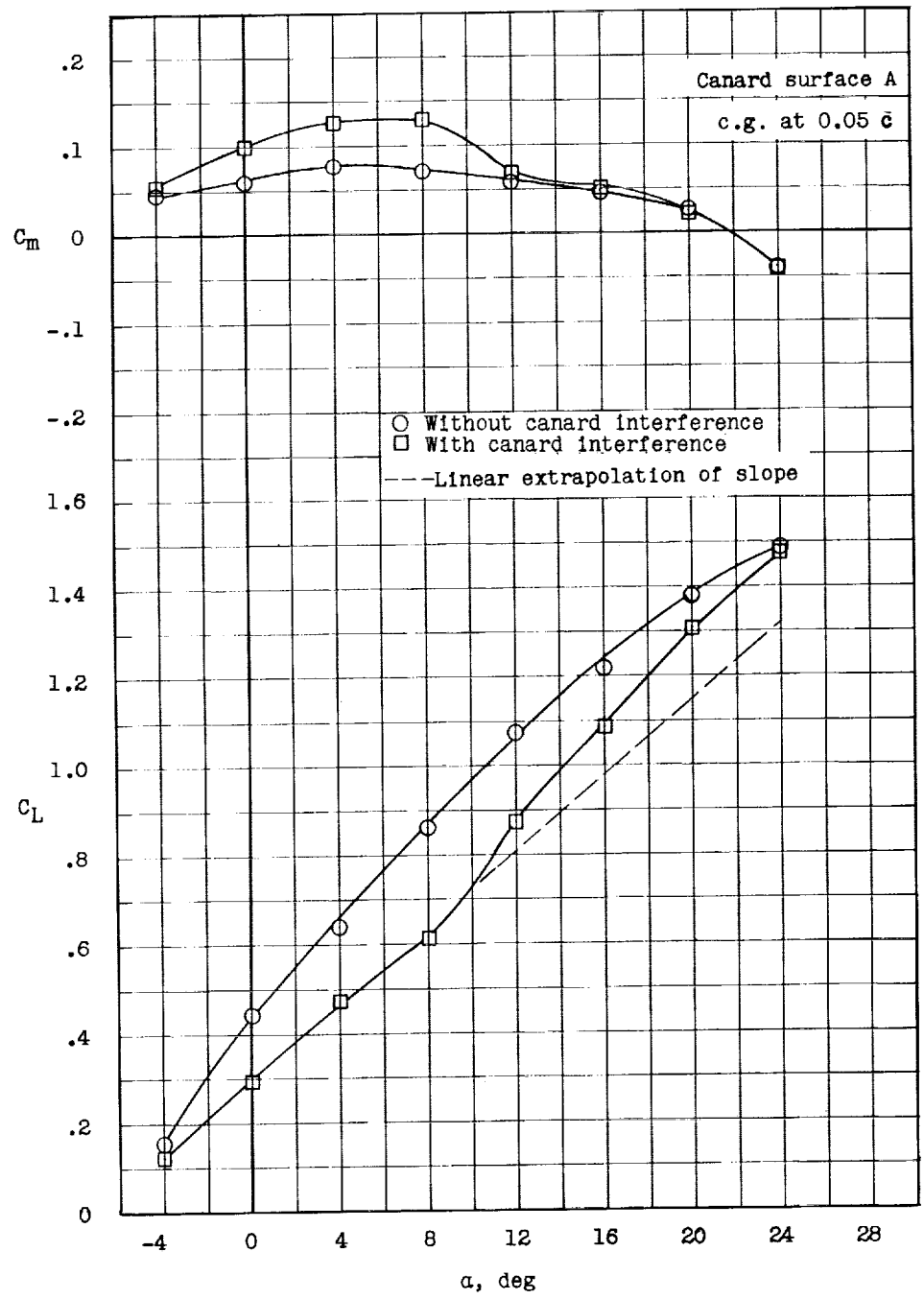

(a) $i_w = 8^o$; $i_t = 0^o$.

Figure 15.- Effect of high-lift canard-surface flow field on lift and pitching moment of model. Center vertical tail; leading-edge extension on complete configuration.

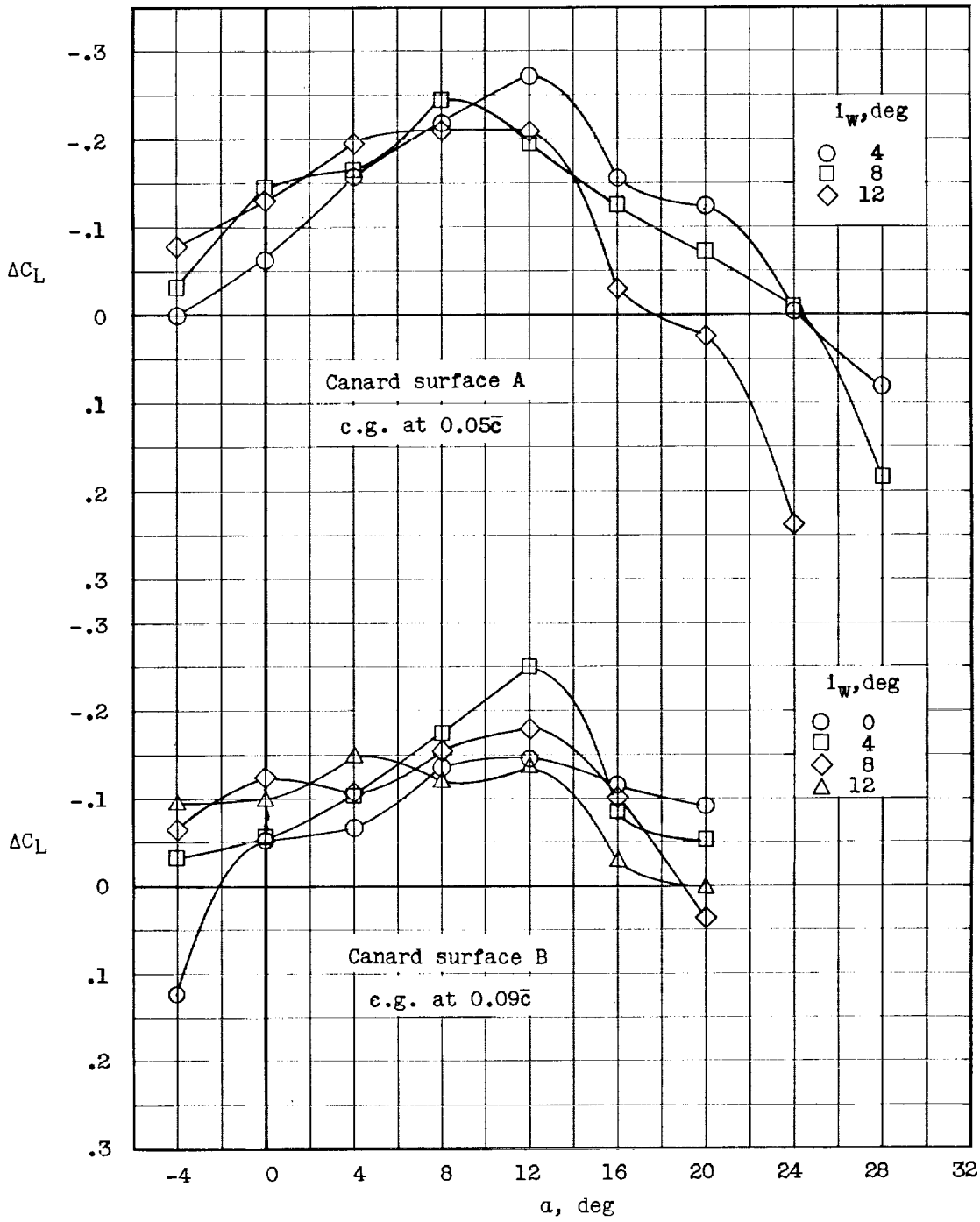

(b) Lift effect.

Figure 15.- Continued.

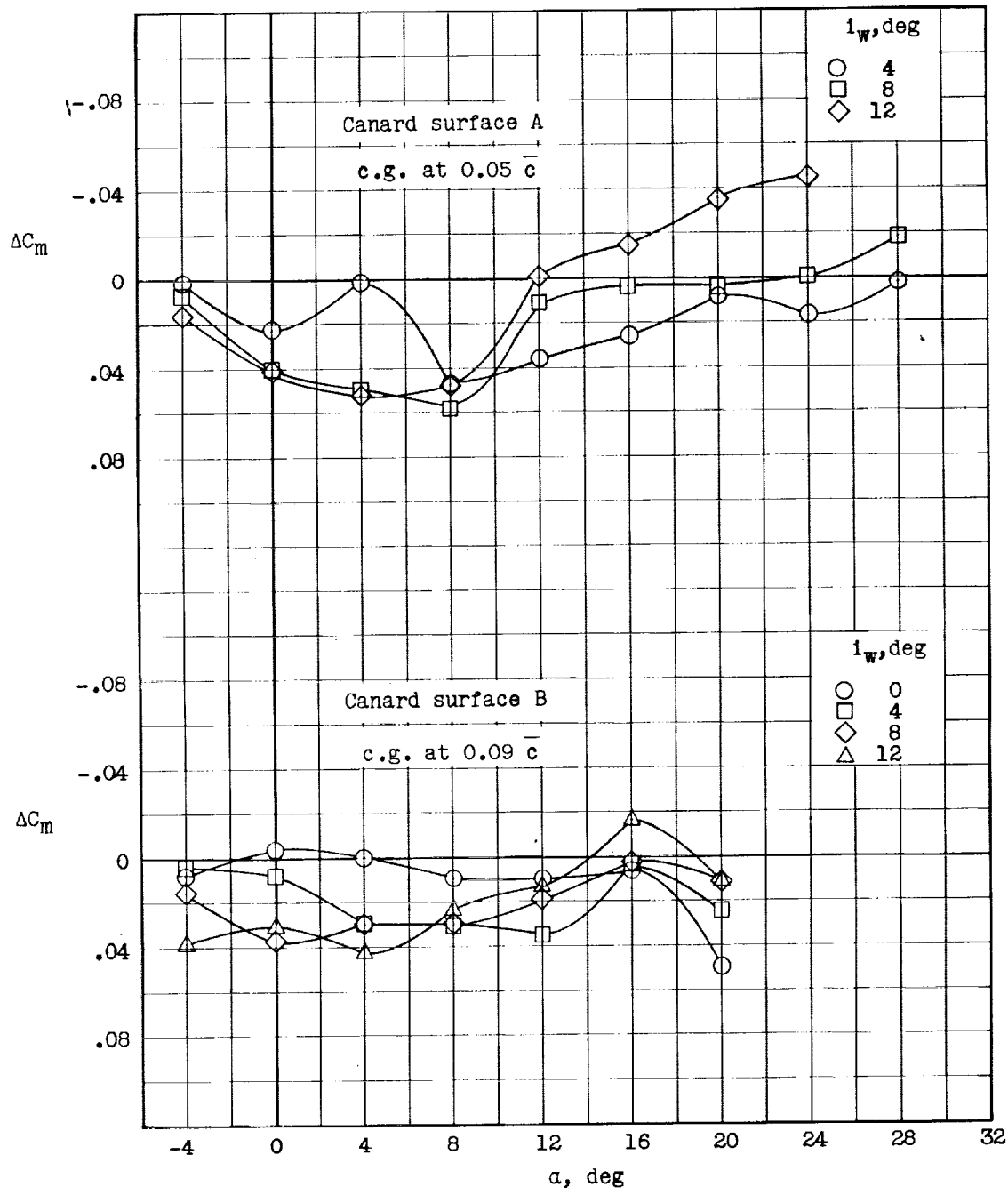

(c) Pitching-moment effect.

Figure 15.- Concluded.

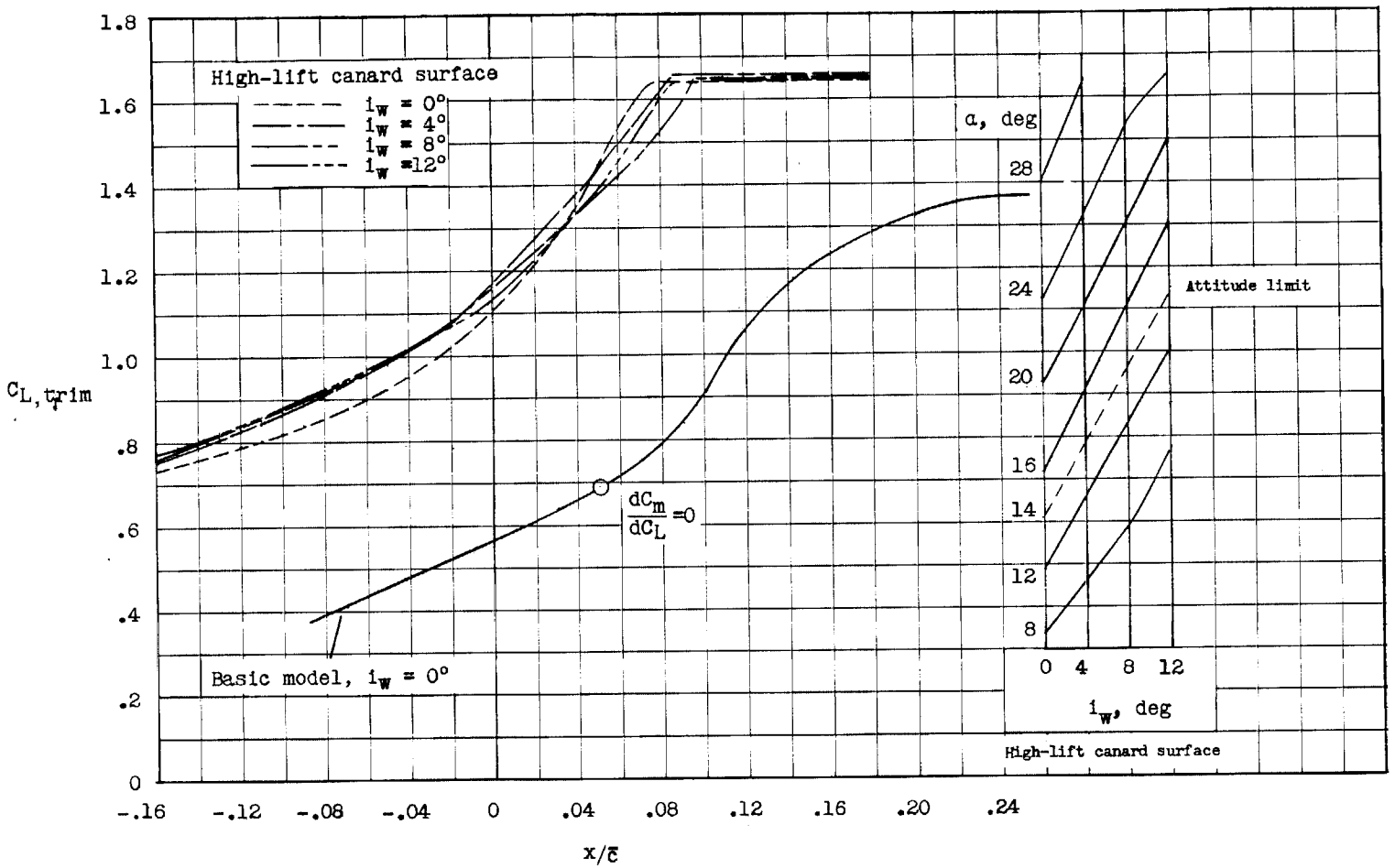

(a) High-lift canard surface A.

Figure 16.- Variation of maximum trim lift coefficient with center-of-gravity position.

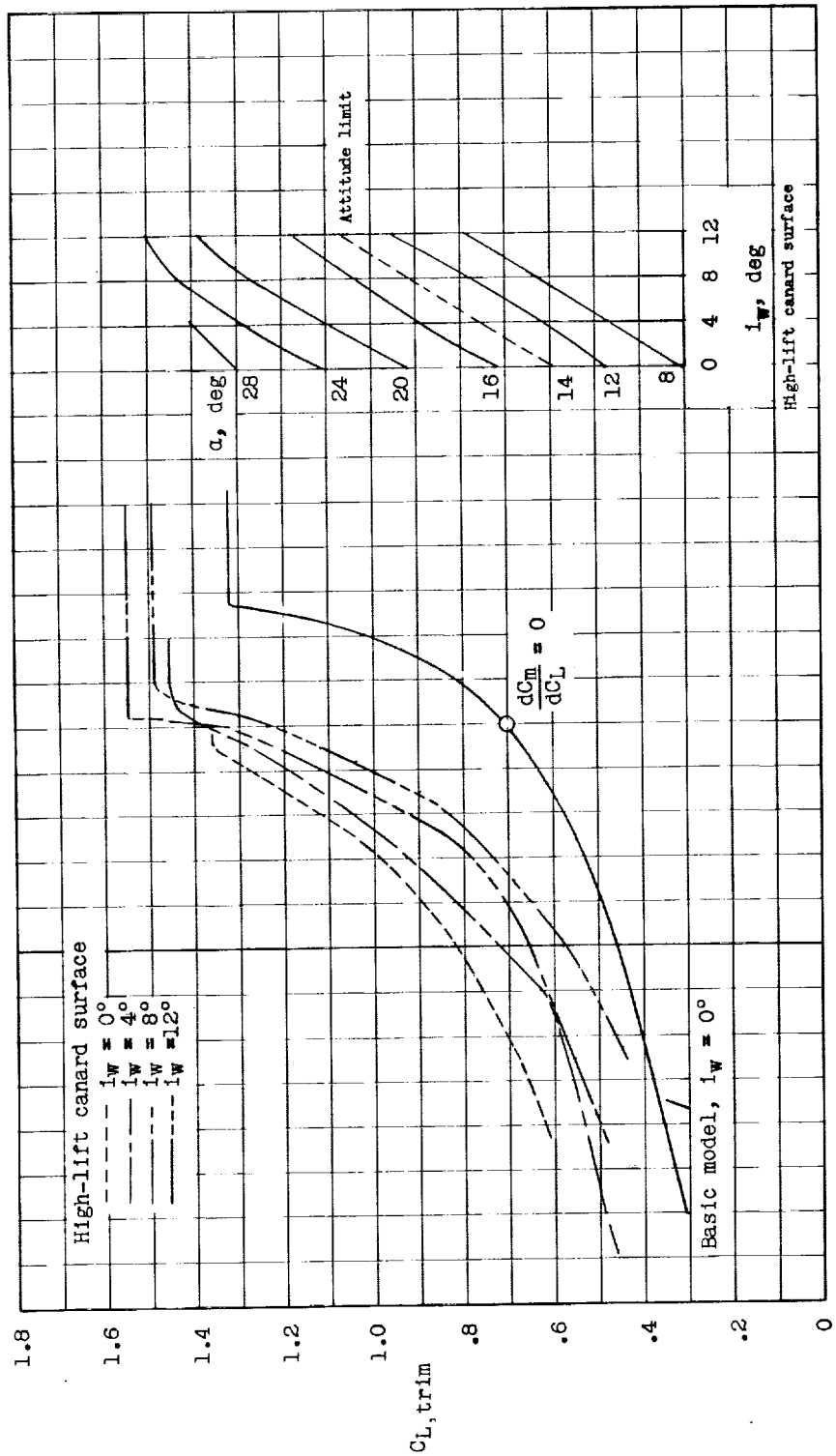

(b) High-lift canard surface B.

Figure 16.- Concluded.

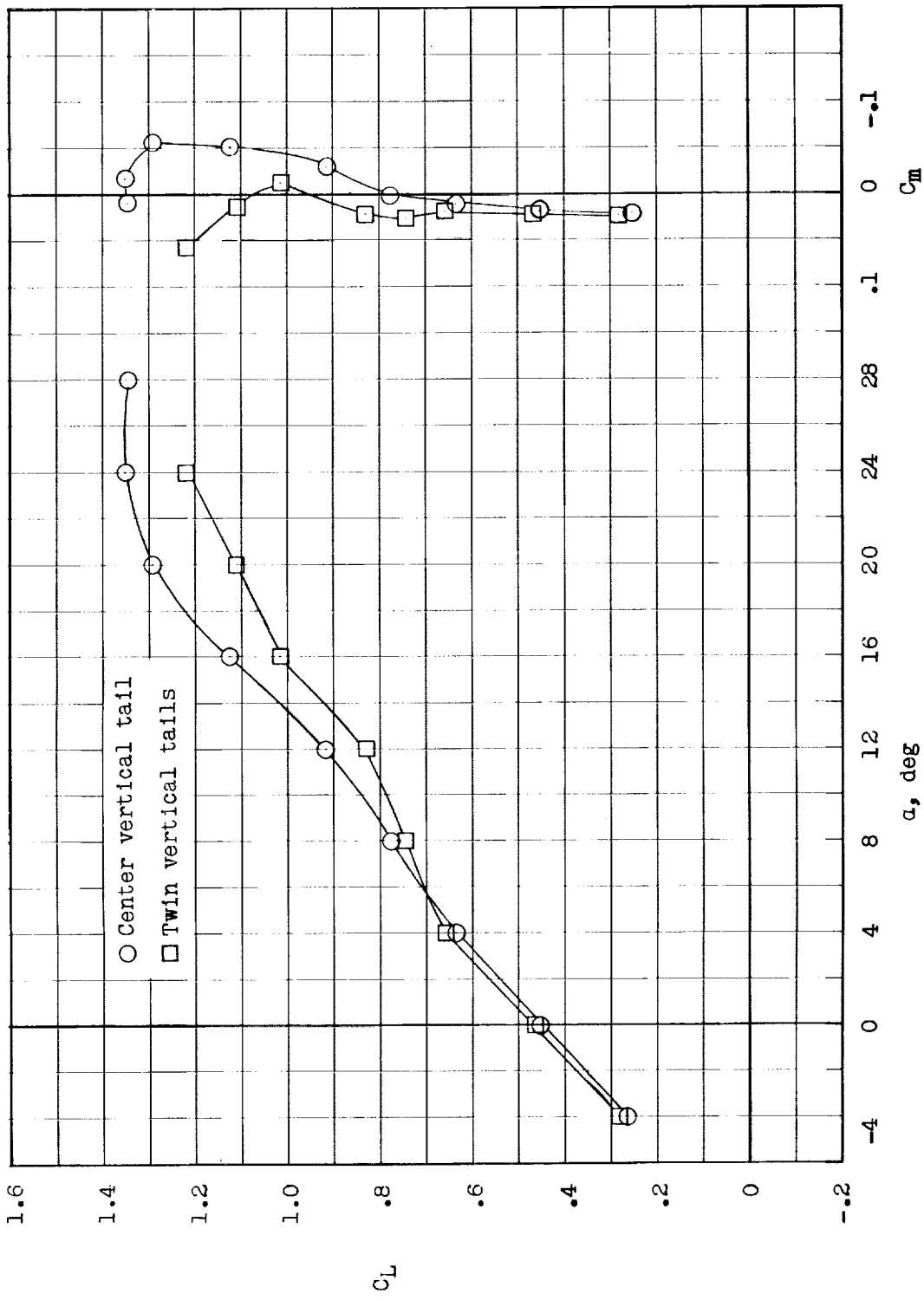

Figure 17.- Effects of twin vertical tails on longitudinal characteristics of model with high-lift canard surface B. $i_w = 12^o$; $i_t = 0^o$; center of gravity at 0.09$\bar{c}$.

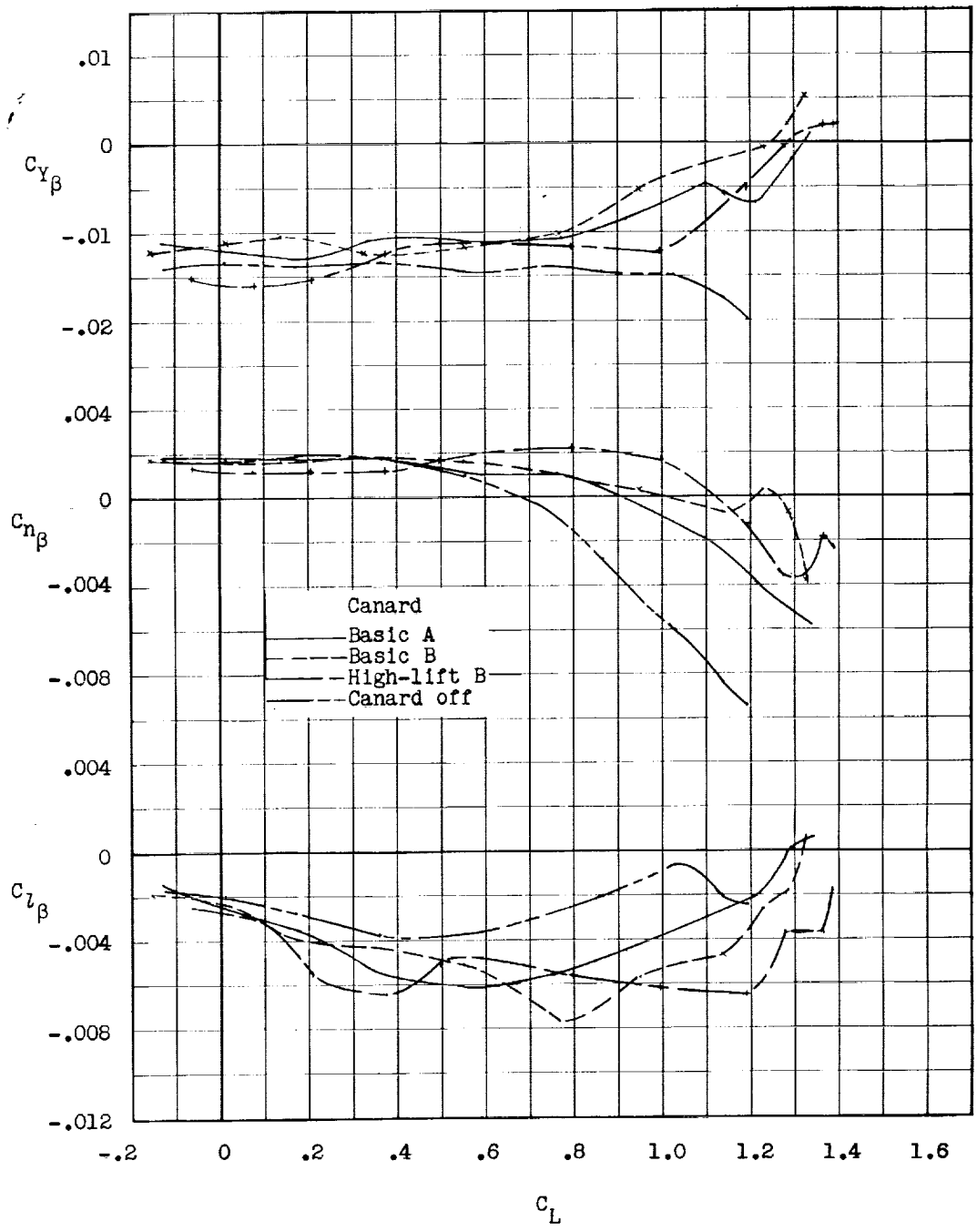

(a) $i_w = 0^o$.

Figure 18.- Effect of canard surface on lateral stability characteristics of model with center vertical tail. $i_t = 0^o$; center of gravity at $0.275\bar{c}$.

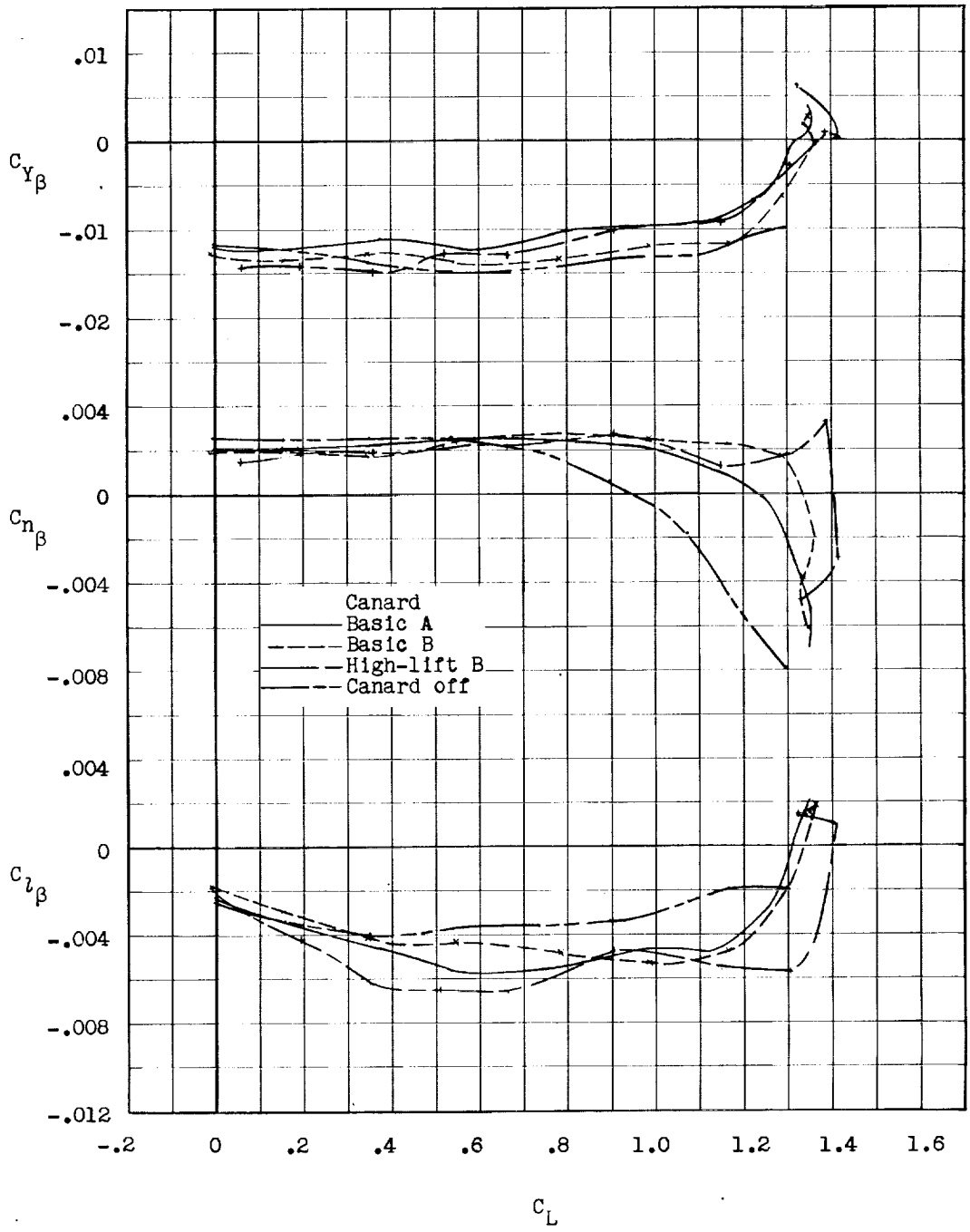

(b) $i_w = 4^o$.

Figure 18.- Continued.

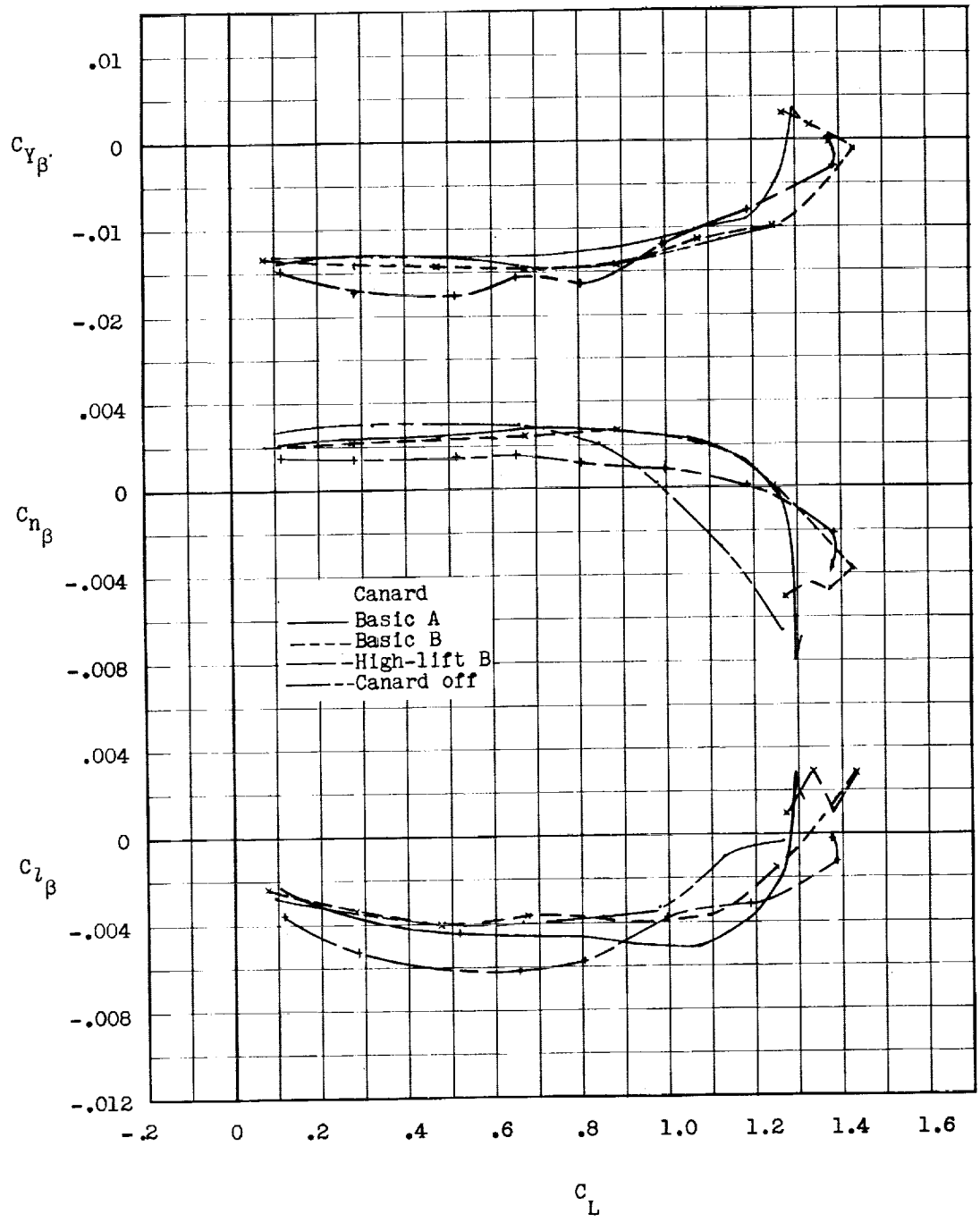

(c) $i_w = 8^\circ$.

Figure 18.- Continued.

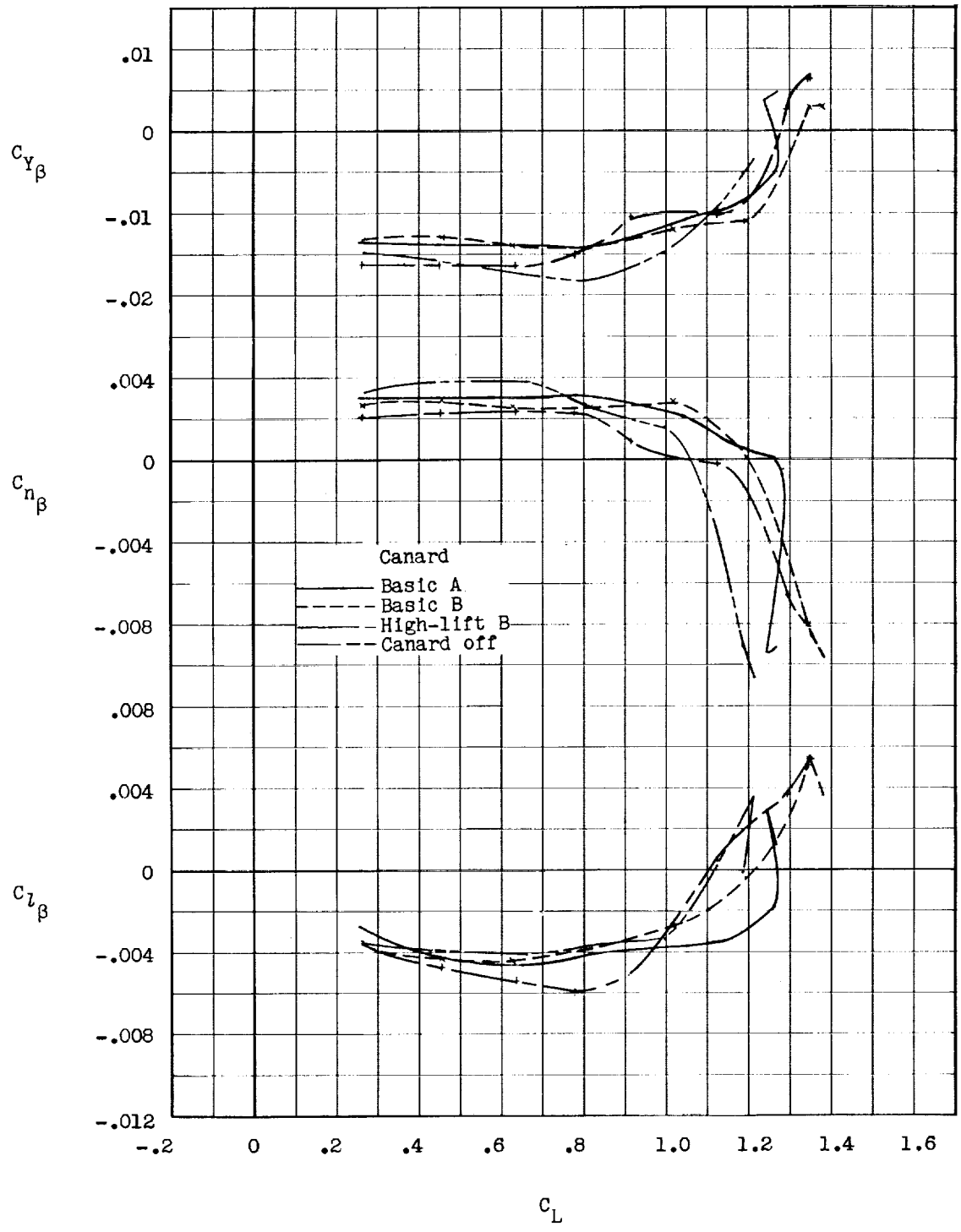

(d) $i_w = 12^o$.

Figure 18.- Concluded.

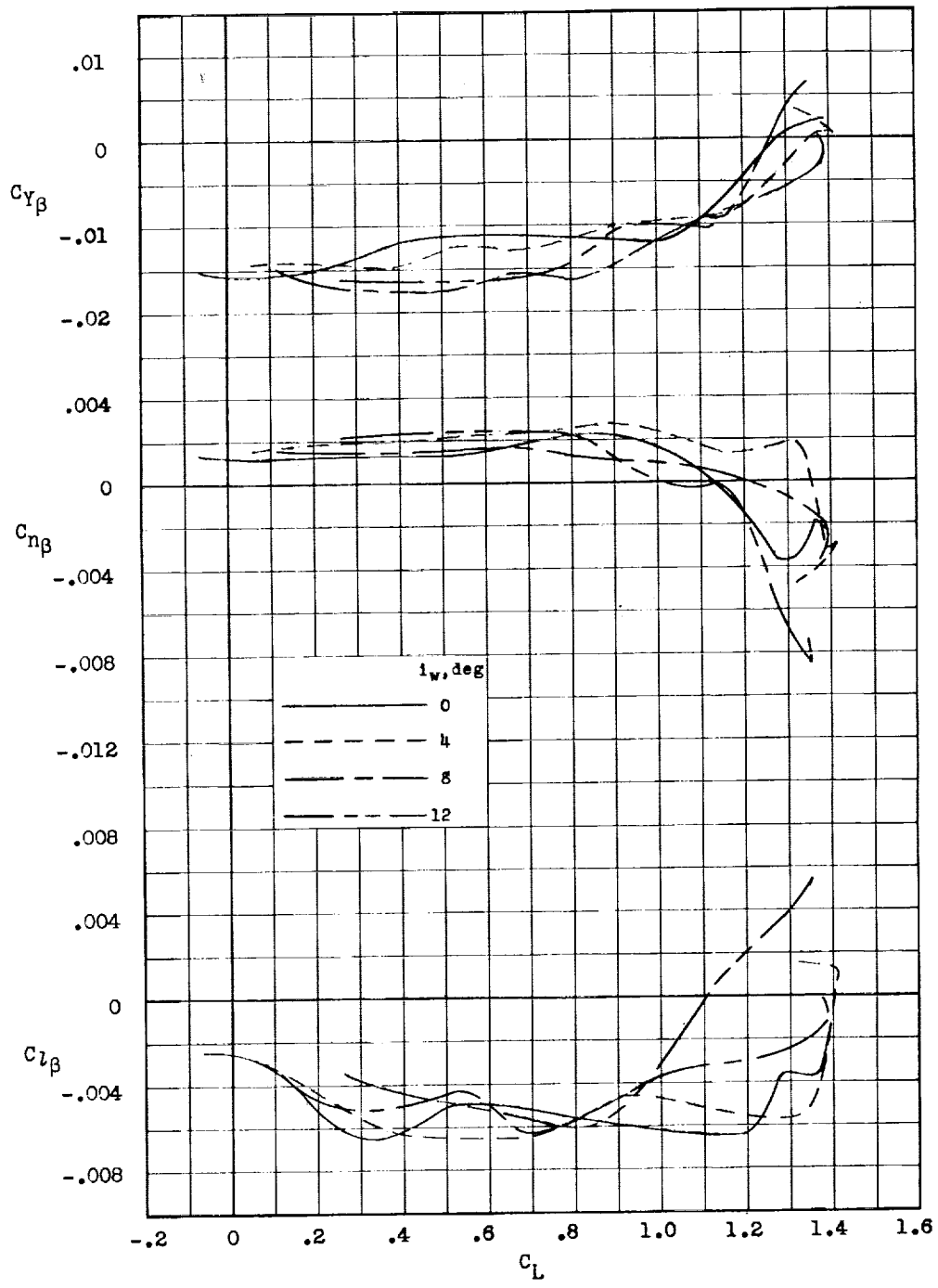

Figure 19.- Effect of wing incidence on lateral stability characteristics of model with high-lift canard surface B. $i_t = 0^\circ$; center vertical tail; center of gravity at $0.275\bar{c}$; leading-edge extension off.

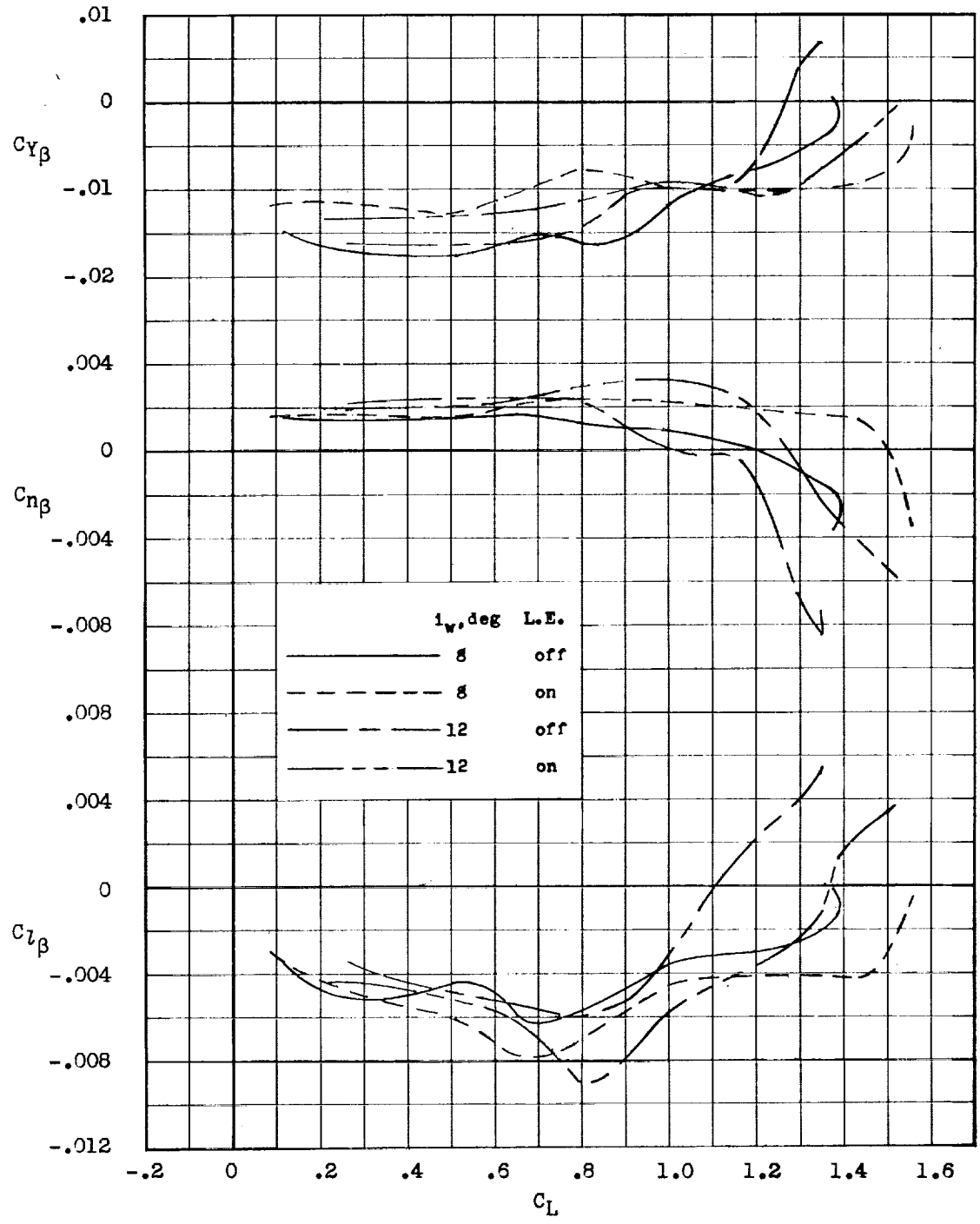

Figure 20.- Effect of wing leading-edge extension on lateral stability characteristics of model with high-lift canard surface B and center vertical tail. $i_t = 0^\circ$; center of gravity at $0.275\bar{c}$.

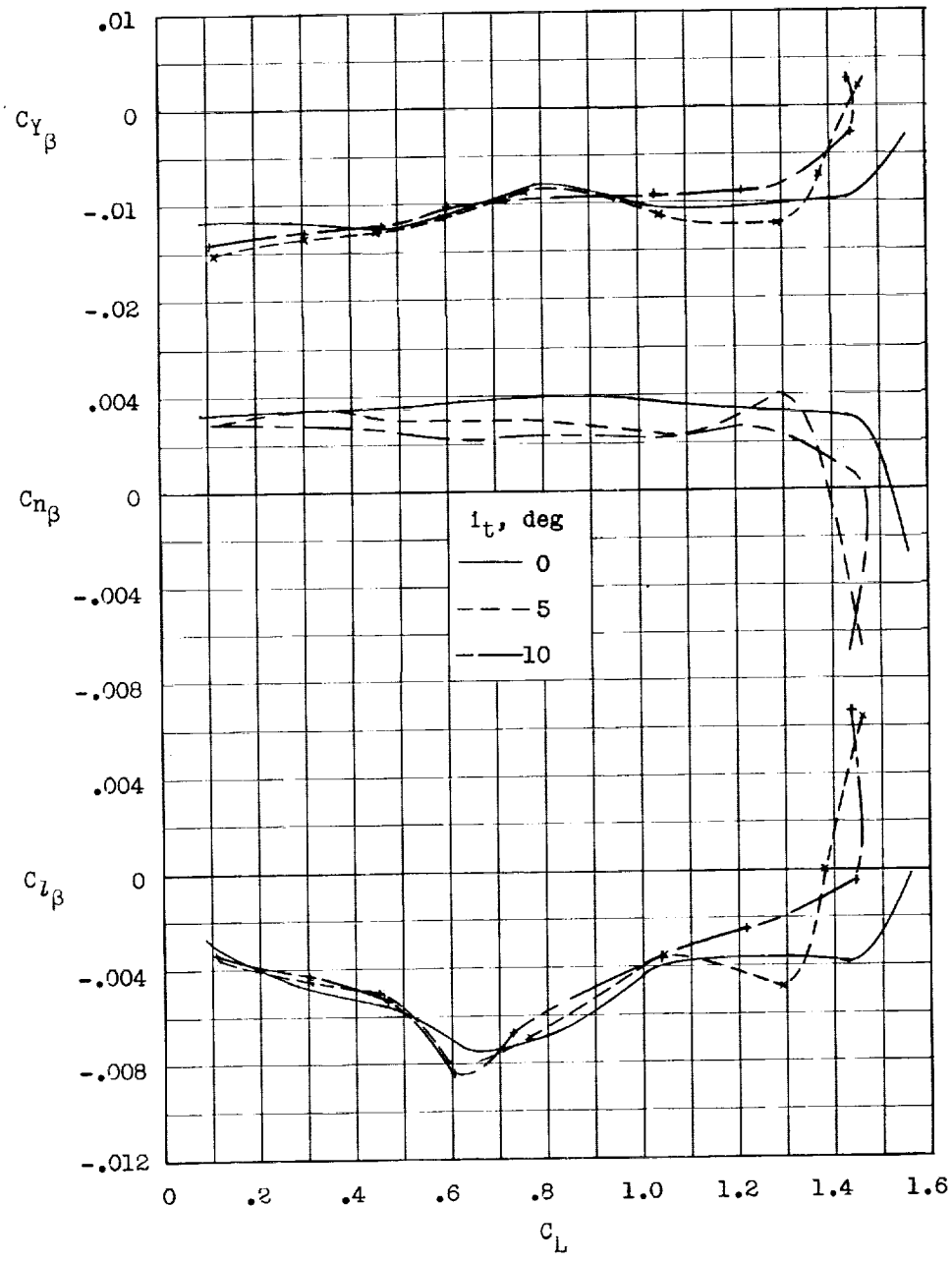

(a) $i_w = 8^o$.

Figure 21.- Lateral stability characteristics of model with wing leading-edge extension, high-lift canard surface B, and center vertical tail. Center of gravity at $0.09\bar{c}$.

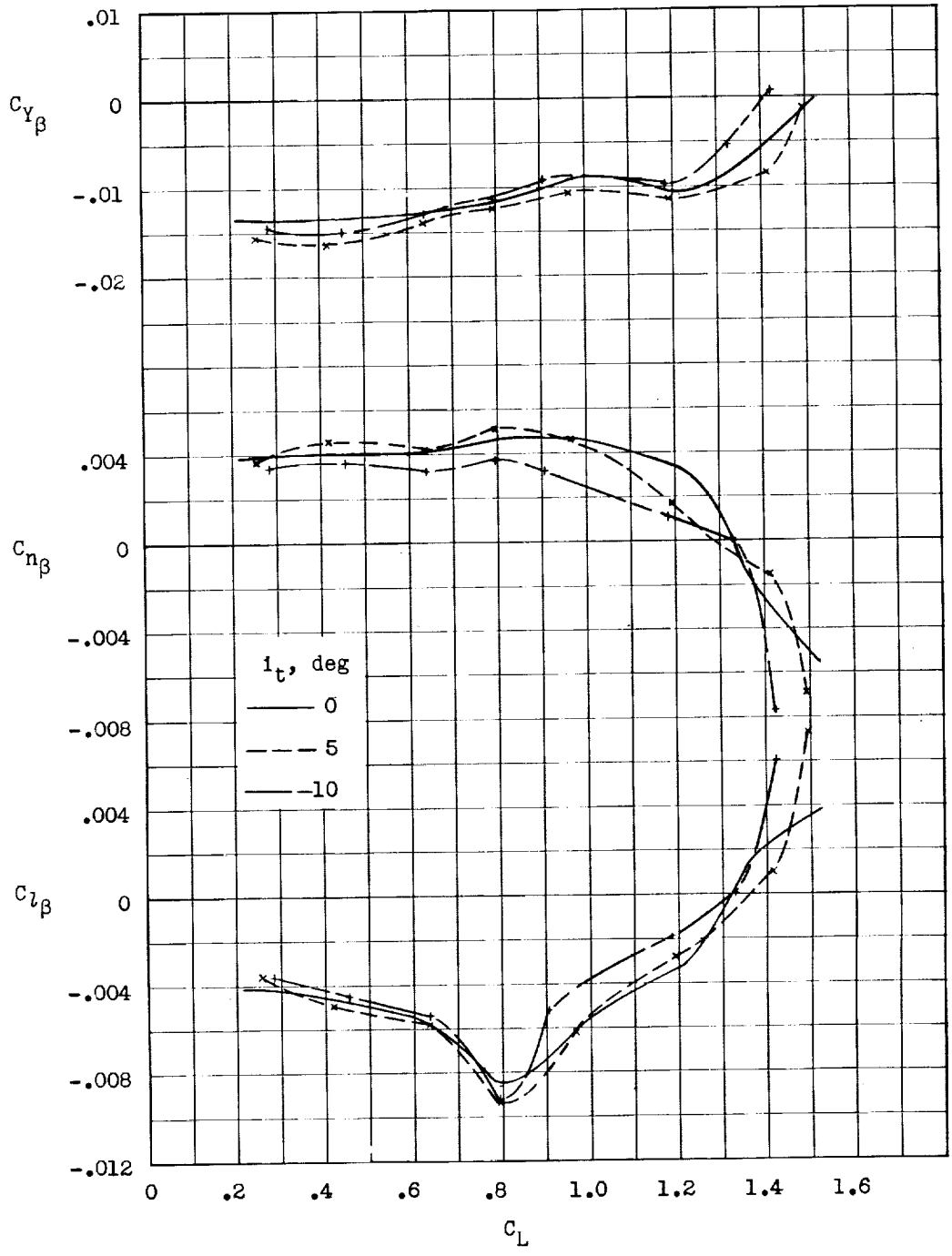

(b) $i_w = 12^\circ$.

Figure 21.- Concluded.

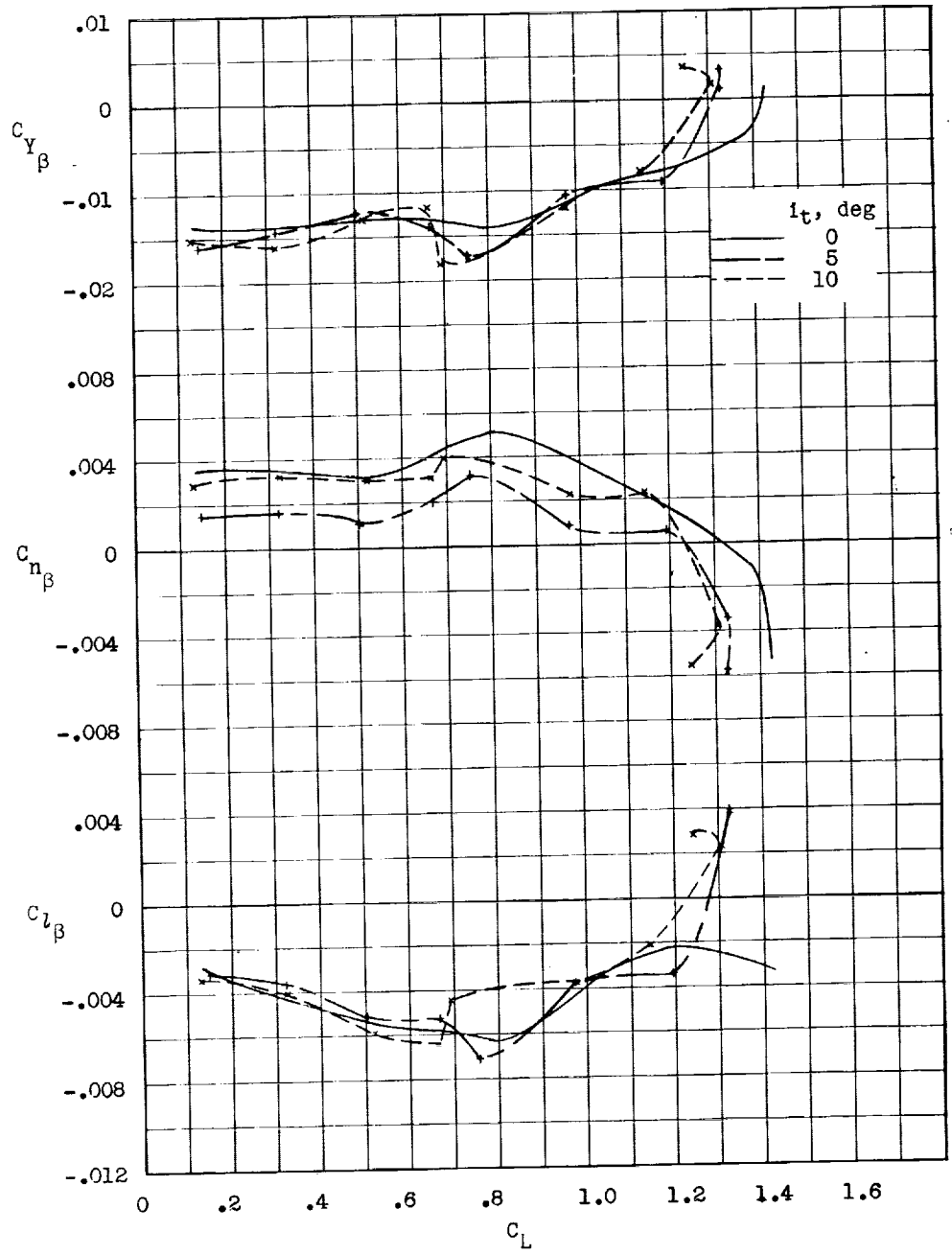

(a) $i_w = 8^\circ$.

Figure 22.- Lateral stability characteristics of model with wing-mounted ventral fins, high-lift canard surface B, and center vertical tail. Center of gravity at 0.09$\bar{c}$.

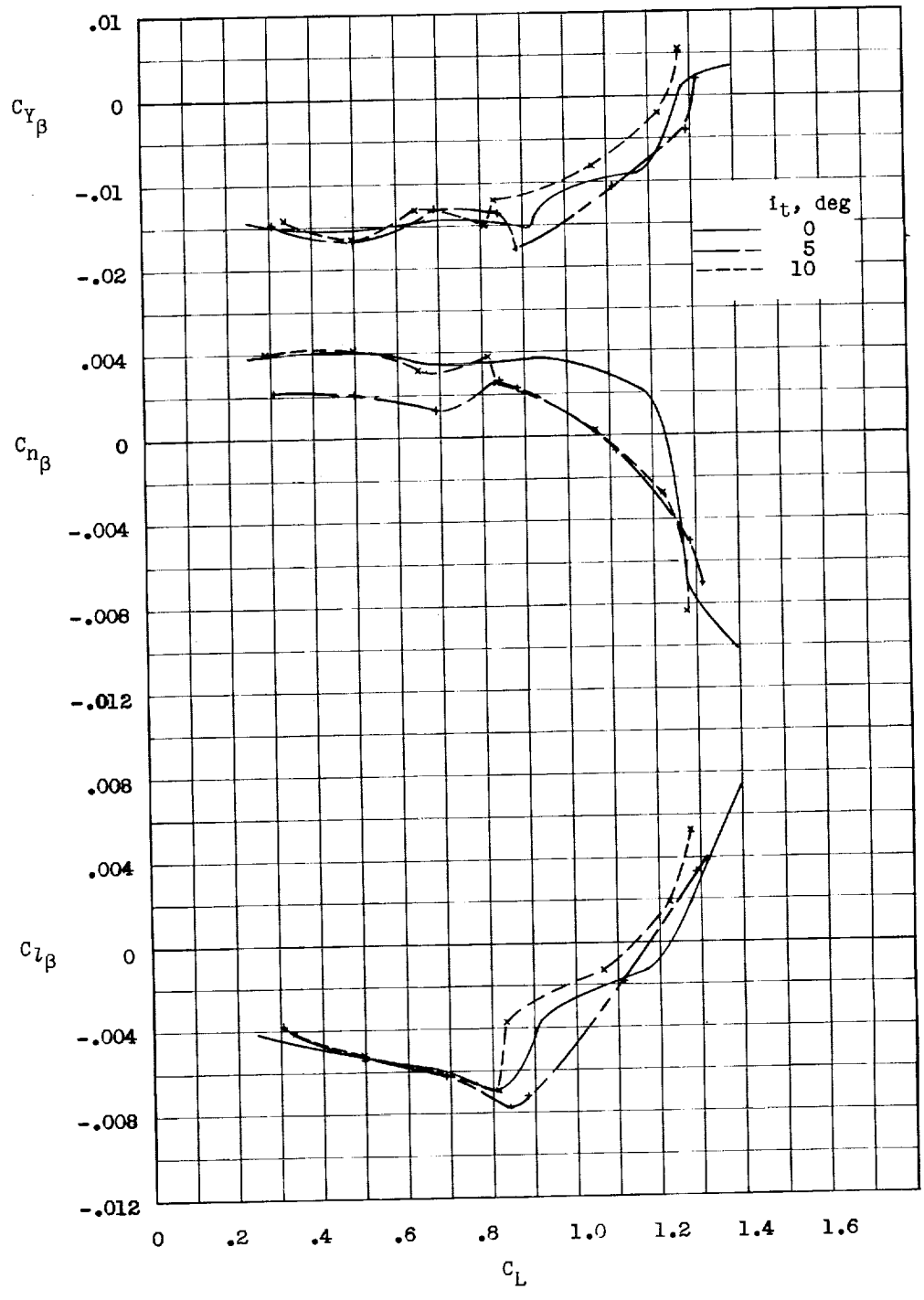

(b) $i_w = 12^\circ$.

Figure 22.- Concluded.

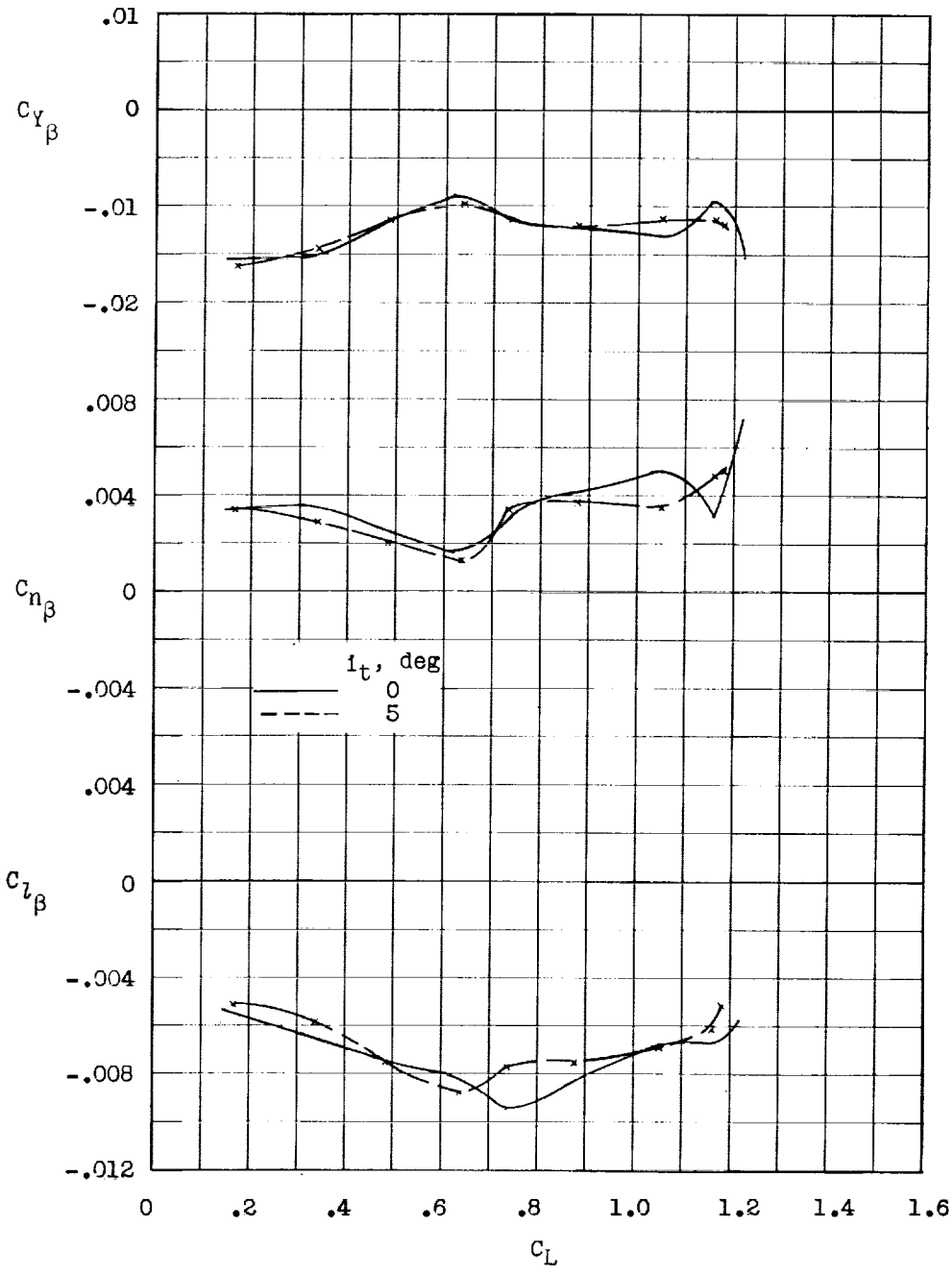

(a) $i_w = 8^o$.

Figure 23.- Lateral stability characteristics of model with twin vertical tails and high-lift canard surface B. Center of gravity at $0.09\bar{c}$.

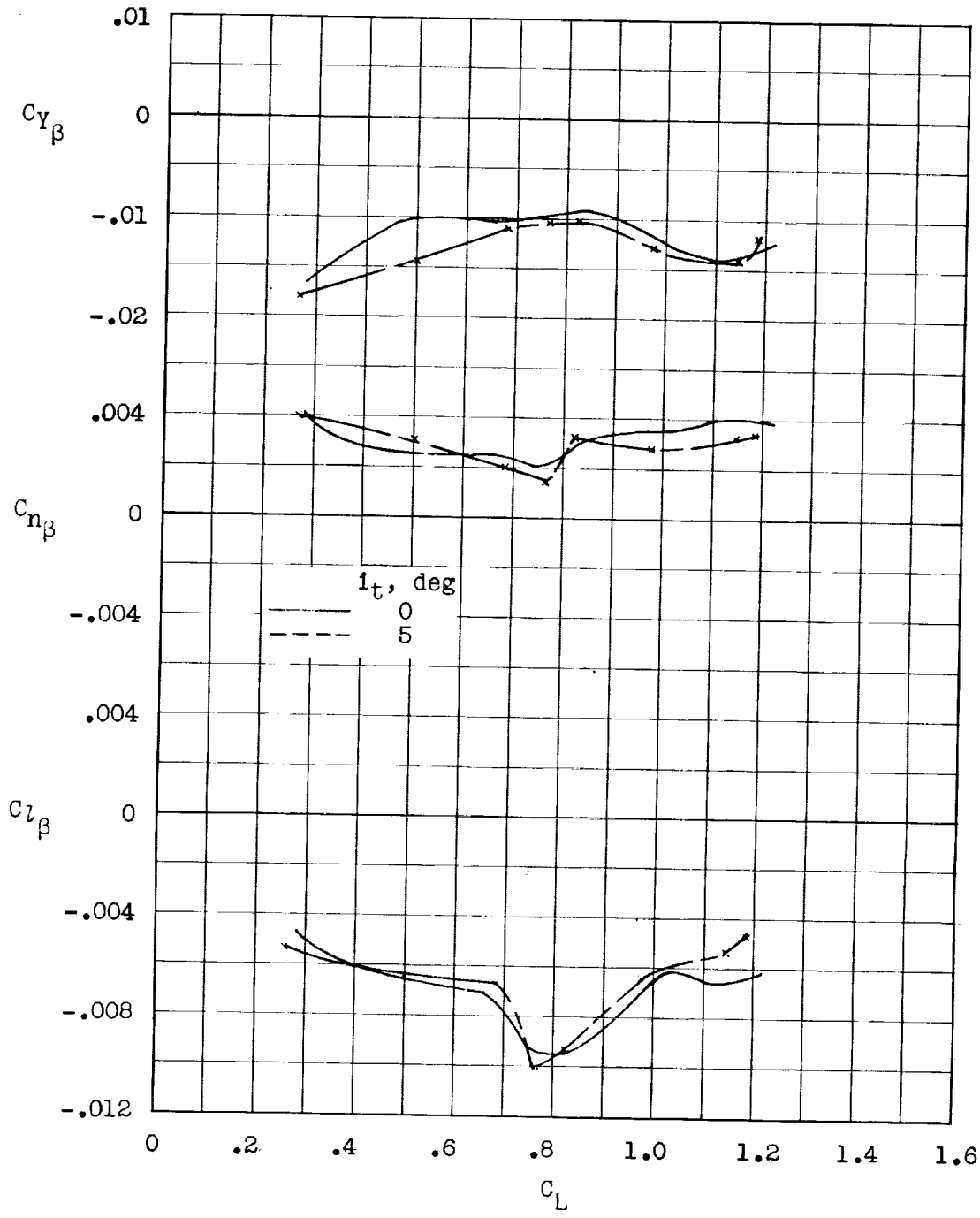

(b) $i_w = 12^o$.

Figure 23.- Concluded.

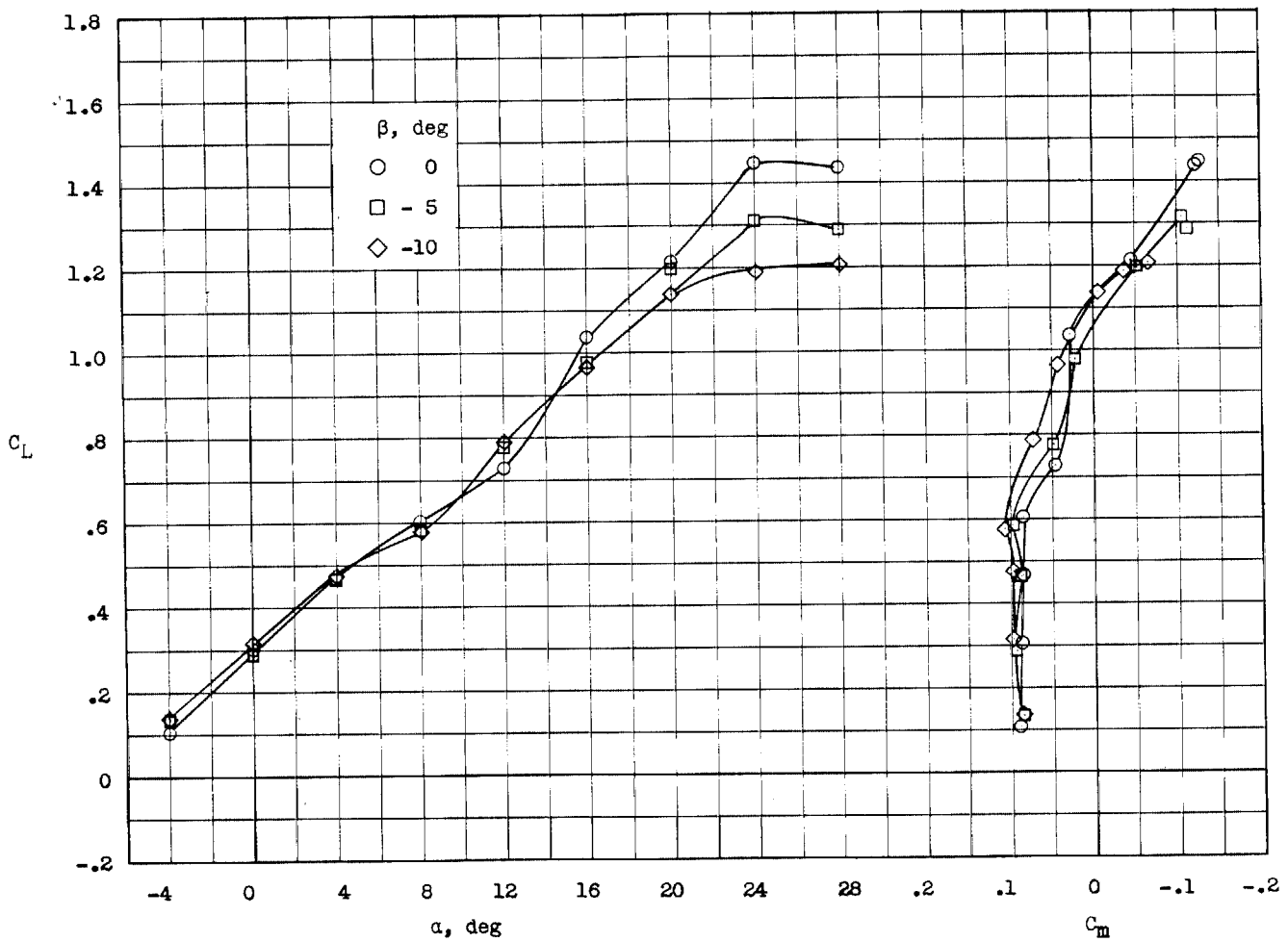

(a) $i_w = 8^o$; $i_t = 10^o$.

Figure 24.- Effect of sideslip angle on longitudinal characteristics of model with leading-edge extension, high-lift canard surface B, and center vertical tail. Center of gravity at 0.09$\bar{c}$.

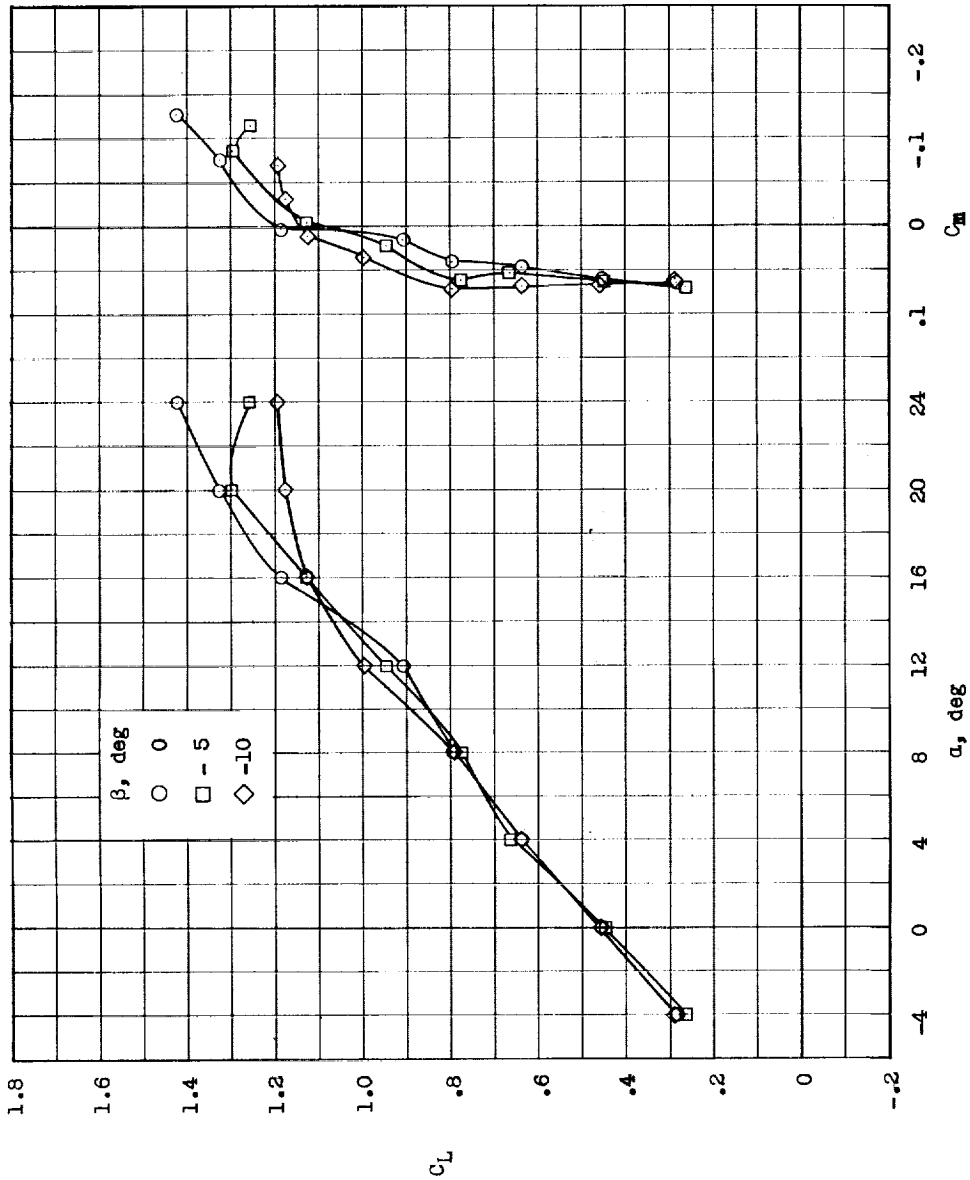

(b) $i_w = 12^o$; $i_t = 10^o$.

Figure 24.- Concluded.